3-25-2021

Correlating the Effect of Dynamic Variability in the Sensor Environment on Sensor Design

Pulak Bhushan
pbhus001@fiu.edu

FLORIDA INTERNATIONAL UNIVERSITY

Miami, Florida

CORRELATING THE EFFECT OF DYNAMIC VARIABILITY IN THE SENSOR ENVIRONMENT ON SENSOR DESIGN

A dissertation submitted in partial fulfillment of the

requirement for the degree of

DOCTOR OF PHILOSPHY

in

ELECTRICAL AND COMPUTER ENGINEERING

by

Pulak Bhushan

2021

To: Dean John L. Volakis
College of Engineering and Computing

This dissertation, written by Pulak Bhushan, and entitled Correlating the Effect of Dynamic Variability in the Sensor Environment on Sensor Design, having been approved in respect to style and intellectual content, is referred to you for judgment.

We have read this dissertation and recommend that it be approved.

_____
Jean Andrian

_____
Shubhendu Bhardwaj

_____
Bruce McCord

_____
Orlin Velev

_____
Michael Daniele

_____
Shekhar Bhansali, Major Professor

Date of Defense: March 25, 2021

The dissertation of Pulak Bhushan is approved.

_____
Dean John L. Volakis
College of Engineering and Computing

_____
Andrés G. Gil
Vice President for Research and Economic Development
and Dean of the University Graduate School

Florida International University, 2021

DEDICATION

To my parents

ACKNOWLEDGMENTS

The last 4 years of graduate school have been a great experience due to the help and support of many people. First and foremost, I would like to thank my advisor, Dr. Shekhar Bhansali, for his invaluable guidance, motivation, and support throughout my doctoral study. You supported me throughout my journey with your knowledge and encouragement while providing me the opportunity to work in my own way. You have always been a role model for me, and I will carry all the training provided by you to guide me in my future career. You provided me with opportunities that I would never have imagined and have always been an incredible mentor and friend. I will always treasure all the academic and non-academic discussions we had during our meetings. I would also like to thank all my dissertation committee members for their insightful comments and guidance throughout my research. You have all been a positive influence on me and have set an example to which I aspire.

I am also thankful to all the active and former graduate students and postdocs of the BioMEMS group for always providing a friendly and helpful work environment. I would like to extend my appreciation to Dr. Yogeswaran Umasankar who guided me through my dissertation and with whom I cherished many wonderful academic discussions. I would like to recognize the support of my current and former lab mates, Apurva Sonawane, Khalid Pasha, Sohini RoyChoudhury, Lamar Burton, and Ahmed Jalal – it was a pleasure working and learning from each one of you. In addition, I thank all the staff members of the Department of Electrical and Computer Engineering for their invaluable support, with special mention to Ms. Pat Brammer, Ms. Luisa Ruiz, and Ms. Layla El-Hilu. I am fortunate to have worked around such people who provided their continual support throughout this amazing journey.

Finally, I will always be indebted to my parents, Akhilendra Bhushan Gupta and Poonam Gupta without whose love and support I would not be where I am today. I have always cherished discussions with my father who has provided me with immense wisdom and advice at crucial junctures of my career. My parents have always been an inspiration to me and without their constant encouragement, I would not have been able to complete this doctoral journey. I would also like to thank my sister, Mahak Bhushan for always raising my spirits whenever I felt dejected. Thank you.

ABSTRACT OF THE DISSERTATION

CORRELATING THE EFFECT OF DYNAMIC VARIABILITY IN THE SENSOR ENVIRONMENT ON SENSOR DESIGN

by

Pulak Bhushan

Florida International University, 2021

Miami, Florida

Professor Shekhar Bhansali, Major Professor

This dissertation studies the effect of biofluid dynamics on the electrochemical response of a wearable sensor for monitoring of chronic wounds. The research investigates various dynamic *in vivo* environmental parameters (pH, temperature, and evaporation) and correlates them with experimentally measured behavior with wound monitoring as a use case. Wearable electrochemical biosensors suffer from several unaddressed challenges, like stability and sensitivity, that need to be resolved for obtaining accurate data. One of the major challenges in the use of these sensors is continuous variation in biofluid composition. Wound healing is a highly dynamic process with wound composition changing continuously, resulting in a dynamic environment. This dissertation investigates the effects of several *in vivo* biochemical and environmental parameters on the sensor response to establish actionable correlations. Real-time assessment of wound healing was carried out through longitudinal monitoring of uric acid and other wound fluid characteristics. A textile sensor was designed using a simple fabrication approach combining conductive inks with a polymeric substrate, for conformal contact with the wound bed. A <3% degradation in the sensor response after prolonged mechanical stress, validated the sensing capability under high mechanical deformation. The nanomaterial-based

enzymatic sensor architecture for UA detection offered a sensitivity of 42.55 nA μM^{-1} cm^{-2}, establishing the applicability of the sensor for accurate measurements in the physiologically relevant range. The sensor was also found to be stable for a period of 3 days when subjected to physiological and elevated temperatures (37^{o}C and 40^{o}C) confirming its relevance for long-term monitoring. Rigorous testing under dynamic *in vitro* conditions showed a direct correlation between sensor response and the dynamic parameters, with the results showing a ~20% deviation from the accurate UA reading. The results confirmed that as a consequence of these parameters temporally changing in the wound environment, the sensor response will be altered. The work thus developed mathematical models correlating the effect of variability of these parameters i.e., pH, temperature, sample volume, evaporation, and biofouling on sensor response to allow for real-time sensor calibration. The clinical validation studies established the feasibility of UA measurement by the developed electrochemical sensor and derive correlations between the wound chronicity and UA levels. The protocols developed in this work for the design, fabrication, and calibration of the sensor to correct for the dynamic *in vivo* behavior can be extended to any wearable sensor for improved accuracy.

TABLE OF CONTENTS

LIST OF TABLES

LIST OF FIGURES

1 Introduction to Wearable Health Monitoring Systems

Continuous monitoring of a person's health parameters can enable timely intervention of healthcare providers and allow for the development of effective disease treatment and management plans; thus, improving the overall therapeutic efficacy. The need for continuous and active healthcare surveillance is fundamental especially in current times of a pandemic.[1,2] Conventional healthcare assessment techniques involve bulky and expensive laboratory equipment, mandating skilled medical personnel for their operation. Moreover, they require invasive procedures for sample collection (e.g., pricking for blood collection) with the general turnaround time being a couple of hours or in some cases several days. The advent of point-of-care devices for bedside assessment, eliminated the need for complex equipment, but still required complex sample collection procedures while only offering single time measurements.[3] This thus necessitated the need for the development of sensing systems that could directly interface to a person's body or a specific organ to continuously measure the physical and chemical signals generated.

1.1 Wearable Sensors

Wearable sensors have provided an elegant alternative to the conventional ways for assessment of a person's physiological status in a continuous and non-invasive manner. They are body-borne systems that interact with the wearer and integrate a biological element to measure health parameters to produce a signal that is then transmitted to an associated electronic device. Over the last decade, the medical sensing paradigm has been completely altered with the dawn of such wearable sensing technologies. The significant advancements made in these devices have enabled clinicians to track vital health parameters such as, body movement,[4–7] heart rate,[8–11] body temperature,[12–15]

glucose[16–19], and lactic acid[17,20–23] levels, etc. in real-time to predict potential future health risks and provide timely treatments. For instance, continuous monitoring of electrograms such as an electrocardiogram (ECG)[24,25] and electroencephalogram (EEG)[26,27] that measure electrical signals from the heart and brain respectively, can allow for diagnosis of potential heart attacks or seizures or timely diagnosis of atrial fibrillation. These devices are particularly beneficial for patients living in remote areas where immediate medical assistance is not available, who require home assistance, or are suffering from chronic diseases, to provide standard medical care remotely while reducing the medical costs. The integration of these sensors into wearable accessories that can be placed onto the body (e.g. watch or headband) or be incorporated within garments can truly help realize personalized healthcare monitoring. The technological advances made in the field of material science, semiconductor technology, sensing mechanisms, miniaturized flexible electronics, and above all the growing awareness of the need for personalized healthcare and treatment plans have led to significant research in wearable technology. Furthermore, the convergence of industrial-scale fabrication technologies, physiological sensing, and predictive data analytics has enabled the translation of wearable devices from research laboratories to commercial medical products.

A majority of the daily activities carried out by a person are inevitably dependent on some physical activity. Continuous measurement of physical stimulus generated by the body through wearable sensing systems provides an opportunity for predictive analysis aiding in early diagnosis of a disease. Extensive research is being carried out to develop systems that are mechanically robust and highly sensitive to accurately detect the body signals while eliminating unwanted noise. While advances in material science have led to the development of sensing platforms that are ultrathin, lightweight,

mechanically resilient, self-healing, and can conformally attach to the human body; implementation of nanostructured architectures[28–32] have resulted in improved sensitivity of the sensors. Some of the vigilant physical monitoring systems include sensors that track heart rate, muscle movement, pressure, strain, and venous pulse (Figure 1.1).

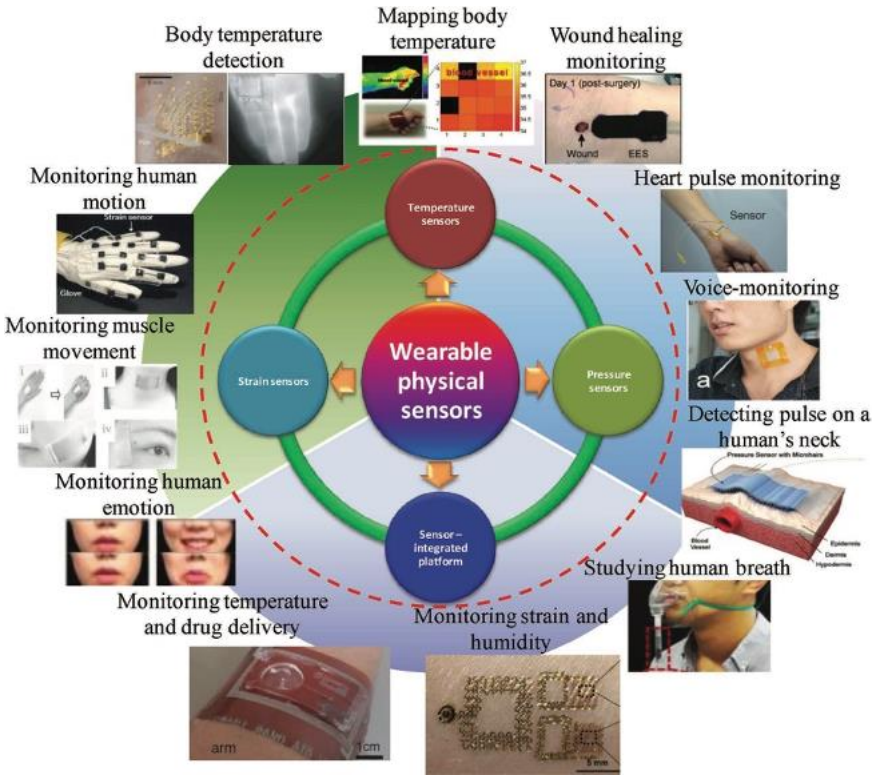

Figure 1.1. Examples of wearable sensing systems for tracking physical stimuli such as heart rate, body temperature, strain, humidity, muscle monitoring, etc. for real-time healthcare monitoring. Reproduced with permission.[33] Copyright 2016, Wiley-VCH.

In addition, integrated platforms are being designed that implement an array of several individual sensors to simultaneously measure multiple health parameters providing a more holistic view of the person's health.[34–38] Although monitoring of physical parameters is essential, biochemical profiling of biofluids can provide an even more comprehensive overview of a person's health. A majority of non-invasive wearable biochemical sensors are still in the research stage and no commercial devices that can provide real-time monitoring and therapeutics exist yet.

1.2 Wearable Chemical Sensors

Chemical sensing involves the detection of a particular analyte using a sensing element and transforming the chemical information into an electrical signal using a transducer. These sensors are particularly vital in the field of healthcare monitoring for the detection of a multitude of diseases. For example, measurement of analytes such as glucose[39] and lactate[40] in blood has been used for the detection of diabetes and kidney-related diseases, respectively. However, the conventional laboratory-based detection techniques require collection of samples in a non-invasive manner (e.g., finger-pricking for blood collection) posing a major healthcare hurdle. The need for sensors for continuous temporal monitoring of analytes with a simple and non-intrusive sample collection procedure is vital. Management of diseases like post-traumatic stress disorder, may require continuous measurement of cortisol to prevent any sudden mental breakdowns in the future.[41] Similarly, complications associated with diabetes can lead to the development of chronic ulcers, which with inefficient wound care management may result in infections and traumatic amputations. However, existing wound care practices are highly subjective, with no existing platforms for vigilant wound monitoring. The development of continuous monitoring platforms for such diseases can aid in clinical decision making thus improving the patient's standard of life. Over the last decade, several wearable chemical sensors have been developed for healthcare diagnostics using optical,[42–45] electrochemical[16,17,21], and piezoelectric[46,47] based transduction mechanisms. Among these, electrochemical sensors have gained particular attention owing to their simplicity, stability, sensitivity, and low cost. A typical electrochemical sensor consists of two fundamental units: i) a receptor, and ii) a transducer (Figure 1.2).

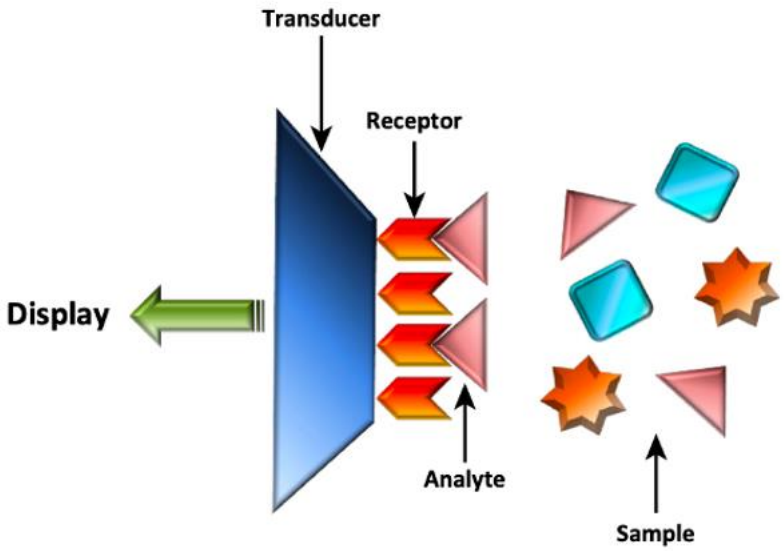

Figure 1.2. Schematic illustrating the different functional components of an electrochemical sensor, which includes a transducer, receptor, target analyte and the sample biofluid. Reproduced with permission.[48] Copyright 2014, Elsevier Inc.

The main role of the receptor is to specifically detect the target analyte in the presence of potentially interfering chemical species, while the transducer is required to convert the generated chemical signal to a readable electrical signal. Electrochemical sensors are further classified based on the receptor type as, catalytic or affinity-based sensors. Amongst these, enzymatic sensors, a class of catalytic-based sensors, have received tremendous attention owing to their high specificity, sensitivity, and their continuous measurement modality. Considerable efforts have been made recently in this field resulting in the development of wearable electrochemical sensors that can detect target analytes in biofluids such as sweat, interstitial fluid, tears, saliva, and wound exudates. The following sections discuss the different electrochemical sensors developed for different target biofluids in further detail.

1.2.1 Sweat-based sensors

Sweat is a complex biofluid containing a wealth of chemical information whose profiling can be potentially utilized to obtain a deeper understanding of a person's health at the biomolecular level. While blood has conventionally been used as a sample

for the detection of several diseases, researchers have established strong correlations between the sweat and blood concentration of certain analytes such as glucose,[39] thereby providing an opportunity to probe sweat for non-invasive long-term medical monitoring. In order to identify the correlations between sweat and blood analyte concentrations, recent research has been focused on understanding the underlying fundamentals of sweat gland physiology.[49,50] The research revealed that sweat conductivity and volumetric sweat rate play a major role in determining the sweat analyte concentrations. Researchers have utilized this rich biofluid to detect several analytes panning from ions such as Na^+,[51–53] K^+,[17,54] Cl^-, [55,56,] and Ca^{+2} [57] to metabolites like glucose,[17,58] lactate,[17,22,54] ethanol,[59–61] uric acid,[38] etc. All the above-mentioned analytes are directly linked to diseases such as diabetes, gout, alcoholism, and chronic liver disease, and their continuous monitoring can allow for improved clinical management of these diseases. Continuous monitoring of glucose using these wearable sensors has been of particular interest since their need is necessitated for efficient diabetes management. Some of the other state-of-the-art sweat based sensors developed recently are shown in Figure 1.3. Different form factors have been explored based on the target application, e.g. wristband or headband type sensors are preferable for monitoring of athletes while patch-type sensors have been used to discretely adhere to jointed areas or areas with a heterogeneous body topography (Figure 1.3). Multiplexed detection platforms have also been explored for the diagnosis of diseases that require the study of the interdependence of several health parameters.[17,34,38] Moreover, systems integrated with transdermal drug delivery modules[62] have been developed to enable active feedback therapy to prevent potential health issues. Such painless delivery modules are highly desirable especially for patients requiring frequent shots, e.g. insulin shots for diabetic patients.

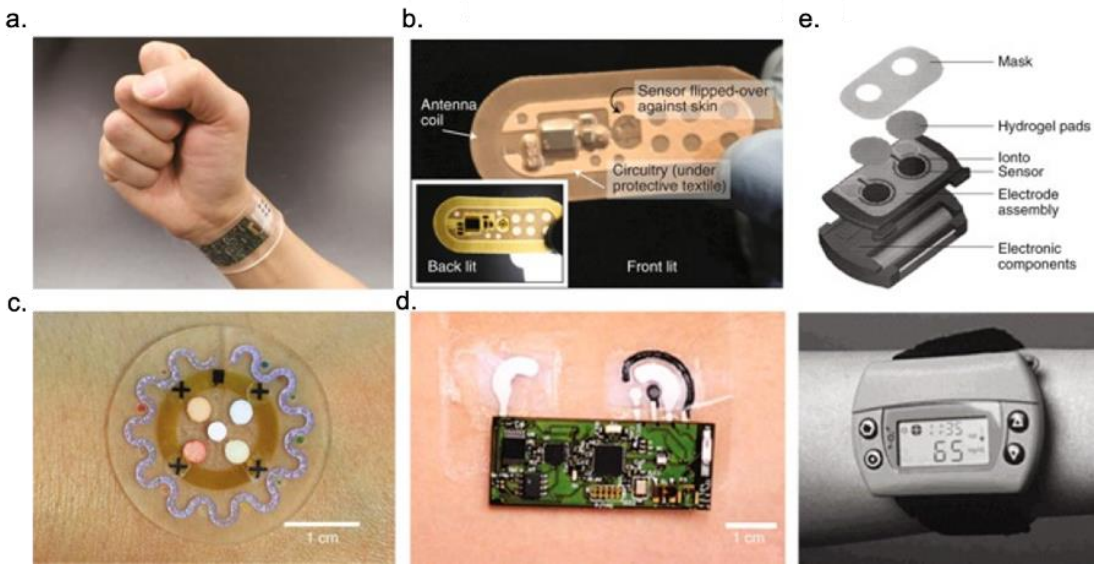

Figure 1.3. Recently developed wearable chemical sensors for continuous monitoring of metabolites in sweat. a. Smart wristband for multiplexed detection of a panel of analytes (glucose, lactate, Na^+ and, K^+) in sweat integrated to a flexible wireless transmission system for easy analyte read-out[17] b. Band-Aid style patch for continuous detection of Na^+ ions in sweat. The sensor patch was further integrated to an RFID antenna for wireless data transmission[63] c. A microfluidic wearable patch for sweat rate measurement and colorimetric detection of analytes present in the sweat (glucose, lactate, pH and chloride) [64] d. Tattoo-based screen-printed electrodes for ethanol detection in sweat. The device consisted of an iontophoretic system to induce sweat and integrated with flexible electronics for data recording and transmission[61] and e. An exploded view of the different layers in the commercial GlucoWatch (top). Photograph representing semi-continuous glucose measurements using the GlucoWatch (bottom)[65]. Reproduced with permission.[66] Copyright 2018, Springer Nature.

1.2.2 Saliva-based sensors

Saliva is one of the biofluids that has been used for a long time for analyte detection using laboratory-based techniques as well. The easy accessibility and richness in biological constituents make saliva an excellent biofluid for non-invasive analysis.[67] However, conventional techniques require processing of the collected saliva for further analysis, which is eliminated by the wearable sensors to a certain extent. Considerable progress has been made in the field of wearable saliva-based sensors, with primary form factor being denture-based or mouthguard-based.[68,69] Sensors have been designed for monitoring a wide spectrum of analytes especially focused on analyzing oral pathology[70,71] and improving pharmacological efficiency. It is well known that the oral cavity is a host to a multitude of bacteria. Analysis of the microbiome composition can

provide valuable insights on the development of any bacterial infections within the cavity due to a dental prosthetic or a secondary manifestation of a certain disease.[72,73] As an examples, monitoring of fluoride activity has been carried out to serve as an indicator of fluoride dentifrice efficacy using these sensors.[74]

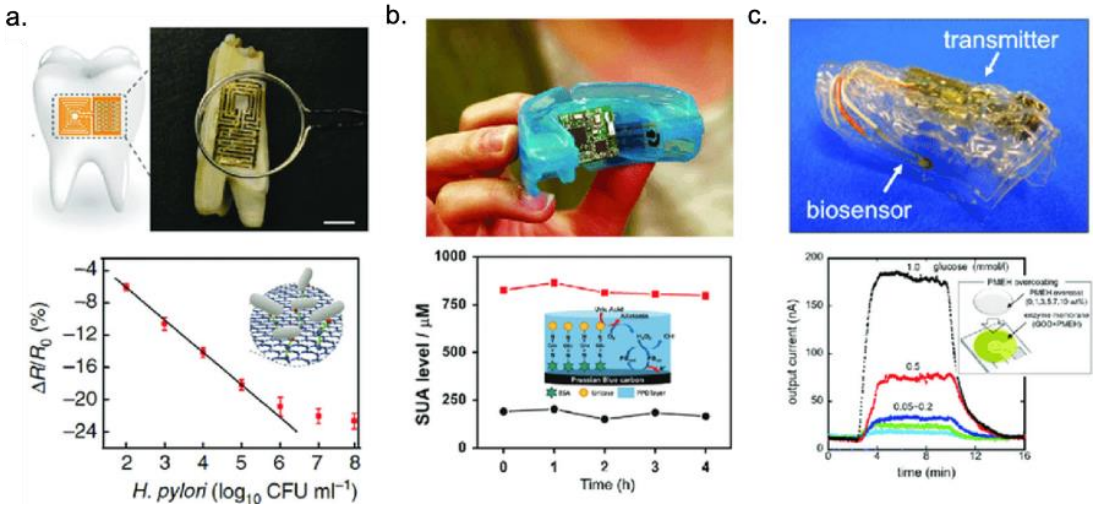

Figure 1.4. Recent wearable chemical sensors for monitoring of metabolites in saliva. a. Photograph of graphene-based sensors integrated onto a tooth for detection of bacterial formation on tooth enamel. The changes in the electrical resistance were used to quantify the growth of bacteria[72] b. A mouthguard-based device for electrochemical detection of salivary uric acid. The results show patients with hyperuricemia exhibiting elevated uric acid levels in the saliva[69] c. A mouthguard sensing platform for measurement of salivary glucose using entrapment of glucose oxidase in poly(MPC-co-EHMA). The results show a linear increase in the output current from the device with increasing levels of glucose[75]. Reproduced with permission.[76] Copyright 2018, The Royal Society of Chemistry.

In addition, saliva contains analytes that permeate via para or transcellular paths and can be used to evaluate systemic disorders. For example, a strong correlation has been established for glucose concentrations in saliva and blood for patients suffering from diabetes.[77] Cortisol is another such analyte that has been used to estimate the stress levels with direct correlation of saliva cortisol concentrations to circadian variations in a person.[78] Other analytes explored for detection using saliva as a biofluid are shown in Figure 1.4. Besides the fact that saliva can be collected in a non-invasive and painless manner, it is particularly compliant for clinical monitoring that requires frequent

sampling. However, a major drawback of saliva-based sensors is the requirement for pre-treatment steps, thus making it a lesser-explored biofluid compared to sweat.

1.2.3 Tear-based sensors

Tear is a biofluid that contains water, lipids, lysozymes, immunoglobulins, ions and, analytes like glucose and urea.[79] It is an easily accessible biofluid and has been considered to be an intermediate fluid between the cerebrospinal fluid and the serum.[79] Tear monitoring can be of particular importance for monitoring ocular and non-ocular disorders.[80] For instance, lipid monitoring in tears has allowed for the detection of diseases like multiple sclerosis.[79] On the other hand, researchers have primarily used tear as a biofluid for measurement of glucose levels for diabetes management.[81,82] An ocular lens-based sensor was developed by a research group that electrochemically measured glucose levels and transmitted the data wirelessly to the user (Figure 1.5).[83]

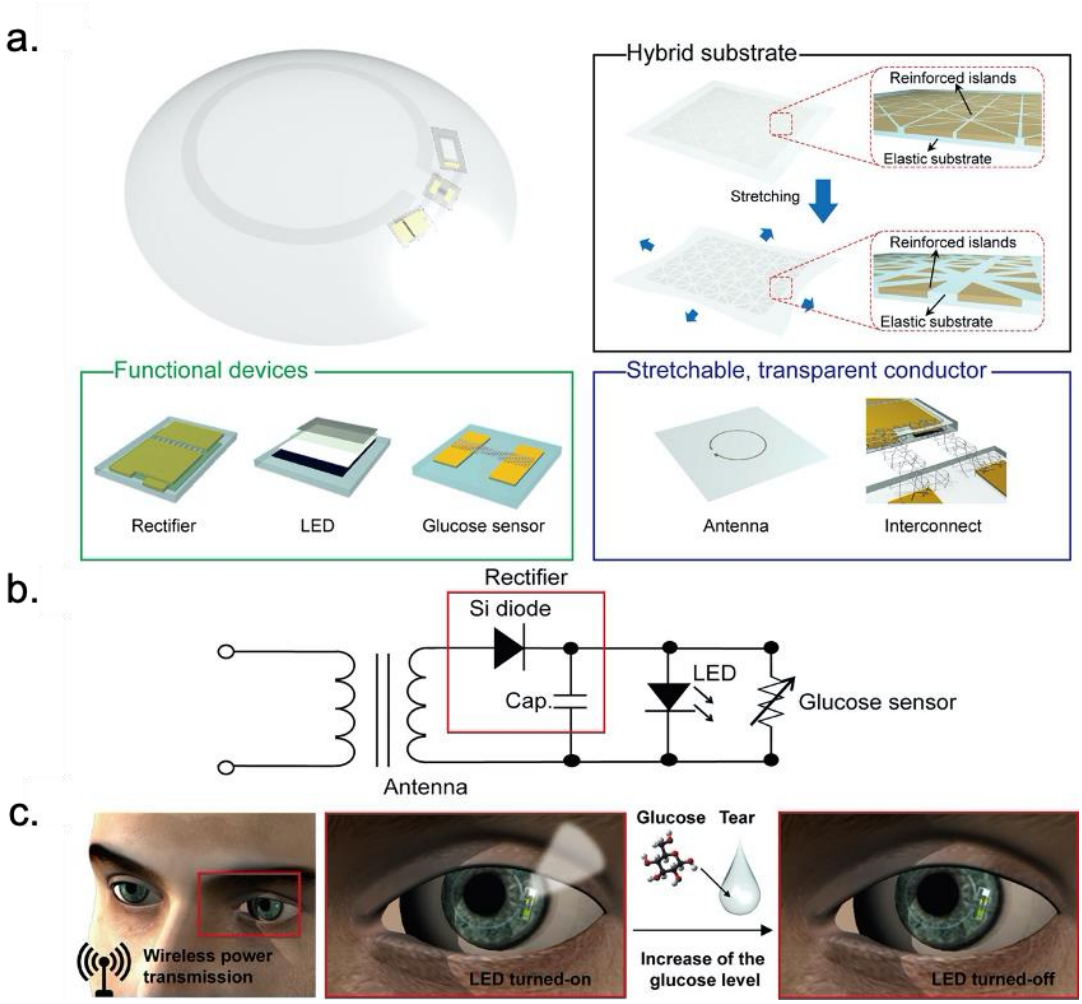

Figure 1.5. A wearable tear-based smart contact lens for glucose monitoring. a. Schematic illustration of the different components used in the developed soft, smart contact lens b. Circuit diagram of the smart contact lens and c. Operation of the soft and smart contact lens. The lens allows wireless transfer of power through the integrated antenna. The LED turns on while the glucose measurements are recorded to indicate the measurement in progress after which the results are wirelessly transferred to the user. Reproduced with permission.[83] Copyright 2018, American Association for the Advancement of Science.

However, accurate correlations between the analyte concentrations present in blood and tear have been rather questionable. Further, tear collection has been a major challenge in the development of these sensors.[84,85] Due to small volumes and fast evaporation rates of the tear, collecting a sufficient amount of biofluid is challenging. Recently, sensor-enabled lenses, also known as lab-on-the-eye devices, are being developed by researchers to eliminate the hurdle of sample collection and tear evaporation.[86–89] Measurement of different metabolites such as lactate is also being

explored to serve as an indicator of hypoxic conditions.[90] However, these sensors are still in infancy and a considerable amount of clinical validation is required to extract actionable information from these sensing platforms.

1.2.4 Wound exudate-based sensors

The biomolecular mechanisms explaining tissue regeneration and the reasons for poor healing of a wound are still poorly understood. Wound exudates are thus being largely explored to elucidate the underlying mechanisms of wound healing for improving the therapeutic efficacy of drugs especially for chronic wounds. Biochemical processes that govern tissue regeneration can be probed to better understand the healing process to allow for improved wound care management. Until recently, while a lot of diagnostic techniques were available for bedside assessment not many real-time wound assessing techniques existed. Most of the traditional techniques relied on visual inspection, subjective assessment, or optical measurements of the wound size and depth, with none of the techniques offering continuous wound measurement modalities.[91,92] Considerable progress has been made now for developing smart bandages that can proactively monitor biomarkers in the wound milieu such as pH,[93–96] temperature,[97,98] uric acid, xanthine[99–102], and bacterial metabolites to track wound healing in real-time. Wound exudate pH has been studied predominantly owing to its direct correlation with the different wound healing stages (Figure 1.6).[103–105] Moreover, the differences in pH variances among acute and chronic wounds allow for differential diagnosis of such wounds.[106] However, pH in a wound milieu is subject to change due to a multitude of reasons. For instance, a bacterial infestation in the wound may tend to acidify the wound environment. Furthermore, the pH may also change as a function of an underlying disease, diet and medication of a person. Likewise, elevated wound bed temperature has been known to suggest the manifestation of bacterial biofilms within the wound.

Periwound temperature mapping has been identified as an easy way to determine the wound areas requiring debridement to accelerate the healing process. However, body temperatures vary from person to person making temperature not a very accurate measure of wound healing. Smart bandages incorporating a multimodal sensing approach are thus required to accurately assess the underlying cause of pH or temperature changes.

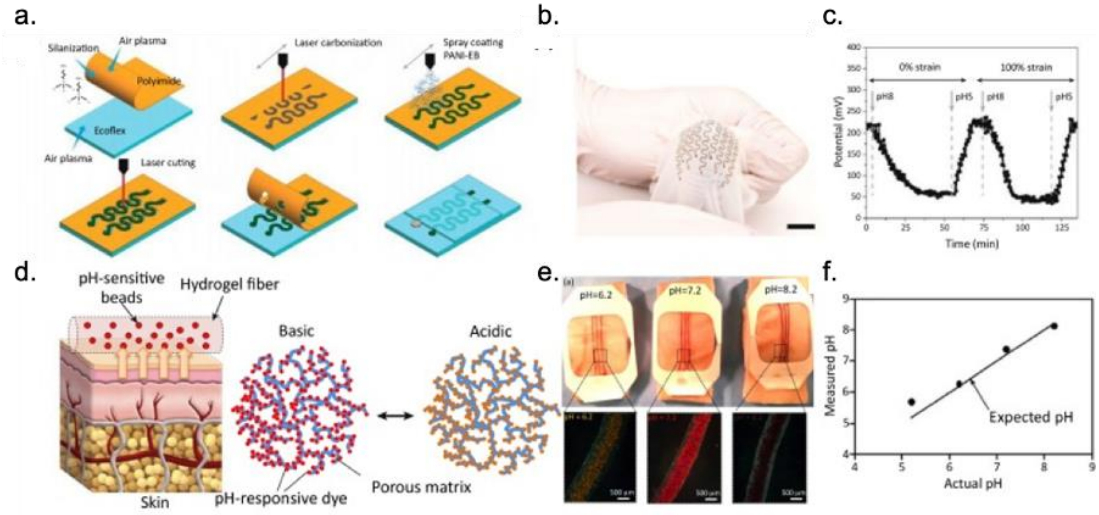

Figure 1.6. Wearable smart bandages for wound bed pH monitoring. a. Schematic illustration of the fabrication steps of a highly stretchable potentiometric sensor for pH measurement b. Photograph of a bandage with integrated flexible pH sensors c. Real-time monitoring of pH and the sensor response under mechanical stress[107] d. Colorimetric pH sensor-based hydrogel loaded with a pH-sensitive dye for long-term monitoring e. Images showing the changes in the color of the dressings when sprayed with different pH solutions and f. Correlation plot depicting the data collected from the images using a smartphone in comparison to a gold standard method[108]. Reproduced with permission.[109] Copyright 2018, Elsevier Inc.

Apart from multimodal approaches, integrated bandages are being designed that combine a controlled drug release mechanism in conjunction with a sensing element to determine when to deliver drugs to combat bacterial infections in wounds (Figure 1.7).[110–112] However, these drug delivery modules are passive in nature, releasing a pre-determined drug dosage. Systems with active spatial and temporal control over the drug release based on the real-time wound status can allow for improved wound treatment. Given the great variations in wound exudates depending on the patient's medical

history, diet, and medication, ambiguity is an ever-present hazard that can be minimized through self-referencing and longitudinal measurements. This provides an opportunity for designing smarter bandages that can tap into an individual's wound exudates to determine proper treatments at a personalized level.

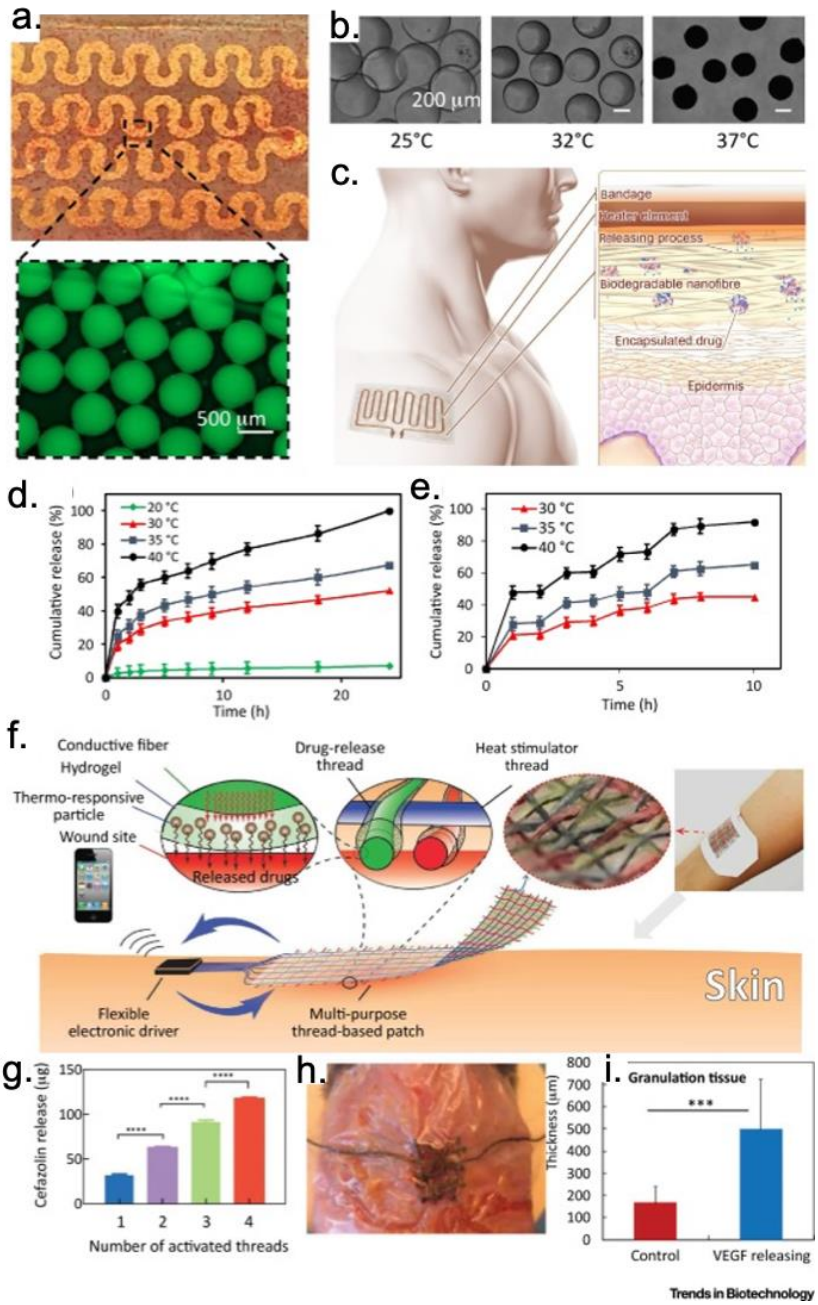

Figure 1.7. Recently developed wearable smart bandages enabled with integrated drug release mechanisms. a. Photograph and micrograph of thermo-sensitive drug carriers encapsulated in an alginate layer cast on a flexible heater b. Response of the thermo-sensitive drugs to varying temperatures[113] c. Schematic showing the operational principle of the engineered platform d. Release profile of cefazolin from the

nanofibrous mesh at four different temperatures e. Effect of temperature on the release rate of ceftriaxone encapsulated within the nanofibrous mesh upon cyclic heating[110] f. Illustration of a thread-based patch enabling active control over the release of different drugs g. Effect of the number of activated fibers on cefazolin release from a textile patch h. Image of the patch on the wound model and i. A typical fabricated bandage used for releasing vascular endothelial growth factor into wounds in diabetic mice[114]. Reproduced with permission.[109] Copyright 2018, Elsevier Inc.

1.3 Challenges of Existing Wearable Systems

Despite all the recent progress made toward realizing wearable enzymatic electrochemical sensors, these sensors still suffer from several unmet challenges that require to be addressed for their successful commercial realization. Among the several challenges that exist related to sensing, resilient materials, data acquisition, and security, a major challenge has been the *in vivo* validation of these sensors.[66] Owing to the great variations in the biofluid composition from one person to another, there is always an ambiguity in the environment that the sensor is placed in. Current wearable electrochemical sensors do not take into account the dynamic environment that is offered by these *in vivo* environments. The conventional electrochemical sensor calibration establishes a mathematical relation between the steady-state environment and the corresponding sensor response. However, in a complex *in vivo* environment, the environment doesn't necessarily assume a steady-state. With a change in the rate of physiological processes the realized biofluid environment varies,[115] subsequently impacting the sensor output. Hence, the ability to model and actively correct for the sensor response with respect to the variations in the environment is required to develop a robust and accurate sensing system.

Enzymatic electrochemical sensing approaches offer significant advantages for longitudinal measurements but suffer from stability issues owing to the loss of enzyme activity due to temporal changes in pH and temperature.[116] Enzymatic activity is primarily dependent on pH and temperature, where the enzyme activity is highly

compromised at high temperatures and deviation from the optimal pH leading to conformational changes in the protein, altering its activity significantly. Alterations in these parameters affect the enzyme activity leading to a sensor drift which further results in erroneous sensor response. For example, the pH of a biofluid like sweat or saliva is highly dependent on factors such as exercise or diet.[117–119] A change in the environmental pH changes the sensor functionality and needs to accounted for. Likewise, the differences in the human physiological response to ambient temperature can result in a different body temperature of a person, with the temperature also being variable for the different body parts e.g. forearm, foot etc.[120] Thus, the wearable systems require an integrated sensing system to measure these parameters in conjunction with the analyte sensor to provide accurate sensor readings. In a recent study, a glucose-sensing patch/strip was developed with an integrated pH sensor for auto-calibration of the glucose sensors.[62] The researchers showed the difference in sensor response before and after correction, demonstrating the importance of simultaneous measurement of these parameters (Figure 1.8).

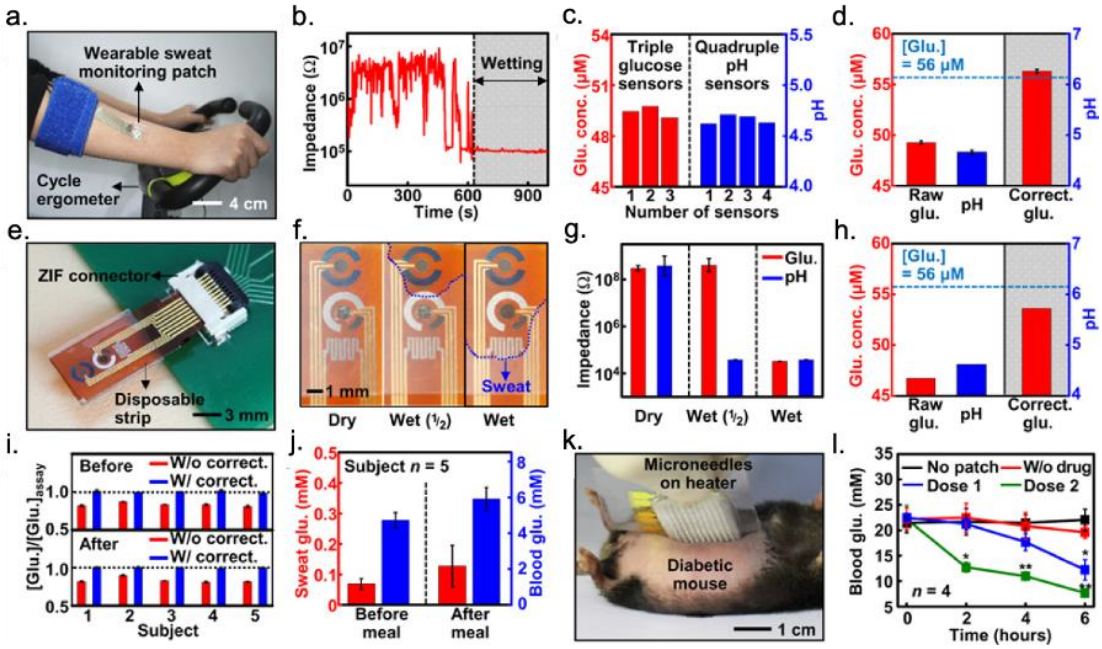

Figure 1.8. Sweat-based glucose monitoring with real-time sensor correction. a. Optical camera image of the subject on a cycle ergometer wearing the wearable patch b. Real-time humidity monitoring to check the sweat accumulation c. Multimodal glucose and pH sensing to improve detection accuracy d. Measured sweat glucose concentrations, pH levels, and corrected sweat glucose level based on the averaged pH (dotted line, glucose concentration measured by a commercial glucose assay) e. Optical image of the disposable strip-type sensors f. Optical images of the sweat uptake via the fluidic channel of the strip g. Humidity monitoring using impedance measurements h. Sweat glucose and pH monitoring using the disposable strip i. Comparison of sweat glucose concentrations measured by the patch and a commercial glucose assay with and without the pH-based correction j. Comparison of the sweat and blood glucose concentrations before and after a meal k. Optical image of the transdermal drug delivery device on a mouse l. Blood glucose levels of the mice for the treated groups (microneedles with the drugs) and control groups (without the patch, microneedle without the drugs). Reproduced with permission.[62] Copyright 2017, American Association for the Advancement of Science.

Over a transient measurement, evaporation of the biofluid is likely to happen depending on the ambient environmental conditions.[121] Sample evaporation has emerged as a potential issue in wearable sensing systems, especially where the sample volumes are low. In case of any biofluid like sweat or tear, the sweat or tear volume and analyte concentration are transient and greatly depend on the environmental conditions. Intuitively, as a result of this evaporation, the analyte concentration in the biofluid will change and can be a significant source of error. The estimation of transient

concentration in the fluid thus becomes highly dependent on the evaporation rate.[122] The evaporation rate is not only governed by the ambient conditions (temperature and humidity) but also by the substrate properties of the sensor[123–125] (ability to retain the sample). A level of complexity is further introduced by the interrelationship between all the above-mentioned parameters. Correlation studies are thus imperative to characterize the dependence of these individual parameters on each other and the sensor response. Very few studies have been carried out to address the effect of evaporation on analyte concentrations. One such preliminary study revealed that the sensor output depends linearly on the evaporation rate assuming steady-state conditions.[126] A similar study modeled the interaction of the fluid with the substrate as a function of the evaporation rate and environmental conditions.[122] A classical convection-diffusion equation was used to develop a correlation between the evaporation rate and salt concentration. Based on the developed model, optimal flow rate conditions were identified for accurate sensing at high time resolution. The evaporation rate not only affects the analyte concentrations but also the sample transport mechanism. With ultra-low sample volumes of the biofluid present (e.g. sweat, tear), transport of sufficient amounts of sample is an issue with evaporation playing a major role. Theoretical models are required to understand the correlation of sample transport on wearable porous substrates while considering the evaporation effect. In a study, the authors report that the rate of evaporation is strongly dependent on the overall geometry of the system. They established a theoretical model to predict the evaporation rate from the substrate and showed that the evaporation rate can be adjusted by modification of the substrate geometry. While certain preliminary studies have been carried out to elucidate these relations in point-of-care devices, novel sensors system architectures need to be developed to address them for wearable sensors where these parameters change in real-

time. Sweat rate is another parameter that varies, even within an individual, and is dependent upon factors like hydration level, heat stress, and physical exercise.[127,128] As mentioned earlier in the chapter, it has been shown that the concentration of certain analytes in the sweat is dependent on the sweat rate.[129] Thus, measurement of sweat rate along with the metabolite measurement is vital to accurately quantify the metabolite levels. Furthermore, enzymes act as catalysts consuming target analytes and are thus sensitive to analyte flux. Any changes in the flow rate of the biofluid will then be accompanied by a change in the sensor output. This necessitates the development of microfluidics integrated sensor systems to measure the sweat rate in tandem with the chemical sensor to account for changes in the fluid flow rate.

Besides the above-described parameters, electrochemical sensing in complex biological matrices is further challenged by sensor fouling resulting from adsorption of extracellular proteins, cellular debris, accumulation of salt residues etc.[130–132] The adherence of these materials to the active area of the electrode impedes the diffusion of the target analyte to the electrode surface, leading to a change in the sensor response. It has been shown that macromolecules adsorb onto the electrode surface inhibiting the electrocatalytic process resulting in a decreased sensor response. Several electrochemical sensors utilize a polymeric gel layer over the active surface area to improve the sensor stability.[133–136] However, a study showed that prolonged exposure of the sensor to human serum resulted in the fouling of the polymeric hydrogel, thus decreasing the glucose diffusivity to the electrode.[137] Therefore, proper selection of the polymeric material and the properties of the designed gel is vital to minimize the deleterious effects of biofouling on the sensor response.

The state-of-the-art wearable enzymatic sensors currently cannot quantify the changes in these parameters in real-time in an *in vivo* setting. Simply, improvements on

the sensing system designs by developing fundamental frameworks to understand the effect of these parameters can contribute to providing reliable and actionable data to aid clinical decision making. More robust and stable systems are required to ensure the translation of these sensors to *in vivo* settings and enable their long-term use.

1.4 Wearable Wound Monitoring: A Use Case

Complications associated with wound care lead to the development of chronic wounds, which with inefficient wound care management lead to increased risk of infections and traumatic amputations.[138] Chronic wounds are a major global healthcare challenge and their real-time monitoring is vital to enable efficient wound care management. Present wound care techniques are limited to analysis of subjective measures such as wound width and depth.[91,92] These approaches cannot be integrated onto a wearable construct and do not offer continuous monitoring modalities. Thus, efforts have been directed towards the development of electrochemical sensors for monitoring wound healing. Smart bandages that employ enzymatic detection mechanisms for detection of purine metabolites and other relevant biomarkers have been reported.[99,102] However, none of the bandages have been validated in an *in vivo* setting to the best of our knowledge.

A chronic wound milieu is a classic example of a dynamic environment owing to its persistent inflamed state for long periods. These wounds are highly heterogenous with the biomolecular signatures of the wound environment changing significantly with time and the different healing stages. The pH of a wound is one such factor that varies according to the wound status. It is well known that as a wound heals, the pH of the wound milieu shifts from alkaline to acidic. Further, as a result of bacterial infestation in a wound the pH of the exudate results in extremely low values.[104] Similarly, temporal changes in the wound temperature are observed as a consequence of several factors like infection, inflammation, and change in the local blood flow rate.[139] These dynamic

changes in the pH and temperature can considerably compromise the enzyme activity subsequently affecting the sensor response. During the inflammatory and proliferative stages of wound healing, a majority of exudate is produced, with the production rate being largely dependent on the characteristics of the wound. The local flux in the wound environment can thus dynamically change as a function of the changing wound conditions. The resulting erratic diffusivity pattern of the target analyte present in the wound exudate due to the flux changes can again substantially affect the sensor response.

A major challenge of low sample volume is further posed by the dry and low exuding wounds. While sensing in low sample volumes is challenging due to insufficient sensor wetting, such low volumes also tend to rapidly evaporate adding to the sensing complexity. Additionally, the substrate properties of the wound dressings play a major role in sample transport. The mass transport dynamics of the analyte to the sensor surface are governed by the wicking properties of the dressing thus governing the sensor response. To add to the complexity, electrochemical sensing in a complex biofluid matrix, like wound exudate, is accompanied by sensor fouling resulting from the formation of biofilms and adsorption of extracellular proteins (ECM) over the sensor surface. The adsorption of these materials not only impedes the diffusion of analyte but can also affect the enzymatic activity significantly. Therefore, there is a need to design smart wound monitoring systems that track these dynamic changes temporally allowing for on-chip calibration of sensing systems to enable the development of wearable wound diagnostic systems. Future research should be focused on understanding and modeling the intrinsic effects of the physiological wound environment to improve sensor accuracy.

1.5 Motivation and Layout of the Dissertation

The dynamic variability existing in biofluids in any wearable construct can result in a confounded sensor response. As discussed earlier, potential factors such as sample volume, evaporation rate, and sample flow rate of a sensor environment can affect the electrochemical measurements and must be accounted for in the sensor design. Yet, rarely does a consideration of the interplay of these dynamic factors motivate the design of a sensor. Despite the extensive efforts dedicated to the development of wearable sensors, a fundamental gap exists in understanding the effect of other existing *in vivo* dynamic parameters in a sensor environment and their interdependence on each other. Fundamental frameworks are required to establish these correlations and their effect on the sensor response for development of robust sensor designs. Moreover, for real-time measurement of parameters like sample volume and evaporation rate, incorporation of conductivity or impedance-based measurements within the sensor design may offer an advantage for quantitative measurements for sensor calibration.

This dissertation aims to study how the dynamic sensor environment affects the sensor response and develop fundamental frameworks to understand the correlations between them. The main focus is to develop analytical models to establish actionable correlations for accurate quantification of target analytes in dynamic *in vivo* environments. The central goal of the research is to develop mathematical frameworks describing the dynamic sensor environment and sensor response, which correlate with experimentally measured behavior with wound monitoring as a use case. The correlations between the different competing parameters will be investigated to predict how the sensor response scales as the environment changes.

Chapter 1 serves as an introduction to wearable sensing systems with a particular focus on enzymatic electrochemical sensing systems. The chapter discusses

the existing sensors that have been developed for quantification of analytes in several biofluids like sweat, tears, wound exudates, and saliva. The existing issues in translational of electrochemical sensors from traditional rigid substrates to flexible and conformal substrates have been explored. Next, the challenge of a variable sensor environment offered by the dynamic variability in biofluids parameters and their effect on the sensor response has been discussed. Wound bed has been taken as a use case to elucidate the different dynamic parameters offered by the biofluid (wound exudate) as a function of wound healing. Subsequently, the capabilities and limitations of the existing sensor systems have been discussed thereby explaining the motivation and rationale of this dissertation. **Chapter 2** elucidates the wound biochemistry and presents an electrochemical approach towards long-term wound monitoring. The work establishes a mediator-free enzymatic detection mechanism for uric acid, as a biomarker for wound healing. A thorough physical and chemical characterization of the proposed electrochemical sensor is presented in the chapter. The proposed mechanism is characterized using a rigid sensor platform under ideal steady-state environments to understand the fundamental reaction kinetics. **Chapter 3** presents a novel method for the fabrication of flexible textile-based electrochemical sensors for wearable applications with wound monitoring as the use case. The fabrication strategy presented allows sensor integration onto any kind of textile by taking advantage of an industrial scale process, screen-printing. Further, the high mechanical durability and electrochemical sensing performance of the fabricated sensors under tensile and flexural stresses have been established in this chapter. **Chapter 4** demonstrates the application of the fabricated flexible sensors presented in Chapter 3 for electrochemical detection of uric acid. An electrochemical sensing platform has been presented consisting of an array of uric acid sensors for spatial mapping of uric acid in the wound.

The physical and electrochemical characterization of the above flexible sensors and their relevance for wound monitoring application has been detailed in the chapter. The chapter further presents the design and characterization of a wearable system-on-chip to be integrated with the flexible sensors for real-time on-body data collection and wireless data transmission. **Chapter 5** discusses the effect of various dynamic environmental parameters on the sensor response. The effect of parameters like pH, temperature, sample volume, and evaporation on sensor response has been discussed. Correlation models between the dynamic parameters and the sensor response have been presented for real-time response correction. **Chapter 6** investigates the biocompatibility of the developed sensor system and the sensor constituents. *In-vitro* toxicity studies have been presented to elucidate the toxicity mechanisms if any, offered by the sensor and the involved sensor materials. The cytotoxicity was assessed at both an intercellular and intracellular level. **Chapter 7** presents the human *in vitro* and *in vivo* clinical validation studies carried out on chronic venous leg ulcer patients using the developed wearable wound monitoring system discussed in the previous chapters. The entire clinical trial protocol has been detailed for both *in vitro* and *in vivo* studies. Correlations derived between the wound chronicity, wound size, and the measured uric acid have been discussed. The sensor accuracy of the electrochemical sensor is further established through validation using standard optical measurements. Confounding of sensor response as a result of biofouling has been further presented in the chapter. Preliminary studies presenting an approach towards real-time monitoring of bacterial infection have also been discussed. The work also presents a new near-wound sensing mechanism to allow for unobtrusive long-term wound monitoring. **Chapter 8** provides a synopsis of the work carried out in this dissertation and discusses the defining problems that remain a challenge for the deployment of wearable sensors in real-time

scenarios. The chapter also provides an outlook towards a future roadmap for creating next generation integrated wearable devices.

2 Uric Acid Detection on Rigid Sensors in a Steady-State Environment

2.1 Introduction

Chronic wounds pose an ever-increasing threat to a large fraction of the population and significantly burden the healthcare economy with annual costs exceeding $25 billion in the US.[140] Wounds and burns represent more than 15% of all skin disease-related deaths, with a reported prevalence of 4.64% in the U.S. population and an estimated cost of $6 billion annually.[141] As the population ages and sedentary lifestyle becomes common, this burden is likely to grow, with wound care centers needing advanced tools for rapid diagnostics and care. Hence, there is an urgent need to develop tools for wound monitoring and healing prediction. Present wound monitoring techniques are largely reliant on visual inspection of the wound and objective measures that can only be performed by specific wound experts. While imaging techniques enable measurement of wound width and depth,[142,143] they are expensive and do not offer continuous measurement modalities. In addition, amidst the repeated visits to the clinic, a delay in medical attention may lead to further deterioration of the wound condition. Therefore, the development of wound care technologies for continuous monitoring of wound healing is imperative to facilitate timely therapeutic interventions for improved patient care.

Efforts have been made recently to develop wound monitoring sensors that enable continuous monitoring of various physical and chemical parameters of the wound environment. Such parameters include pH and pressure,[144–147] bacterial metabolites[148,149] and metabolites from the purine degradation pathway.[150–153] The estimation of these parameters would provide real-time insight into the wound status. Placing or positioning these sensors directly over the wound bed may lead to sensor

fouling and limit their lifetime, due to adsorption and occlusion of the active surface by the wound debris. For example, the dead parenchymal cells and fibrinogen present in the wound fluid can accumulate over the active surface area limiting the interaction between the biomarker and the catalyst. This will result in lower sensitivity, degraded detection limit, and a lifetime of the sensor. Furthermore, the materials utilized in the sensor interface directly with the open wound and may pose biocompatibility issues restricting the practical applicability of the sensor.

Uric acid (UA), a product of the purine metabolic cycle, is considered to be an endogenous biomarker for wound healing assessment. As a consequence of cell rupture at the wound site, adenosine triphosphate is released into the extracellular matrix. It further breaks down into several metabolites, where the final reaction in the pathway is the conversion of xanthine to UA.[154] The UA levels at the wound site are known to decrease as the wound heals, and hence serves as an accurate diagnostic indicator for wound healing.[155]

In this chapter, a bi-enzymatic electrochemical sensor for monitoring UA levels in human wound fluids is presented. This biosensor utilizes uricase (UOx) for UA oxidation and horseradish peroxidase (HRP) for shuttling electrons between the electrode surface and UOx. A nanocomposite of MWCNTs and AuNPs has been investigated for improving the sensor response. In order to establish the feasibility of the sensor to measure UA levels and understand the reaction kinetics of the sensor, the sensor functionality in a steady-state environment using a rigid sensor has been explored. The proposed electrochemical sensing approach utilizing uric acid as a potential biomarker for continuous monitoring of wound healing may enable to advance the existing wound care management technologies.

2.2 Experimental

2.2.1 Materials

AuNPs (20 nm diameter) and MWCNTs (9.5 nm × 1.5 μm, CAS No. 308068-56-6) were purchased from Sigma Aldrich, USA. Analytical grade horseradish peroxidase (HRP, CAS No. 9003-99-0, 0.2 U ml^{-1}) was purchased from ThermoFisher Scientific. Lyophilized UOx powder (CAS Number 9002-12-4) containing 15∼30 U mg^{-1} was purchased from Sigma Aldrich. UA, sodium hydroxide (CAS No. 1310-73-2), 30% hydrogen peroxide (CAS No. 7722-84-1), sulfuric acid (95.0-98.0% H_2SO_4, CAS No.7664-93-9), dimethylformamide (99.9% DMF, CAS No. 68-12-2), sodium phosphate monobasic (NaH_2PO_4, CAS No. 10049-21-5) and sodium phosphate dibasic (Na_2HPO_4, CAS No. 7558-7-4) were used of analytical grade. All aqueous solutions were prepared in phosphate buffered saline (0.02 M, pH 7.8), prepared using NaH_2PO_4 and Na_2HPO_4 salts.

2.2.2 Methods and apparatus

Screen-printed carbon electrodes (SPCE) purchased from CH Instruments, Inc., United States, were used to prepare the sensors. The working electrode was functionalized with MWCNT solution prepared in DMF and dried at 60^{o}C. Subsequently, AuNP solution was drop-casted and dried at 60^{o}C. Enzymes, HRP and UOx, were then immobilized over the electrode by drop-casting, nitrogen drying, and subsequent washing in PBS. All steps involving enzyme immobilization were carried out in an icebox to prevent enzyme denaturation. Scanning electron microscopy (SEM JEOL 6330) and transmission electron microscopy (TEM Philips CM200) was carried out to examine the surface morphology of the nanocomposite electrodes. Electrochemical impedance spectroscopy (EIS) was performed using an Autolab impedance analyzer to study the nanocomposite-enzyme effect on the sensor property. All the readings were taken in a

frequency range of 1 mHz to 100 kHz at a potential of 5 mV in a ferri/ferrocyanide buffer. Various functionalized electrodes were studied to observe the influence of nanomaterials and enzymes on the electron transfer resistance.

Cyclic voltammetry (CV) studies were performed using the analytical system model CHI-230B potentiostat (CH Instruments, Inc.). A conventional three-electrode cell assembly consisting of SPCE, Ag/AgCl as a reference electrode, and a Pt wire as a counter electrode was used for the experiments. CV was performed to assess the performance of the nanocomposite-enzyme functionalized electrode in varying concentrations of UA. The measurements were performed at a scan rate of 0.02 V s^{-1} in a potential window of 0.2 V and -0.6 V. Control studies were carried out in the absence and presence of different nanomaterials (Au and MWCNT) with the working electrode being either bare, or nanomaterial and enzyme functionalized SPCE. A Multiskan™ FC microplate reader (ThermoFisher Sc., USA) was used for absorbance measurements.

Sensor stability was characterized under room temperature, physiological conditions (37^{o}C) and elevated temperature (40^{o}C) over 7 days. The sensor response was recorded every 8 h, and the electrode was left immersed in the UA solution in between the sequential readings.

2.3 Results and discussion

2.3.1 Active surface area characterization of the biosensor

The surface morphology and the electron transfer resistance of the active surface were characterized using SEM, TEM, and EIS respectively. A uniformly distributed structure was observed for the MWCNTs modified electrodes, with MWCNTs having an average diameter of 10 nm (Figure 2.1a). The darker area on the edges seen in the representative TEM image shown in Figure 2.2a showed the multi-walled structure of the carbon

nanotubes. This homogeneous topography as observed from the images offers accelerated electron transfer.

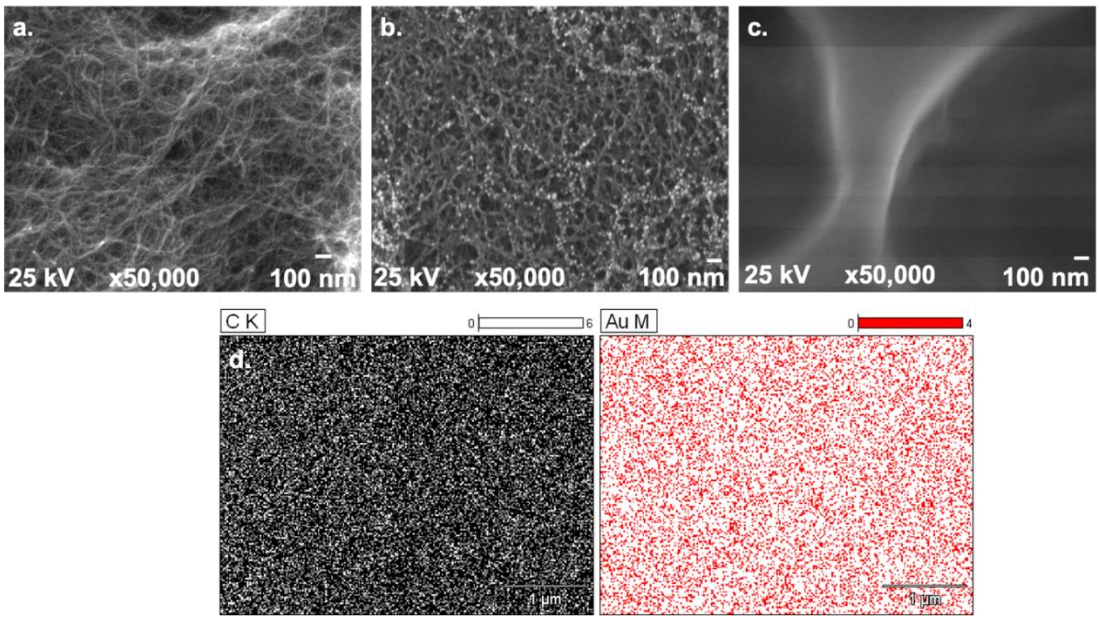

Figure 2.1. SEM images of electrodes modified with a. MWCNTs b. MWCNT/Au and c. MWCNT/Au/HRP/UOx. The MWCNT scaffold allowed for uniform distribution of AuNPs on the electrode surface. The enzyme blanket over the nanocomposite structure enabled efficient electron transfer between the enzymatic active site and the electrode. d. Elemental mapping of AuNPs on MWCNT surface showing the even distribution of nanoparticles over the MWCNT network.

Compared to the bare electrode, an increase in the R_{ct} (semicircle area) for the MWCNT electrode was observed from the Nyquist plot (Figure 2.3a). This decrease in electron transfer resistance from 7.35 kΩ to 2.34 kΩ can be attributed to the conductive properties offered by the MWCNT matrix. Subsequently, AuNPs were deposited over the MWCNTs functionalized electrodes, resulting in a smoother and more uniform surface as seen in Figure 2.1b. The AuNPs can be seen as bright spots and were spatially distributed across the MWCNT framework. A low agglomeration level was observed for the NPs, with a size distribution of 21.54 ± 1.7 nm.

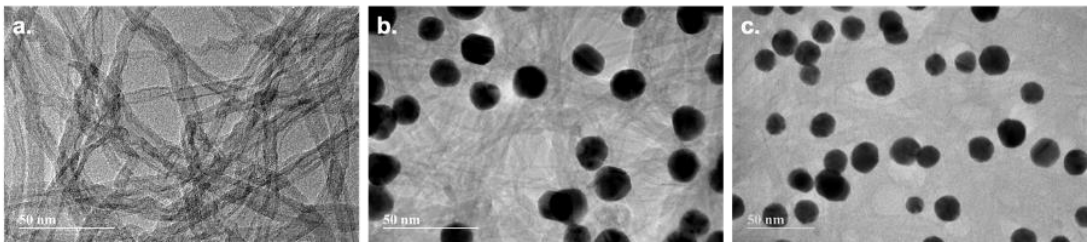

Figure 2.2. TEM images of electrodes modified with a. MWCNTs b. MWCNT/Au and c. MWCNT/Au/HRP/UOx. The images show the synergistic interaction between the walls of carbon nanotubes and AuNPs facilitating electron transfer over the electrode surface. The immobilization of the enzyme on the electrode was confirmed when the MWCNT matrix became indistinct as a result of enzyme deposition.

The elemental mapping of the composite surface further confirmed the uniform distribution of MWCNTs and AuNPs over the electrode surface (Figure 2.1d). The white pixels for MWCNT mapping represent their spatial distribution on the electrode surface, while the distributed red pixels for the AuNPs show their assembly on the MWCNT matrix. The TEM image revealed a physical interaction between the AuNPs and the MWCNT walls which may enable accelerated electron transfer between the two nanomaterials (Figure 2.2b). The resulting synergism due to the interactions between the MWCNTs and AuNPs augmented their electron transfer properties; as reflected by the decrease in R_{ct} to 764.21 Ω after AuNPs deposition. The decrease in the charge resistance suggested improved transfer kinetics offered by the nanocomposite.[156]

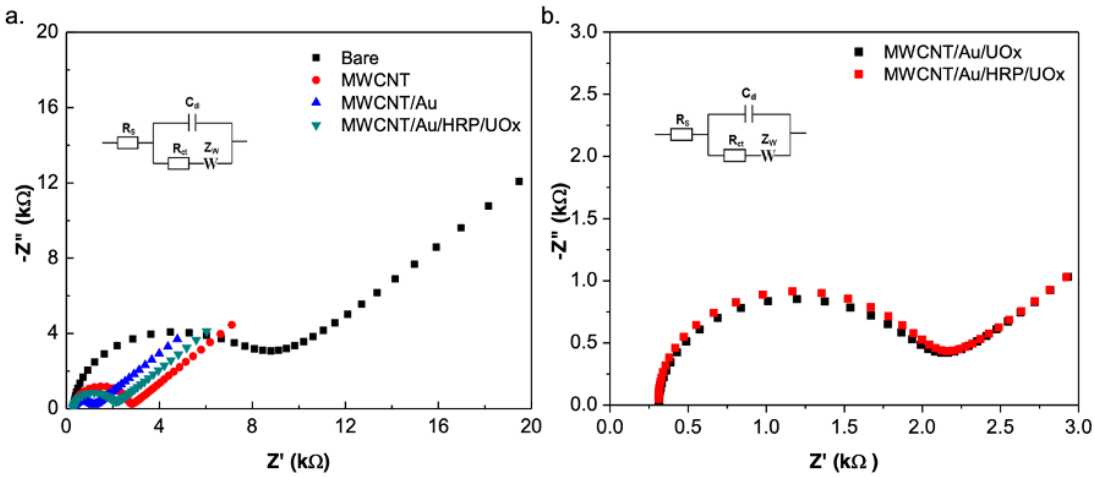

Figure 2.3. Nyquist plots of nanomaterial(s)-modified electrodes from 1 mHz to 100 kHz at a potential of 5 mV in ferri/ferrocyanide buffer. a. Plots of a bare electrode and electrodes modified with MWCNT, MWCNT/Au and MWCNT/Au/HRP/UOx. A decrease in the electron transfer resistance after MWCNT/Au immobilization showed the improved electron transfer characteristics offered by the nanomaterials. b. Plots of a MWCNT/Au/UOx electrode in presence and absence of HRP. An increase in the charge transfer resistance confirmed the successful immobilization of the enzymes. Randles equivalent circuit (inset) was used to fit the experimental data, where R_s is the solution resistance, R_{ct} is the charge transfer resistance, C_{dl} is the double layer capacitance and Z_w is the Warburg impedance.

Such a network of nanostructures allows for robust immobilization, improved stability, and reduced leaching of the enzyme.[157,158] It was observed that no nanoparticles were visible after enzyme deposition, confirming the deposition of an enzyme blanket over the nanocomposite matrix (Figure 2.1c). The high-resolution TEM images showed the AuNPs, however, the MWCNT matrix was indistinct as a result of the deposited enzyme layer (Figure 2.2c). This was further established by the increase in the charge transfer resistance from 764.21 Ω to 1.06 kΩ, due to the enzyme blanket over the nanomaterials. The EIS plot also shows an increased R_{ct} after HRP immobilization (from 1.06 kΩ to 1.66 kΩ) compared to the only UOx immobilized electrode (Figure 2.3b). Immobilization of HRP over the UOx enzyme resulted in inhibition of ions reaching the nanocomposite substrate, hence limiting the charge transfer process.[159]

2.3.2 Biosensor response to uric acid

UOx is a peroxisomal enzyme that belongs to the purine degradation pathway. It catalyzes the oxidation of UA to 5-hydroxyisourate, which is followed by the generation of hydrogen peroxide (H_2O_2) (Eq. 1). The formed 5-hydroxyisourate then reacts with water to produce carbon dioxide and allantoin which is a soluble form of urate (Eq. 2).

$$\mathrm{UA} + \mathrm{O_2} + \mathrm{H_2O} \rightarrow 5-\mathrm{hydroxyisourate} + \mathrm{H_2O_2} \quad (1)$$

$$5-\mathrm{hydroxyisourate} + H_2O \rightarrow \mathrm{allantoin} + CO_2 \quad (2)$$

In this work, the UA levels were quantified by measuring the amount of H_2O_2 generated by the UOx from a given sample. CV measurements were carried out at a scan rate of 0.02 V s^{-1} to monitor the production of H_2O_2 on the electrode. The H_2O_2 produced as a result of UOx reduction binds to the heme (Fe(III)) group present in HRP. This leads to the heterolytic cleavage of the oxygen-oxygen bond of H_2O_2.[160] The process resulted in the formation of a water (H_2O) molecule and oxidation of the heme group to form an intermediate product. The electron transfer from the electrode was further accelerated by the presence of MWCNT/AuNPs nanocomposite (Figure 2.4). The use of AuNPs supported on carbon fibers has been reported earlier to enhance the electrochemical response of biofuel cells.[161–163] Recently, bi-enzymatic sensors have been widely used to develop biosensors owing to their improved performance characteristics.[164,165] An oxidase/peroxidase cascade leads to the reaction process occurring at a lower potential, in turn improving the selectivity of the sensor.[166]

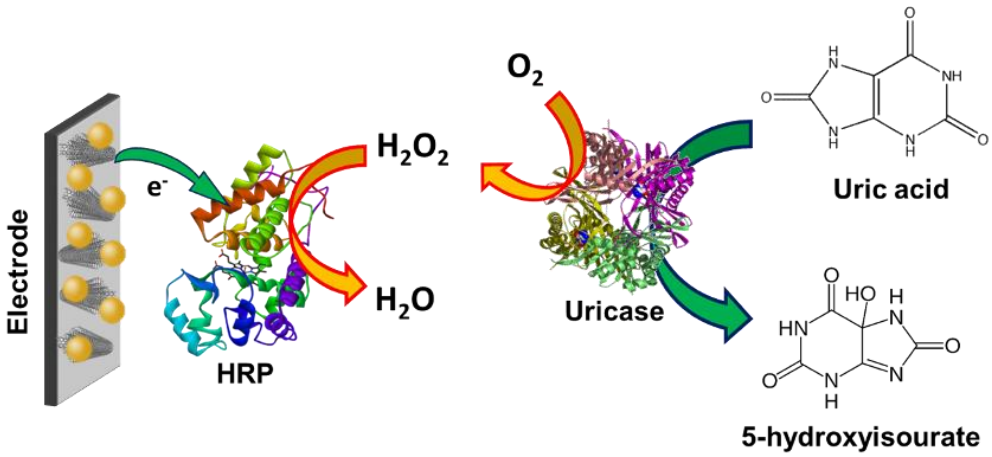

Figure 2.4. Schematic representation of uric acid oxidation by UOx and hydrogen peroxide reduction via HRP on a MWCNT/Au functionalized electrode. The illustrated reaction was used in the sensor to quantify the UA levels in a given sample.

An Ip_c of 7.8 µA was observed for the nanocomposite modified electrode in presence of HRP compared to an Ip_c of 3.86 µA without HRP, while the Ep_c of the reaction was maintained at a potential of -0.4 V (Figure 2.5a). The double-fold increase in the current response implied an accelerated electron transfer offered by the bi-enzyme system. The higher rate of increase in the cathodic current and a 0.2 V decrease in the onset potential of the bi-enzyme system further confirmed the high electron mobility offered by the electrode in the presence of HRP. The electrostatic interactions in a coupled HRP-UOx system, lead to a decrease in the distance to be traversed by the produced hydrogen peroxide to the active site of HRP, which in turn results in an improved sensor response.

The electrodes modified with the individual nanomaterials, MWCNT, or AuNPs, presented a 1.2 and 1.5 fold higher current intensities with respect to the bare electrode (Figure 2.5a). The enhanced effect of AuNPs in comparison to the MWCNTs can be attributed to the redox effect presented by gold. Owing to the redox reaction happening on the surface of these nanoparticles, gold undergoes transitions in the oxidation state facilitating the reduction of hydrogen peroxide.[167] The presence of the nanocomposite accelerates the electron transfer rate from the electrode, resulting in the

increased current response. The nanocomposite modified electrode exhibited an Ip_c of 7.8 µA, which was a ~2.5-fold improvement over the electrodes modified with the individual nanomaterials. The inter-nanomaterial interaction between the MWCNTs and AuNPs provides an efficient conducting interface for the electrons.[168,169] While the edged planes of the MWCNTs offer increased surface interactions owing to their high surface-to-volume ratio, the AuNPs offer enhanced sensitivity through increased conductivity. Moreover, the increased current response can be attributed to the synergistic interaction of the enzyme with the nanocomposite. The UOx enzyme has an isoelectric point of 7.5, and at a physiological pH of 7.8, the overall charge on the enzyme is negative.[170] This negative charge results in electrostatic interactions between UOx and the positively-charged AuNPs (amine-functionalized), leading to greater retention of the enzyme. Concomitantly, MWCNTs provide a nanoscale environment for effective enzyme adsorption.[171] The hydrophobic amino acid residues of the UOx enzyme interact with the hydrophobic sidewalls of the MWCNTs allowing for facile enzyme immobilization.[172]

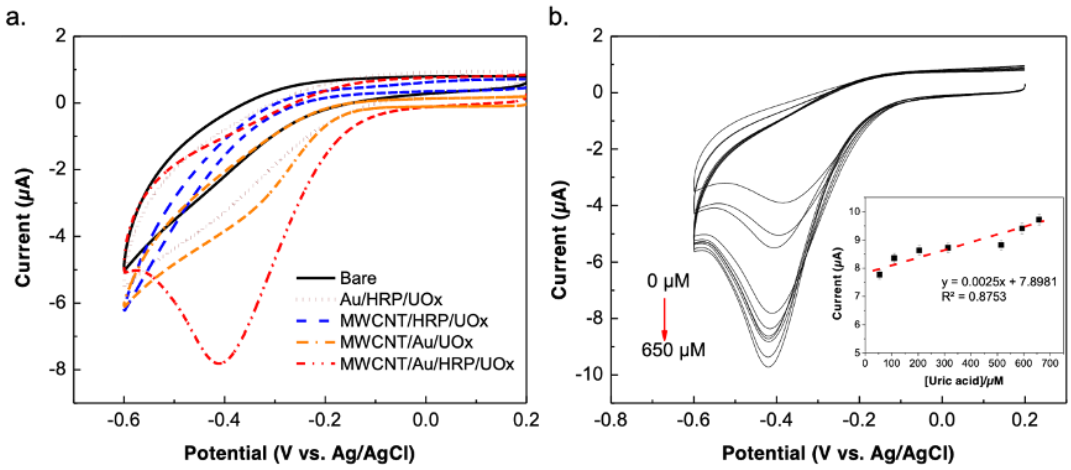

Figure 2.5. a. CV response of 53 µM UA on a bare electrode, UOx electrode modified with Au/HRP, MWCNT/HRP, MWCNT/Au, and MWCNT/Au/HRP. The higher slope and lower overpotential of the MWCNT/Au modified bi-enzyme electrode showed the improved reaction kinetics of the system. b. CV response of the nanocomposite bi-enzyme system as a function of UA concentration. Inset shows the linear plot of Ip_c vs.

UA concentration, with a sensitivity of 2.5 nA μM^{-1}. Each experiment was carried out in triplicate (n = 3), and the data is represented as mean ± SD.

The nanocomposite bi-enzymatic sensor was evaluated with various concentrations of UA through cyclic voltammetry. An increase in the cathodic peak current was discerned as depicted in Figure 2.5b and was correlated with the UA concentration. A linear current response was observed in the range of 50 µM to 650 µM, with a correlation coefficient (R^2) of 0.87 (Figure 2.5b inset). The sensor sensitivity was calculated from the slope of the calibration plot and found to be 2.5 nA μM^{-1}. The sensor responded to a lowest concentration of 9.91 µM suggesting its applicability over the clinically relevant range of UA in wound fluids i.e. 236-823 µM.[173] While the reported sensitivity of the sensor was marginally lower compared to previously reported sensors (Table 2.1), the sensor is capable of detecting UA in the physiological range. Moreover, none of the previous sensors report the sensor stability at physiological conditions which is an important factor for wearable sensing purposes. In any enzymatic sensor, elevated temperatures can result in an unstable sensor response due to enzyme denaturation. This restricts the usage of these sensors under physiological conditions over a long period of time.

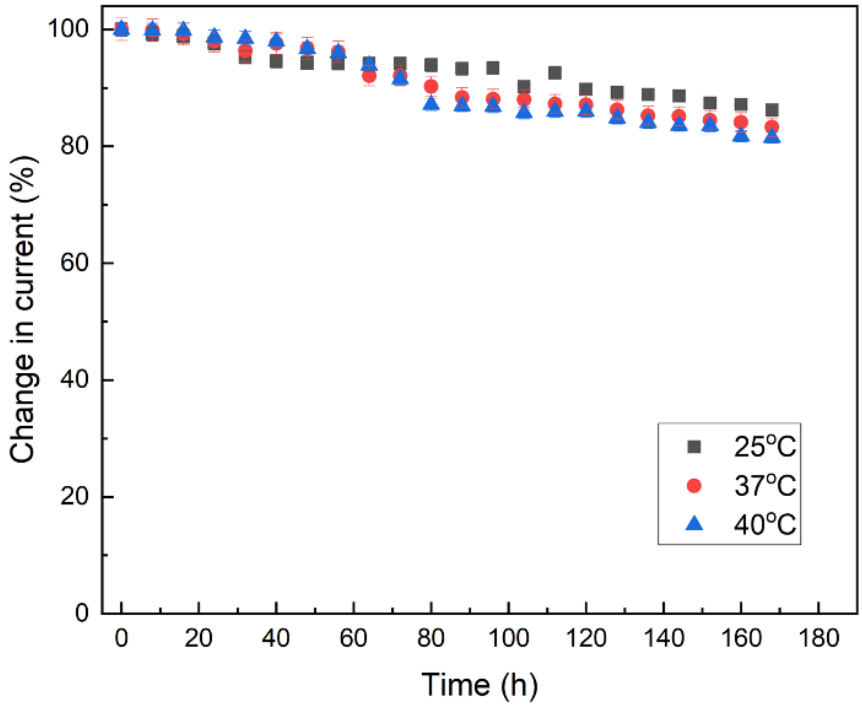

Figure 2.6. Change in the UA current response of a MWCNT/Au/HRP/UOx sensor under room temperature, physiological conditions (37°C) and an elevated temperature (40°C) over a period of 7 days. The electrodes showed a stable response for up to 2 days, after which the sensor response degraded. The sensors showed the highest degradation rate when kept at an elevated temperature of 40°C. Each experiment was carried out in triplicate (n = 3), and the data is represented as mean ± SD.

The long-term stability study of the developed sensor was carried out over a period of 7 days under physiologically relevant conditions at a UA concentration of 250 µM. The time frame for the study was chosen since the dressings for chronic wound patients is typically changed once per week. A 13% decrease in the current response was observed for the sensor at room temperature, and the sensor also exhibited a stable response at a physiological temperature of 37°C with just a 16% decrease in the current (Figure 2.6). However, at an elevated temperature of 40°C, the sensor response was seen to degrade by 18%. The stable response offered by the sensor under physiological conditions for a long period demonstrates its feasibility for utilization in a wearable construct.

Table 2.1. Comparison of uricase sensors for electrochemical detection of UA.

Sensor	**Linear range**	**Sensitivity**	**Limit of detection**
Graphene oxide-UOx[174]	20-490 μM	-	3.45 μM
Cu_2ZnSnS_4/UOx[159]	0.05-700 μM	0.0018 μA mM^{-1} cm^{-2}	0.066 μM
Nafion/UOx-Zinc oxide nanorods[175]	10-456 μM	239.67 μA $mM^{-1}cm^{-2}$	5 nM
Zinc oxide quantum dots/UOx[176]	1000-10000 μM	4.0 μA mM^{-1} cm^{-2}	22.97 μM
Au-rGO/UOx[177]	50-800 μM	2.89 μA mM^{-1} cm^{-2}	7.32 μM
CNT/Au/HRP/UOx (This work)	50-650 μM	35.71 μA mM^{-1} cm^{-2}	9.91 μM

2.4 Conclusion

A UA based enzymatic electrochemical sensor for continuous wound monitoring has been reported in this chapter. The sensor comprises of a bi-enzymatic system coupled with a nanocomposite of MWCNTs and AuNPs for signal enhancement. While the bi-enzymatic system facilitated an accelerated electron transfer rate, the presence of the nanocomposite matrix allowed for higher enzyme loading. The sensor was capable of sensitively detecting UA under the physiologically relevant range of UA levels found in chronic wounds. The high stability of the sensor exhibited at physiological conditions demonstrated its applicability for sensing in a wearable setting. Although the specificity and selectivity of the sensors remain to be evaluated for practical applicability of the sensor, the proposed approach is a step forward towards long-term wound monitoring.

3 All-Printed Textile-Based Wearable Electrochemical Sensors

3.1 Introduction

Wearable sensors enabling on-body monitoring of health-related parameters have the potential to revolutionize personalized healthcare technology. These sensors have attracted significant attention owing to their ability to non-invasively monitor human health and provide predictive analytics and treatment. Textiles represent an appealing class of substrates for realizing such wearable sensors, especially where sensor durability and wearability are essential requirements. Over the past few years, several such sensors have been developed to monitor physical parameters such as body temperature,[178,179] electrocardiogram (ECG),[180–182] body motion,[183,184], and respiration rate[185,186]. Unlike the notable effort that has been aimed at physiological monitoring, research directed towards the development of textile-based electrochemical sensors has been limited. Chemical sensors can provide real-time information about the biochemical profile of an individual's health yielding an in-depth insight into the overall health status. They offer significant advantages for longitudinal measurements, providing high sensitivity, specificity, and rapid response. Owing to the completely printed embodiments of textile-based electrochemical sensors, these sensors can be easily integrated into garments to provide vital health data for extended periods without compromising user comfort.

The successful realization of textile-based electrochemical sensors requires the translational of these systems from traditional rigid and planar substrates to flexible and conformal substrates. Further, a fundamental requirement is that these sensors maintain their sensing capabilities while accommodating high mechanical deformations, thus

imposing additional fabrication constraints. While the rough topography offered by the textile hinders the fabrication of planar surfaces, the strain-limiting materials lead to a low mechanical durability of the sensors. Recently several fabrication techniques[187–191] have been implemented, however not every textile is compatible with the fabrication process or in compliance with the operational environment. Techniques like inkjet printing and dyeing allow for sensor integration within the knitted structure providing high mechanical durability but require complex processing and are expensive. Thick film patterning techniques such as screen-printing[187,192,193] and stamp transfer[188] have thus been commonly employed to fabricate sensors on a large scale at lower costs. Screen-printing offers several advantages such as ease of printing and easy design customization, however, concerns raise due to its incompatibility with non-planar and highly porous substrates. Sensors printed on porous substrates tend to crack and delaminate from the textile under mechanical deformation, leading to a sensor failure.[194] On the other hand, though the stamp transfer technique allows for printing on rough substrates, it results in low sensitivity sensors due to nonplanar electrode surfaces and exhibits low mechanical durability. The low sensor sensitivity can be attributed to the discontinuous and rough surface offered by the printed sensor resulting in poor electron transfer on the surface. Despite the considerable attempts made towards realizing textile-based electrochemical sensors, fabrication routes to mechanically robust and substrate compliant sensors are still lacking.

This chapter presents a facile approach towards fabrication of flexible textile-based electrochemical sensors for healthcare monitoring. The approach combines screen-printing of flexible conductive inks with a low modulus polymeric substrate (TPU), to yield a rugged platform for flexible electrochemical sensing. The utilization of a thin stretchable polymeric substrate allows the sensor to intimately mate with the

wearer's body for conformal attachment. Sandwiching the inks between highly stretchable TPU films led to the sensor exhibiting high mechanical resilience, and a stable electrochemical response under high mechanical deformation. Furthermore, the fabricated flexible electrochemical sensors can be ironed onto any textile substrate, allowing for easy customization for any application. As a proof-of-concept, the printed sensors were transferred onto a cotton gauze to be used as a breathable sensing substrate for real-time wound monitoring. In addition, given a low softening point of the TPU film (80^{o}C), the transfer process is compatible with even heat-sensitive textiles.

3.2 Experimental

3.2.1 Materials

Flexible conductive Ag/AgCl (Creative Materials, 127-48E) and carbon inks (DuPont^{TM} Intexar^{TM} PE671) were purchased for screen-printing the sensors. Potassium ferricyanide ($K_3[Fe(CN)_6]$, CAS No. 13746-66-2), potassium chloride (KCl, CAS No. 7447-40-7), sodium phosphate monobasic (NaH_2PO_4, CAS No. 10049-21-5) and sodium phosphate dibasic (Na_2HPO_4, CAS No. 7558-7-4) were obtained from Sigma-Aldrich. All aqueous solutions were prepared in phosphate buffered saline (0.02 M, pH 7.8), prepared using NaH_2PO_4 and Na_2HPO_4 salts.

3.2.2 Flexible electrochemical sensor fabrication

The electrochemical sensors were fabricated by printing commercial flexible conductive inks onto a stretchable thermoplastic polyurethane (TPU, TE-11C DuPont^{TM}) film, and subsequently heat laminating over a cotton gauze (thickness: 100 µm). Screen-printing technique was used for the fabrication of flexible sensors on fabric, given its known advantages of low cost and large-scale production. The bilayer TPU film consisted of a high recovery (50 µm) and a melt adhesive layer (25 µm), backed by an adhesive barrier layer. Printing was performed using a hand-operated

screen-printing setup. The sensor pattern was designed in SolidWorks 2013 software and the design mask was cut out on an adhesive vinyl using a Silhouette cameo 3 die cutter. The mask was then placed on a polyester screen (200-mesh size) and the ink was transferred to the TPU substrate through a hand-held squeegee angled at 45°. A sequential printing of the silver/silver chloride (Ag/AgCl) and carbon inks was carried out following a curing step of 15 minutes at 80^{o}C in a convection oven after each print (Figure 3.1). The conductive inks were known to have excellent adhesion to the elastomeric TPU substrate while exhibiting resistance to flexing and creasing. Subsequently, an encapsulating TPU layer (TE-11C DuPont^{TM}) was placed over the printed sensors to define the working area (Ø:3 mm) and the contact pads resulting in the flexible sensor construct. The entire assembly was later heat laminated over a cotton gauze with a heat press at 130°C for 2 min, to obtain a textile-based sensor.

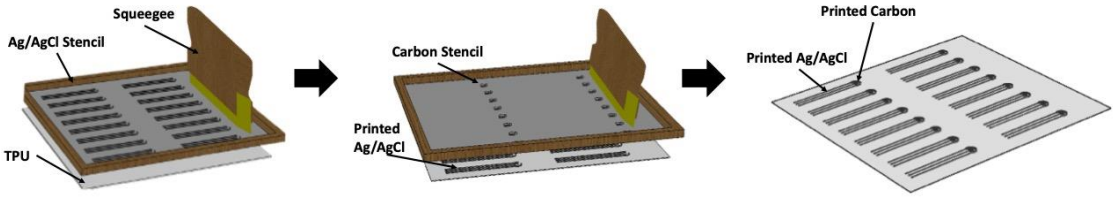

Figure 3.1. Schematic illustration of the flexible sensor fabrication process using the screen-printing technique. Flexible inks (Ag//AgCl and carbon) were sequentially screen-printed and cured onto the TPU substrate. To define the electrode area, the printed electrodes were encapsulated with a TPU layer resulting in the complete flexible sensor construct.

3.2.3 Mechanical Characterization

Linear stretching and bending characterization of the sensors was carried through a custom-designed micro-tensile tester. The sensor was subjected to increasing levels of strain up to 100% in 10% increments at a rate of 50 mm/min. The lateral bending study was conducted by bending the sensor up to an angle of 180^{o} in increments of 45^{o}. Optical and scanning electron microscopy (SEM JEOL 6330) was performed to analyze

the changes at a microscopic level. The change in resistance as a function of stretching and bending was logged to assess the changes in sensor conductivity.

3.2.4 Electrochemical Characterization

Cyclic voltammetry (CV) was performed using a CH Instruments (CHI-230B) electrochemical analyzer. A 5 mM $K_3[Fe(CN)_6]$ solution in 0.1 M KCl was used as the electrolyte for the studies. CV plots were acquired in a potential range of 0.5 V to -0.5 V with a scan rate of 20 mV/s. All electrochemical characterization was performed by either continuously applying a strain of 25% or a lateral bending of 90^o and recording CV every 15 minutes for a total of 60 minutes.

3.3 Results and Discussion

The fabricated electrochemical sensor was designed to have a three-electrode assembly, wherein the Ag/AgCl ink serves as the pseudo-reference electrode (RE), while the chemically inert carbon ink is used to realize the working (WE) and counter electrodes (CE) (Figure 3.2a). A layer of TPU was heat laminated on the printed sensor to serve as an encapsulation layer and define the working area and the contact pads. An optical micrograph of the printed sensor along with the scanning electron micrograph illustrating the planar surface morphology and cross-sectional structure of the sensor are shown in Figure 3.2b, c, and d. Using mechanically flexible inks in combination with an elastomeric substrate, led to the printed electrochemical sensors demonstrating high resilience to stretching, torsional, and bending stresses (Figure 3.2e-g). Owing to the low thickness of the TPU substrate, the sensor can also intimately couple with the complex contours of the skin surface (Figure 3.2h).

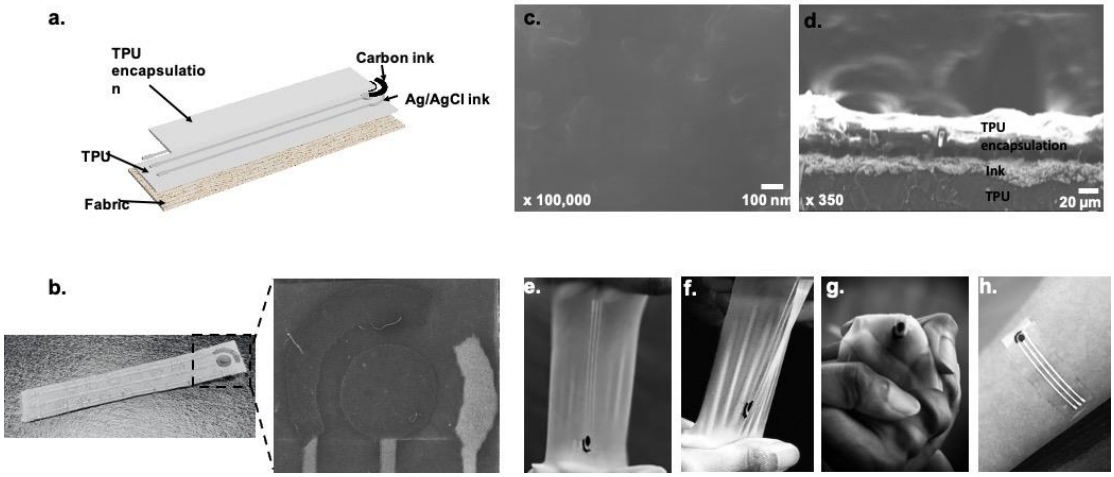

Figure 3.2. a. Schematic representing the exploded view of the entire sensor assembly b. Optical micrograph of the top view of the sensor (Inset: magnified image of the three electrodes) c. SEM image of the working electrode illustrating the smooth surface morphology d. Cross-sectional profile of the sensor, showing the TPU substrate, ink and the encapsulation layers. Images depicting the sensor under e. tensile f. flexural and g. torsional stress and h. conformal attachment of the sensor to the epidermis.

A crucial step towards obtaining the proposed flexible sensor was the heat lamination of the TPU encapsulation layer over the printed sensor. The heat lamination process thermally anneals the sensor surface resulting in reduced ohmic resistance. The higher temperature of the heat lamination process (130^{o}C) compared to the ink curing temperature (80°C) results in rearrangement of the conductive particles in the ink resulting in a 50% decrease in the resistance for the working and counter electrodes (

Table 3.1). Another key challenge is the protection of sensors at high peak strains that can occur upon large-scale deformation, thereby creating a potential for sensor failure. The TPU encapsulation layer addresses this challenge by providing the sensor with an additional degree of stretchability. Preliminary work aimed at quantifying the flexibility of the printed sensor with and without the encapsulation layer. The micrographs of the sensor surface under strain illustrate that the ink starts to debond and develop cracks at a low strain level of 25% for a non-encapsulated sensor (Figure 3.3a). On applying a tensile force to the underlying TPU substrate the printed ink experiences shear stress. As a consequence of relatively low stretchability of the

ink compared to TPU, the printed sensor starts to develop cracks and consequently peel off the substrate. On removal of the external force, the ink is unable to recover its electrical conductivity which would consequently affect the sensor response. In contrast, an encapsulated sensor exhibited excellent mechanical resiliency even under a strain of 100%. Sandwiching the printed ink between two highly stretchable TPU layers resulted in the sensor undergoing a large ductile deformation before failing, in contrast to the non-encapsulated sensor. As clearly evident from the micrographs shown in Figure 3.3a, minimal cracks were seen to develop even at higher strains for the encapsulated sensor. This can be attributed to the TPU encapsulation layer preventing the propagation of transverse cracks across the ink layer. The blockage of crack propagation thus allows the ink layer to reach its ductile yield point and stretch out together with the TPU layers to large elongations causing no appreciable damage to the sensor.[195] The sensor thus exhibits a self-healing property causing only an 11% increase in the resistance upon returning to an unstrained state.

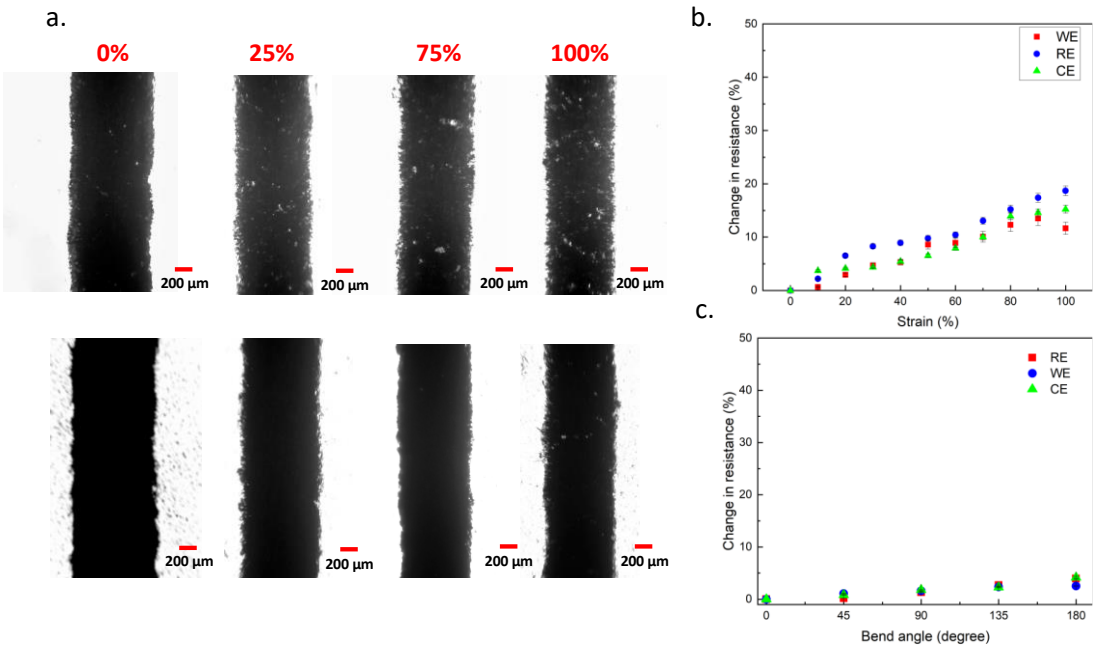

Figure 3.3. a. Optical micrographs of a printed non-encapsulated (top) and encapsulated (bottom) sensor when subjected to different strain levels (0%, 25%, 75% and 100%). Change in the ohmic resistance (△R/R) of the three electrodes (WE, CE and RE) as a

function of b. strain and c. bending stress. A minimal change in △R/R validated the sensor's durability under mechanical stress. Each experiment was carried out in triplicate (n = 3), and the data is represented as mean ± SD.

Table 3.1. Change in ohmic resistance (△R/R) of the three electrodes (WE, CE and RE) after heat lamination of the TPU encapsulating layer onto the screen-printed electrodes. The data is represented as mean ± SD.

Sensor	**Electrode**	**Resistance (Ω)**	
		Before encapsulation	**After encapsulation**
1	RE	2.4 ± 0.2	1.83 ± 0.06
	WE	24.37 ± 0.25	12.1 ± 0.1
	CE	26.23 ± 0.12	13.63 ± 0.15
2	RE	2.17 ± 0.06	2.1 ± 0.1
	WE	27.77 ± 0.15	12.47 ± 0.06
	CE	34.43 ± 0.35	13.17 ± 0.12
3	RE	2.5 ± 0.00	2.07 ± 0.06
	WE	24.6 ± 0.00	10.47 ± 0.12
	CE	31.13 ± 0.06	13.43 ± 0.12
4	RE	2.02 ± 0.03	1.87 ± 0.06
	WE	26.33 ± 0.06	16.47 ± 0.23
	CE	30.2 ± 0.10	18.17 ± 0.12
5	RE	2.6 ± 0.00	1.93 ± 0.06
	WE	28.73 ± 0.06	15.33 ± 0.06
	CE	34.5 ± 0.17	19.67 ± 0.06

The electrochemical characteristics of the sensor were examined by performing cyclic voltammetry using potassium ferricyanide as the electrolyte (Figure 3.4a). The electroactive surface area of the printed sensor was estimated to be 0.05 cm^2 using the

Randles-Sevčik equation (Equation 3.1) for a quasi- reversible electron transfer process.

$$i_p = 0.446\, nFA\, C^0 \left(\frac{nF\upsilon D_0}{RT}\right)^{1/2} \qquad \text{Equation 3.3.1}$$

where i_p is the peak cathodic current, n is the number of electrons transferred in the redox process, F is Faraday's constant, A is the electrochemical active area, D is the diffusion coefficient, C is the bulk concentration of the analyte, R is the universal gas constant, T is the temperature, and υ is the scan rate.

In a wearable environment, sensors are required to operate accurately under continuous mechanical stress. Chronic wounds such venous leg ulcers or diabetic foot ulcers are found in the gaiter area of the leg or on the foot, respectively. Previous studies have shown an average radius of curvature found in these regions to be around 20^o [196,197]. Thus, when the sensor is placed on a wound, the typical stretching and bending stresses can be expected to be 0% and 20^o, respectively. In the case of sensor mishandling or a sensor being subjected to extreme conditions, a strain of 25% and a bending of 90^o may be expected. To ensure proper sensor functionality under these conditions, the sensor was tested under continuous mechanical stress both under normal and extreme conditions. Subsequently, the change in electrochemical response of the sensor as a function of applied strain and bending moment was evaluated. The sensor was subjected to a continuous strain of 25% with CV response recorded after every 15 minutes for a total of 60 minutes.

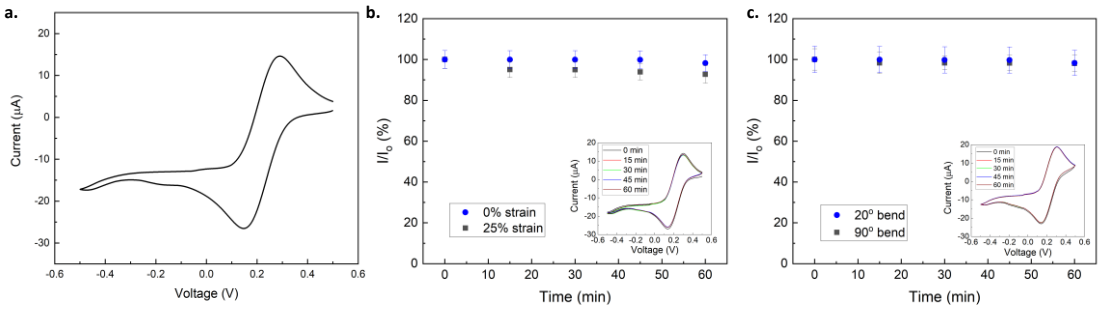

Figure 3.4. Electrochemical sensor response using a ferricyanide probe a. while the sensor was under no mechanical stress. b. while the sensor was under a 0% and 25% strain for a total of 60 min (inset: CV recorded every 15 min). c. while the sensor was under 20^o and 90^o bending stress for a total of 60 min (inset: CV recorded every 15 min). Negligible changes in the Ep_c and Ip_c were observed illustrating the sensor's ability to withstand prolonged mechanical deformations. I and I_o represent the average cathodic peak current obtained from the CV plot with and without mechanical strain (stretching or bending) respectively. Each experiment was carried out in triplicate (n = 3), and the data is represented as mean ± SD.

A minimal deterioration in the sensor response was seen as indicated by the small shifts (7.29%) in the cathodic peak current and the redox potentials (0.05%) under a 25% strain. Applying an external tensile stress on the printed sensor results in development of cracks given the plastic nature of the components. At an increased level of stress, the cracks start to widen resulting in a loss of electrical conductivity, which in turn affects the ion transport properties on the active area. However, no noticeable change in response after 15 minutes implies that cracks develop in the printed traces within the first few minutes after which they remain latent (Figure 3.4b). The high resilience of the sensors is indicative of the preservation of the surface microstructure, a key characteristic of electrochemical sensing. A lateral bending study was performed next, to study the sensor compliance toward bending stresses. The sensor was held bent at an angle of 20^o or 90^o with CV being recorded every 15 minutes. As depicted in Figure 3.4c, even under extreme conditions (90^o), bending had no discernible effect on the peak current (1.93%). As was seen earlier, bending stresses lead to a less than 5% change in the electrical conductivity of the printed sensors even when bent at 180^o. Thus, a bending moment of 90^o, causes no change in the microstructural properties of

the sensor, thus resulting in a stable sensor response. The mechanical characterization studies reveal that even though minor deformations may appear in the printed traces; they have a negligible effect on the overall electrochemical behavior of the sensor. While the sensors fabricated in this study are mechanically reliable for the wound monitoring use case, previous studies have reported sensors with higher levels of tolerance where negligible effect on the electrochemical response even after a 150% strain for an extended period of time (150 min) was seen.[198] Several other studies have also explored the effect of ink composition on the conductivity and mechanical robustness of the printed traces.[199,200] In the future, different formulations of the printed inks may be further explored to develop highly robust inks for fabricating wearable sensors.

As mentioned earlier, these flexible sensors can be easily translated to any textile substrate to well-suit any apparel-based application. To align with the use case of this study i.e., wound monitoring, the printed sensors were transferred onto a cotton gauze as the substrate (Figure 3.2b). Such sensors can be used for real-time monitoring of wound severity and help determine proper treatment and therapeutic efficacy.

3.4 Conclusion

In summary, a flexible electrochemical sensor exhibiting high mechanical resilience has been demonstrated. The sensor is realized by screen-printing conductive inks on a polymeric elastomeric substrate, TPU. By integrating a stretchable encapsulation layer, the printed sensor can withstand high mechanical stresses. Tensile and flexural characterization of the sensors revealed that a linear stretching of up to 100% and bending up to 180^{o} have a negligible effect on the mechanical properties of the sensor. Furthermore, the thermal annealing of the printed sensors during the encapsulation process resulted in a uniform surface terrain and a ~50% reduction in the ohmic

resistance. The electrochemical characteristics of the sensor were also shown to be highly resilient (<5% deviation) to any mechanical deformations. This work also presents a facile and inexpensive process for the integration of flexible electrochemical sensors on textiles to ensure user comfort and wearability. Further improvements can be targeted towards tailoring the pristine inks and the substrates to impart additional levels of stretchability to the sensors. Coupling electrochemical sensing modalities with flexible and stretchable platforms can offer unprecedented opportunities for the development of next-generation electrochemical sensors. Novel processes for synthesizing stretchable inks and large-scale fabrication of electrochemical sensors hold great promise to transform personalized healthcare monitoring.

4 Uric Acid Detection on Flexible Sensors in a Steady-State Environment

4.1 Introduction

Flexible biosensors have been extensively explored for a plethora of applications, in particular for healthcare monitoring owing to its advantage of continuous montioring.[17,201,202] Apart from the sensors that track physiological parameters[203,204] of the body, electrochemical sensors have been explored for monitoring of the chemical information present in biofluids like sweat,[17,205] interstitial fluid,[206] wound exudates[100,102], etc. Chemical sensors have the potential to capture real-time changes in the biomarker levels in a rapid, continuous and a non-invasive manner. Coupled with physical sensors, these sensors can provide a comprehensive overview of a person's health. For example, uric acid concentration in wound exudates can be explored as a biomarker for real-time monitoring of the progress of wound healing coupled with a pressure sensor to monitor chronic pressure ulcers. Unlike conventional rigid electrochemical systems, flexible sensors offer extended scope for high degree of functional integration while conformally interfacing with the human body. Translational of the traditional sensing mechanisms to wearable substrates has eliminated the need for sophisticated equipment and skilled personnel providing real-time actionable data directly to the healthcare provider.

Potential flexible substrate materials that have been considered for development of such sensors include, polyimide (Kapton),[62,207] polyethylene terephthalate,[208,209] paper[210–212], and textiles.[189,213] Plastic-based substrates such as polyimide, offer a planar surface for efficient electrochemical sensing and allow for easy bending, however, they do not entail stretching capabilities restricting their use in many applications. Further,

owing to the plastic component of these substrates they have a compromised user compliancy. For instance, a plastic substrate like polyimide may result in patient discomfort when placed directly on an open wound; that may subsequently result in an inflammatory response. Thus, textile-based substrates for these sensors[213,214] have been extensively explored to overcome the comfortability issues. In addition to their excellent mechanical resiliency, these sensors can be seamlessly integrated to any apparel for user comfort especially accommodating long-term monitoring applications. However, due to the non-planar surface characteristics (dependent on the type of textile) of these sensors they generally demonstrate low sensor sensitivities owing to the poor electron transfer. Despite the major advances made towards development of flexible electrochemical sensors significant amount of effort is required to couple mechanically compliant substrates with efficient electrochemical sensing capabilities to develop sensitive next-generation devices.

In this chapter, a textile-based flexible electrochemical sensor has been reported for detection of uric acid (UA) for real-time wound monitoring. The flexible sensors fabricated in the earlier chapter have been assessed for their electrochemical properties for detection of UA. While the elastic nature of thermoplastic polyurethane (TPU) allowed the sensors to undergo high mechanical stress, its biocompatibility made it a suitable candidate for wound monitoring. The detection platform implements an enzymatic electrochemical sensing modality to measure UA for longitudinal wound monitoring. The tested sensing system consisted of an array of four UA sensors integrated onto a single wound dressing to spatially map the UA levels across the wound area. The electron transfer mechanism and the sensor's applicability to sense UA in real biofluids has been explored in detail. The flexible sensors have been further interfaced with a low-cost custom designed wearable electronic system to enable real-

time collection and wireless transmission of the sensor data to achieve a fully integrated wearable system.

4.2 Experimental

4.2.1 Materials

AuNPs (20 nm diameter) and MWCNTs (9.5 nm × 1.5 μm, CAS No. 308068-56-6) were purchased from Sigma Aldrich, USA. Analytical grade horseradish peroxidase (HRP, CAS No. 9003-99-0, 0.2 U ml^{-1}) was purchased from ThermoFisher Scientific. Lyophilized UOx powder (CAS Number 9002-12-4) containing 15∼30 U mg^{-1} was purchased from Sigma Aldrich. UA (CAS No.: 69-93-2), sodium hydroxide (CAS No. 1310-73-2), 30% hydrogen peroxide (CAS No. 7722-84-1), sulfuric acid (95.0-98.0% H_2SO_4, CAS No.7664-93-9), dimethylformamide (99.9% DMF, CAS No. 68-12-2), potassium chloride (KCl, CAS No. 7447-40-7), sodium phosphate monobasic (NaH_2PO_4, CAS No. 10049-21-5) and sodium phosphate dibasic (Na_2HPO_4, CAS No. 7558-7-4) were used of analytical grade. All aqueous solutions were prepared in phosphate buffered saline (0.02 M, pH 7.8), prepared using NaH_2PO_4 and Na_2HPO_4 salts.

4.2.2 Sensor functionalization

Fabricated screen-printed flexible electrodes were used for UA detection. The working electrode of the fabricated sensor was first functionalized with a MWCNT dispersion prepared in DMF and dried at 60^oC to evaporate the solvent. This was followed by casting of AuNP solution (OD: 50) and drying at 60^oC for 5 minutes. The enzymes HRP and UOx, were then immobilized over the electrode via physisorption, nitrogen drying and thorough washing with PBS. All steps involving enzyme immobilization were carried out in an icebox to prevent enzyme denaturation. For control studies, a

monoenzymatic (UOx) electrode was functionalized containing either of the nanomaterials (MWCNTs or AuNPs).

4.2.3 Sensor characterization

The surface morphology and nanoparticle distribution of the functionalized working electrode was studied through scanning electron microscopy (SEM JEOL 6330) and transmission electron microscopy (TEM Philips CM200). Electrochemical impedance spectroscopy (EIS) was performed using an Autolab impedance analyzer to study the effect of nanoparticles on the charge transfer properties of the functionalized sensors. The readings were taken in a frequency range of 1 mHz to 100 kHz at a potential of 5 mV using a 5 mM ferricyanide ferrocyanide buffer as the probe. Electrochemical active surface area characterization of the electrodes was carried out via cyclic voltammetry (CV). CV was performed using a CH Instruments (CHI-230B) electrochemical analyzer, with a 5 mM $K_3[Fe(CN)_6]$ solution in 0.1 M KCl used as the electrolyte. The control measurements were acquired in a potential range of 0.5 V to -0.5 V with a scan rate of 0.02 V s^{-1}. In order to estimate the reaction kinetics of the functionalized electrode, measurements at eight different scan rates (10, 20, 50, 100, 200, 300, 400, and 500 mV s^{-1}) were carried out.

Chronoamperometric studies were performed using an analytical system model CHI-230B potentiostat (CH Instruments, Inc.). Chronoamperometry was performed to assess the response of the functionalized electrode to varying concentrations of UA. Following sensor conditioning, each measurement was performed for 60 s at an applied potential of -0.6 V. Control studies were carried out to assess the sensor response with respect to each functionalized layer. Sensor stability was characterized at room temperature (25^{o}C), physiological conditions (37^{o}C) and at an elevated temperature

(40°C) over a period of 7 days. Sensor response was recorded every 12 h, and the electrode was left immersed in the buffer solution in between the sequential readings.

4.2.4 Wearable electronic system design

A miniaturized electronic circuit system was designed for electrochemical and temperature measurements. The potentiostat system was capable of performing chronoamperometry measurements from each of the four sensors individually. Each 3-electrode potentiostat channel contains an analog front-end (AFE, LMP9100 from Texas Instruments (TI)) with software-adjustable bias and gain. The system also contains a 100 kΩ negative temperature coefficient (NTC) thermistor in a voltage divider circuit with a 49.9 kΩ resistor. The system is controlled by a Bluetooth Low Energy (BLE) system-on-chip (SoC, BLE113 from TI) which reads the output of each AFE through a quad analog-to-digital converter (ADC, ADS1115 from TI), and digitizes the analog output of the potentiostat. Another analog input pin on the SoC is used to read the output of the thermistor to determine the wound bed temperature. After reading the electrochemical and temperature data, the SoC was programmed to operate in either stream mode or save mode. In stream mode, the device samples the channels at 5 Hz and transmits data over BLE to a data aggregator. In save mode, the device wakes up once per hour and samples at 1.3 Hz for 1 minute per channel, then saves the data to an on-board 2 Mb flash memory chip (M24M02, StMicrolectronics) and goes back to sleep. For long-term use, the system was powered by a 350 mAh 3.7 V lithium polymer battery and was encapsulated in flexible silicone to protect the electronics from environmental moisture and ensure user comfort. A custom Python user interface was also designed for device configuration and data aggregation. After connecting to the device, the user can initialize the measurement, configure the gain and bias of the potentiostat, and view a graphical display of the potentiostat currents, temperature

value, and battery level. The user can then either stay in stream mode or switch to memory mode for long-term studies. The same interface is used to retrieve, view, and save the data in memory after the study is complete.

A custom rigid-flex interconnect was further designed to interface the backend electronic system and the flexible UA sensors. A 12-pin Flat Flex Connector (FFC) ribbon cable was attached to the two 12-pin FFC headers connected on the electronic system and a breakout PCB board. The breakout board is then attached to the contact pads on the fabricated sensors with a room-curable conductive silver epoxy to complete the connection.

4.3 Results and Discussion

4.3.1 Sensor surface characterization

Owing to the fast electron mobility offered by MWCNTs and AuNPs, they were used as catalysts in the UA detection mechanism. The nanomaterials provide a high surface area for enzyme immobilization allowing for higher loading, improved stability and reduced leaching of the enzyme. The surface morphology (Figure 4.1a) and electron transfer characteristics of the electrode were analyzed through SEM, EIS and cyclic voltammetry, respectively. The scanning electron micrograph of the MWCNT functionalized electrode illustrated the mesh-like distribution of the MWCNTs over the electrode surface (Figure 4.1b), with an average nanotube diameter of 10.05 ± 1.5 nm. The images revealed that the uppermost layer consisted of a low-density network of randomly oriented nanotubes. The porous structure (higher surface area) offered by the MWCNTs facilitates higher enzymatic loading resulting in improved current density. The different shades of black in the TEM images represented the multi-walled structure of the nanotubes (Figure 4.1d),. The unique electron transfer properties offered by the nanotubes as a result of this planar structure was further confirmed by the reduction in

charge transfer resistance from 2.4 kΩ to 698 Ω after their deposition (Figure 4.2). Furthermore, an increase in the double layer capacitance after MWCNT deposition revealed their capacitive nature.

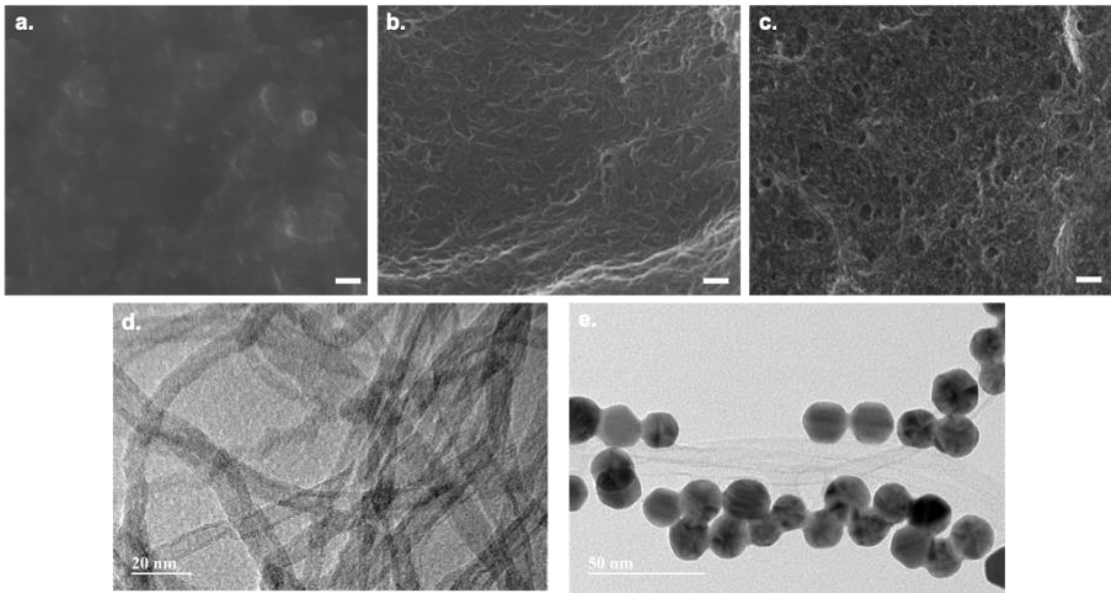

Figure 4.1. Representative SEM and TEM images of functionalized flexible electrodes illustrating the uniform nanoparticle distribution over the electrode surface. SEM images of a. Bare b. MWCNT c. MWCNT-AuNPs functionalized electrodes. Scale bar: 200 nm, TEM images of d. MWCNT e. MWCNT-AuNPs. The synergistic interaction between the nanomaterials resulted in improved electron transfer between the active site of the enzyme and the electrode.

The immobilization of AuNPs over the MWCNT network, resulted in a homogenous topography of the electrode surface (Figure 4.1c). Spheroidal shaped nanoparticles were seen decorated over the MWCNT network, with a mean particle size of 20.75 ± 1.2 nm implying a spatial distribution of the gold nanoparticles with a low agglomeration level. The synergistic interaction between the two nanomaterials, improved their electron transfer properties; as was reflected by the decrease in Rct to 270 Ω (Figure 4.2). The TEM image illustrated the Van Der Wall interactions between the AuNPs and the MWCNTs, where the AuNPs were seen to strongly cohere to the walls of the nanotubes (Figure 4.1e). The decrease in the charge resistance suggested an improved transfer kinetic characteristic offered by the MWCNT-AuNPs

nanocomposite.[156] The successful immobilization of the enzyme was signified by the increase in the Rct of the electrode to 582 Ω as shown in Figure 4.2. Immobilization of the enzymes over the nanocomposite functionalized electrode resulted in inhibition of ions reaching the nanocomposite substrate, hence limiting the charge transfer process.[215]

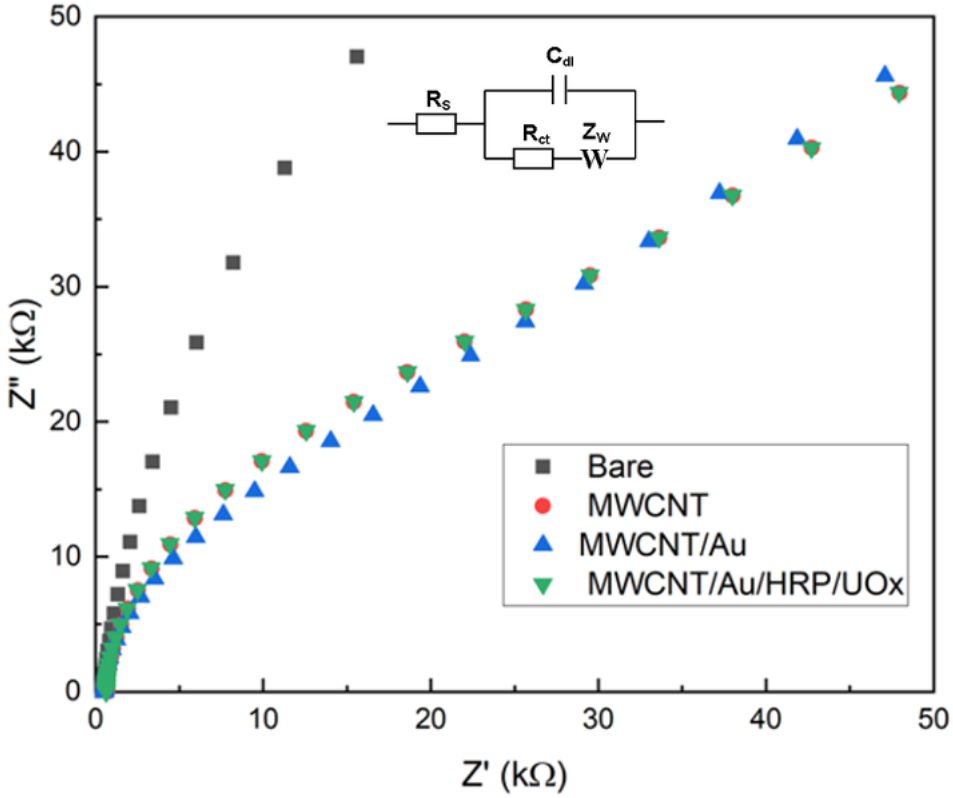

Figure 4.2. Nyquist plot of bare, MWCNT, MWCNT-AuNPs and MWCNT-Au-HRP-UOx functionalized flexible electrodes showing the improved electron transfer rate as a result of nanoparticle immobilization. A ferri/ferrocyanide probe was used to take impedance readings in the frequency range of 1 mHz to 100 kHz at a potential of 5 mV. Randles equivalent circuit (inset) was utilized to fit the experimental data, where R_s is the solution resistance, R_{ct} is the charge transfer resistance, C_{dl} is the double layer capacitance and Z_w is the Warburg impedance.

The electrochemical active surface area of an electrode represents the area of the functionalized electrode available for charge transfer. The active area of the MWCNT-AuNPs functionalized electrode was found using the Randles-Sevčik equation and was estimated to be 0.062 cm^2, which was 1.24 times higher than that of a bare electrode (Figure 4.3a). Furthermore, a linear relationship between the anodic

and cathodic peak currents (R = 0.89 and 0.93 respectively) as a function of the square root of scan rate verified that the redox process was diffusion-limited (Figure 4.3b and c).

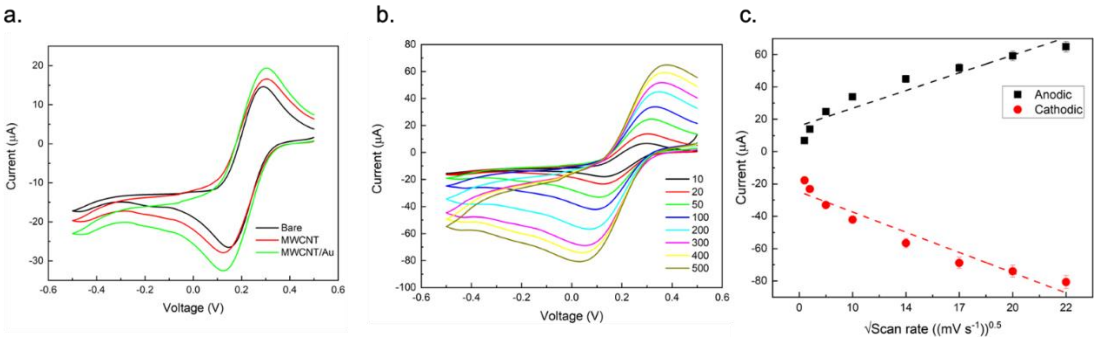

Figure 4.3. Cyclic voltammograms of a 5 mM $K_3[Fe(CN)_6]$ solution in 0.1 M KCl for a. Bare, MWCNT and MWCNT/Au functionalized electrodes. The higher surface area provided by the nanomaterials was reflected by the higher cathodic and anodic currents. b. Current response of a MWCNT/Au functionalized electrode at different scan rates c. Calibration curve of peak current vs. square root of scan rate. Each experiment was carried out in triplicate (n = 3), and the data is represented as mean ± SD. The linear fit confirmed the diffusion-controlled reaction kinetics of the electrode.

4.3.2 Bienzymatic uric acid detection mechanism

Uricase is a peroxisomal enzyme that catalyzes the oxidation of UA to 5-hydroxyisourate. The UOx functionalized electrode selectively oxidizes uric acid to form hydrogen peroxide. H_2O_2 then serves as a substrate for HRP, where it gets reduced as a result of the heterolytic cleavage of the oxygen-oxygen bond (Figure 4.4a). The sensor quantifies the UA concentration by measuring the amount of H_2O_2 reduced at the electrode through amperometric measurements at a certain working potential. Control studies were performed to understand the functionality of the MWCNT-AuNPs nanocomposite on the sensor response. The accelerated electron transfer facilitated by the nanocomposite was reflected by the higher current response observed in the study (Figure 4.4b). The MWCNT electrode showed 4.02 times increase in the current density, while a 4.67 times increase was observed for the nanocomposite-casted electrode in comparison to a bare electrode. The observed signal enhancement can be attributed to the prevention of unfavorable lateral interactions between the enzymes on

the electrode surface due to the MWCNT curvature.[216] Additionally, the synergistic non-covalent interaction between the MWCNTs and AuNPs provides an efficient conducting interface for fast electron transfer.[168,169] The improved signal in presence of the nanocomposite can also be ascribed to the electrostatic interaction existing between the UOx enzyme and AuNPs. The amine groups functionalized on the AuNPs impart a positive charge on them, which then interacts with the negative charge of the UOx leading to higher enzyme retention on the electrode surface. It was further seen that the co-entrapment of the HRP and UOx enzymes within the MWCNT-AuNPs matrix allowed for a faster electron transfer from the enzyme to the electrode. Control studies showed that the current density improved by a factor of 2.0 on co-immobilization of HRP (Figure 4.4b). This can be attributed to the electrostatic interactions between the enzymes, that allows for easy diffusion of H_2O_2 to the active site of HRP site and exchange electrons with it.

The sensor response of a MWCNT/Au/HRP/UOx functionalized electrode on successive additions of UA was assessed next using chronoamperometric technique (Figure 4.4c). An increase in the reduction current corresponded to an increase in the UA levels. The linear response range of the sensor was found to be from 50 μM to 720 μM with a correlation coefficient of 0.97 (Figure 4.4d). The electrocatalytic activity of the UA sensor exhibited a sensitivity of 42.55 nA μM^{-1} cm^{-2}, and a lowest detectable concentration of 5.54 μM which was better than the sensors reported till date (Table 4.1). The results demonstrated that the sensor can accurately measure UA in the clinically relevant range; 200-750 μM. Sensor selectivity is a critical parameter to determine the practical applicability of any sensor in a complex biofluid. The effect of possible interferents (dopamine (DA), ascorbic acid (AA), hypoxanthine (HX) and xanthine (XA)) present in the wound exudate on the sensor response was evaluated.

The UA sensor showed good selectivity over other analytes at physiologically relevant concentrations, with a comparatively higher increase (8.9%) in the current response observed on addition of AA (Figure 4.5).

Further, the electrochemical characterization of the flexible sensors integrated with the wearable SoC was carried out using chronoamperometry (Figure 4.4e). As before, an increase in the current was observed as a function of increasing UA concentration (Figure 4.4f). The linear response range of the sensor lied between 50 μM to 600 μM with a correlation coefficient of 0.95 (Figure 4.4g), and a sensor sensitivity of 40.32 nA μM^{-1} cm^{-2}. The lower current values obtained from the wearable SoC can be attributed to the lower sensitivity offered by the miniaturized potentiostat compared to a benchtop potentiostat. Also, the sensor response obtained from the electronic system was noisier compared to the benchtop results since it doesn't include any signal filtering circuitry as integrated within a benchtop potentiostat. The results were thus smoothed using a least-square method with a window of 5 data points.

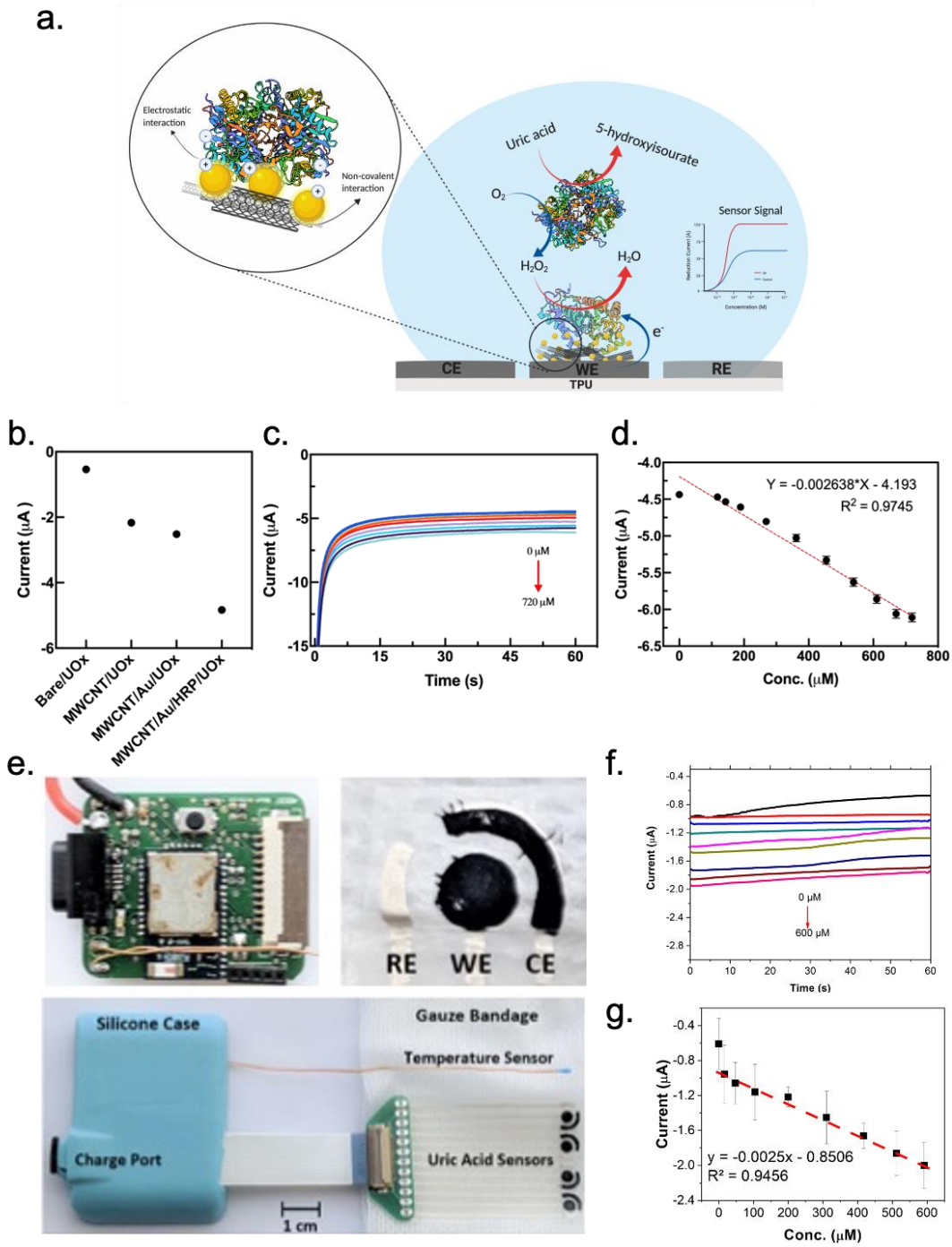

Figure 4.4. a. Schematic illustration of UA oxidation through a bi-enzymatic detection mechanism b. Current response of a bare electrode modified with UOx, UOx electrode modified with MWCNT, MWCNT/Au and MWCNT/Au/HRP to 250 μM UA, with the latter exhibiting the highest current density c. Chronoamperometric sensor response of the nanocomposite functionalized electrode (MWCNT/Au/HRP/UOx) as a function of UA concentration d. Linear plot of cathodic current vs. UA concentration. The sensor showed a linear range of 20 – 720 μM with a sensitivity of 42.55 nA μM^{-1} cm^{-2}. Each experiment was carried out in triplicate (n = 3) and the data is represented as mean ± SD. e. Photograph of the wearable electronic system integrated with the flexible UA sensors. The electronics was encased in a silicone elastomer (blue) to allow for easy

conformation and prevent any patient discomfort f. Chronoamperometric sensor response of the nanocomposite functionalized electrodes as a function of UA concentration as recorded using the wearable electronic system g. Linear plot of cathodic current vs. UA concentration obtained from the wearable electronic system. The sensor showed a linear range of 50 – 600 µM with a sensitivity of 40.32 nA μM^{-1} cm^{-2}. Each experiment was carried out in triplicate (n = 3) and the data is represented as mean ± SD.

Table 4.1. Comparison of recently developed flexible sensors for electrochemical detection of UA.

Sensor	**Linear range**	**Sensitivity**	**Limit of detection**
Carbon/UOx[189]	0-800 µM	4.375 µA $mM^{-1}cm^{-2}$	-
Graphene oxide[207]	0-200 µM	3.5 µA μM^{-1} cm^{-2}	0.74 µM
Carbon black/potassium ferricyanide/UOx[214]	200-1000 µM	2.25 µA mM^{-1} cm^{-2}	200 µM
CNT/Au/HRP/UOx (This work)	50-720 µM	37.3 µA mM^{-1} cm^{-2}	5.54 µM

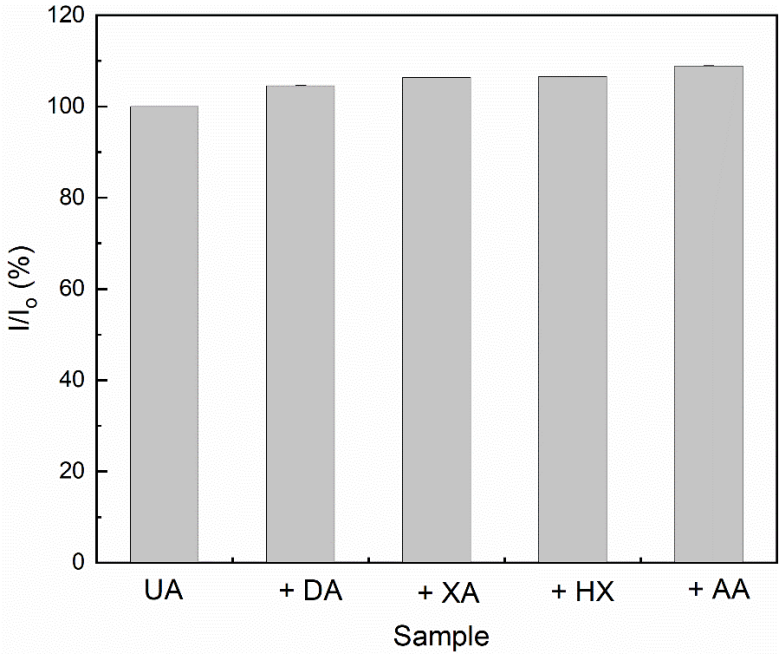

Figure 4.5. Sensor selectivity of a MWCNT/Au/HRP/UOx functionalized electrode in presence of potential interfering electroactive compounds present in the wound exudate: DA (196 pM), XA (50 µM), HX (8 µM), and AA (50 µM). The results showed

that the sensor response was minimally affected only in the presence of AA (8.9% increase in sensor response) in a 50 µM UA solution. Each experiment was carried out in triplicate (n = 3) and the data is represented as mean ± SD.

Enzymatic sensors are known to degrade with time due to enzyme denaturation at elevated temperatures, affecting their stability and thus restricting their use under physiological conditions.[217] The long-term stability of the sensor was evaluated over a period of 7 days under both laboratory and physiologically relevant conditions at a fixed UA concentration (250 µM). While a 16.8% decrease in the sensor response was observed for the sensor at room temperature (25°C), the sensor exhibited a 21.9% decrease in the current at the body temperature (37°C) (Figure 4.6). At a further elevated temperature of 40°C, the current decrease around 22.7%. The stable response offered by the sensor under physiological conditions demonstrates its feasibility for utilization as a wearable sensor for prolonged time periods. In the future, the sensor can be calibrated to compensate for the changes in sensor response as a function of temperature.

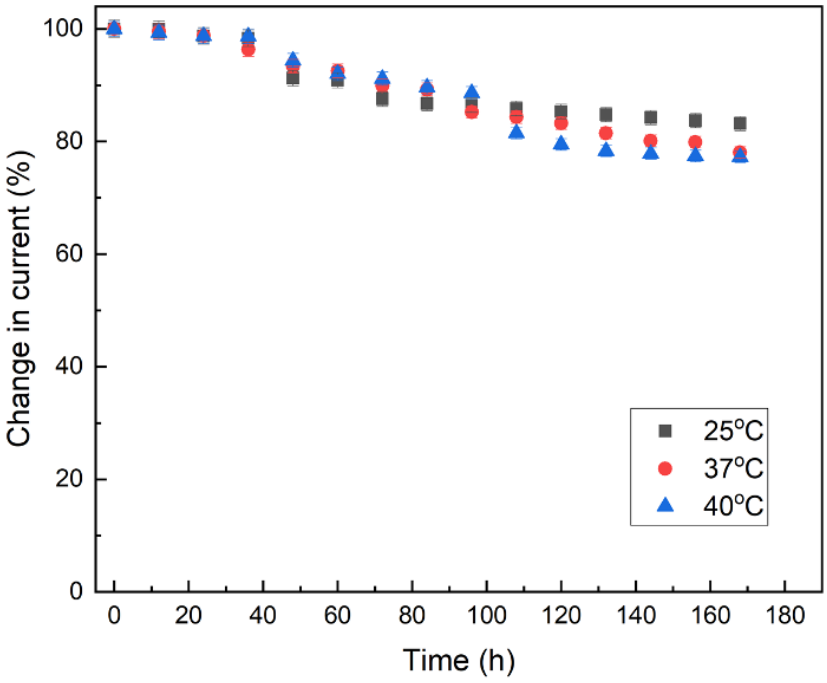

Figure 4.6. Sensor stability of a MWCNT/Au/HRP/UOx functionalized electrode under room temperature (25°C), physiological conditions (37°C) and an elevated temperature (40°C) over a period of 7 days. A degradation in sensor response was seen after 2 days,

with the electrode subjected to an elevated temperature of 40^{o}C showing the highest degradation rate. Each experiment was carried out in triplicate (n = 3) and the data is represented as mean ± SD.

4.4 Conclusion

This work reports a wearable sensing system consisting of an array of UA sensors and a wearable electronic system for continuous monitoring of wound healing. Owing to the mediator-free enzymatic approach, the sensor achieved stable (16.8% degradation at 25^{o}C, 21.9% at 37^{o}C and 22.7% at 40^{o}C) and accurate measurements over a period of seven days for the UA sensor. A sensitivity of 42.55 nA μM^{-1} cm^{-2} enabled the sensor to accurately measure uric acid in the clinically relevant range. An integrated wound monitoring system was further fabricated by interfacing the flexible sensors to custom-designed wearable electronics. An electrochemical characterization of the system for UA detection revealed a sensitivity of 40.32 nA μM^{-1} cm^{-2}. While the system demonstrated a lower current response compared to the benchtop testing, no significant decrease (~1.05 times) in the sensor sensitivity was observed. Given the rich biochemical markers present in the wound exudate, the transition from traditional visual inspection to electrochemical monitoring can provide a non-invasive real-time means to monitor wound chronicity. A multiplexed sensing system can be used to provide feedback to the system-on-chip in the future to allow for an on-chip real-time calibration. Future work could also focus on *in vivo* studies on healing wounds to better understand the correlation of UA concentration with wound healing.

5 Uric Acid Detection on Flexible Sensors in a Dynamic Environment

5.1 Introduction

Continuous monitoring of relevant chemical biomarkers can provide valuable insights on sudden changes in a person's physiology. In comparison to intermittent assessments, continuous monitoring can provide data that can help predict any future episodes. Analysis of such data can help improve therapeutic efficacy and aid in better clinical decision making. Several wearable sensors for continuous monitoring of metabolites such as glucose,[58,62,218,219], uric acid,[153] and, lactate[21,23,220] have been developed. The estimation of these analytes in biofluids such as sweat is a potential alternative to blood-based detection mechanisms. For example, direct correlations between glucose sweat and blood concentrations have been established thus allowing a non-invasive continuous means for monitoring of diabetes.[221] Similarly, lactate in sweat has been studied for monitoring physiological performance,[21] cystic fibrosis[222,223] and oxygen level.[224] Enzymatic sensors have especially been used, owing to their advantages of continuous monitoring modality, sensitivity and selectivity. These sensors offer significant advantages for longitudinal monitoring of health to provide actionable data to the healthcare provider.

However, the deployment of these sensors in *in vivo* environments is faced with several challenges. Owing to the great variations in the biofluid composition at an individual level, there is always an ambiguity in the environment that the sensor is placed in. As a function of the physiological processes, dietary habits, medication and the underlying health condition of a person, the biofluid composition may change. These changes in turn may affect the sensor response thus resulting in erroneous data.

A fundamental drawback of enzymatic sensors is their sensitivity to the sensor's microenvironment. This becomes a major challenge when the sensor is placed in a dynamic environment e.g., wound bed. The current wearable enzymatic sensors do not take into account this dynamic variability offered by a wearable environment. The conventional electrochemical sensor calibration is carried out assuming a steady-state environment under controlled environmental conditions. However, in a complex wearable environment, the environment does not necessarily assume a steady-state. Only one study has been reported till date that incorporates a pH sensor in conjunction with an enzymatic glucose sensor for real-time data correction.[62] Thus, there is an existing need to understand and model the sensor response with respect to the variations in the environment for real-time calibration of the response to obtain accurate readings.

In this chapter, the effect of a dynamic environment offered by a wound on the developed UA sensor has been investigated. The chapter focuses on the challenges faced when a sensor is placed in an *in vivo* environment and how developing correlation models can help reduce the error in the sensor response. The different parameters that change as a function of wound healing were identified and varied according to the expected physiological values. The identified parameters include, pH, temperature, sample volume and evaporation. The effect of each parameter on the sensor response was recorded and correlations were derived to develop mathematical models to correct for the sensor response. The chapter further explores the effect of biofouling on the sensor response. Two independent studies were conducted, with one correlating the effect of physical adsorption of extracellular matrix components on the sensor response, and second the effect of biofilm formation on the sensor surface.

5.2 Experimental

5.2.1 Materials

Analytical grade UA (CAS No.: 69-93-2), LA (CAS No.: 50-21-5), sodium acetate (CAS No.: 127-09-3), acetic acid (CAS No.: 64-19-7), sodium hydroxide (CAS No. 1310-73-2), hydrogen chloride (HCl, CAS No.: 7647-01-0), sodium hydroxide (CAS No.: 1310-73-2), sodium bicarbonate (CAS No.: 144-55-8), sodium carbonate (CAS No.: 497-19-8), sodium phosphate monobasic (NaH_2PO_4, CAS No. 10049-21-5) and sodium phosphate dibasic (Na_2HPO_4, CAS No. 7558-7-4) were purchased from Sigma Aldrich. Luria Bertani (LB) broth was purchased from Sigma Aldrich. All aqueous solutions were prepared using DI water.

5.2.2 Dynamic variability study

The parameters considered for the study included pH, temperature, sample volume, and evaporation. Buffer solutions of varying pH (5, 6, 7, 7.8, and 9) were prepared using the relevant salts and the sensors were tested in the buffers for electrochemical characterization. To study the thermal effect on the sensor response, the sensor was immersed in an electrochemical cell with varying temperatures of 25^{o}C, 30^{o}C, 35^{o}C, and 40^{o}C. To ensure uniform distribution of the sample over the sensor surface for the volume study, a small circular piece of wound dressing (d = 5 mm) was placed covering the three electrodes of the sensor. Different volumes (0.5, 1, 2, 3, 4, and 5 µl) of the UA solution were then drop casted at the middle of the dressing to allow for uniform diffusion of UA across the electrodes. Likewise for the evaporation study, a 10 µl droplet of the UA solution was casted onto the dressing placed on the sensor and kept at constant laboratory conditions of 25^{o}C and 50% humidity. All the above studies were carried using a 250 µM UA solution and performing chronoamperometry using a CHI-230B potentiostat (CH Instruments, Inc.) at a bias potential of -0.6 V.

5.2.3 Biofouling study

The adsorption study was carried out by drop-casting different volumes of wound exudates or skin sweat extracts collected from discarded wound dressings and drying them at room temperature. *Pseudomonas aeruginosa* (PA01) strain was used for the biofilm studies. A preculture was obtained by inoculating 10 ml of LB media with a single colony of bacteria and the cultures were incubated overnight at 37°C at 200 rpm on a shaker-incubator. The UA sensors were placed in a 200 µl of the prepared bacterial inoculation over a period of 7 days. The cathodic current was measured continuously, and the suspension was not disturbed over the entire course of study to prevent any disruption of the biofilm. Scanning electron microscopy (SEM JEOL 6330) was carried out to observe the biofilm growth over the sensor surface with respect to time.

5.3 Results and Discussion

5.3.1 Effect of pH and temperature

The pH and temperature of a wound bed are two parameters that are highly dependent on the wound health.[225,226] It has been established that the pH of a wound shifts from alkaline (pH ~ 9) to acidic (pH ~ 4.7) as it heals.[105] Moreover, development of bacterial infections or inflammations in chronic wounds lead to an acidification and increased temperature of the wound bed.[144] Two of the major factors affecting the catalytic activity of an enzyme are pH and temperature of the operational environment. A change in these parameters can lead to conformational changes in the enzyme's structure thus affecting its catalytic activity. The pH and temperature range for the optimal functionality of an enzyme varies with the enzyme used and the composition of the matrix it is placed in. The current response of an enzymatic sensor may thus vary as a consequence of these structural changes in the enzyme resulting in a confounded response. Furthermore, protonation-deprotonation in the biofluids as a function of

changing pH can result in a change in the ion transport, directly affecting the sensor response.[227,228]

The optimal pH range defined for the uricase enzyme is between 7.5 – 8.5. We investigated the effect of pH (5 - 9) on the sensor response and it was seen that the highest response was recorded at a pH of 7.8, while the current decreased for both more acidic and alkaline environments (Figure 5.1). Earlier studies have shown that UOx precipitates at pH levels lower than 8.0 resulting in a considerable loss of activity, which can be attributed to the observed lower sensor response.[217] Hence, measurement of sensor's environmental pH in conjunction with UA measurements is required to correct for the UA sensor response.

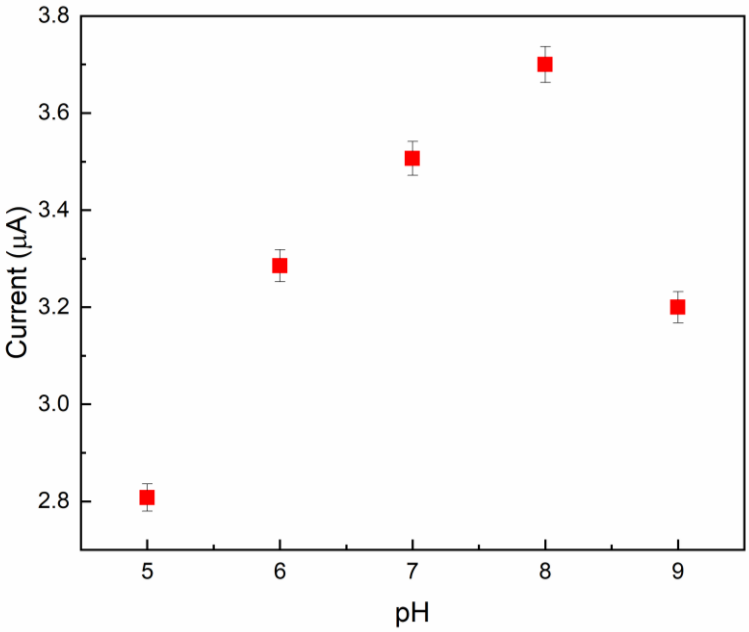

Figure 5.1. Change in UA sensor response of a MWCNT/Au/HRP/UOx functionalized electrode as a function of varying pH (5, 6, 7, 7.8, and 9). Highest sensor response was observed at a pH of 7.8. Each experiment was carried out in triplicate (n = 3) and the data is represented as mean ± SD.

To that effect, a flexible pH sensor was designed and tested to allow for simultaneous wound pH measurements. The working principle of the sensor was based on the protonation of a conductive polymer, polyaniline. As a result of change in the pH, the nitrogen atoms consisting the backbone of polyaniline protonate/deprotonate on

interacting with the protons and the hydroxide ions in the solution. This change can be captured by measuring the resulting potentiometric changes. The response curve of the constructed pH sensor is shown in Figure 5.2a, and the sensitivity of the sensor was calculated to be 81.63 mV pH^{-1} (Figure 5.2b).

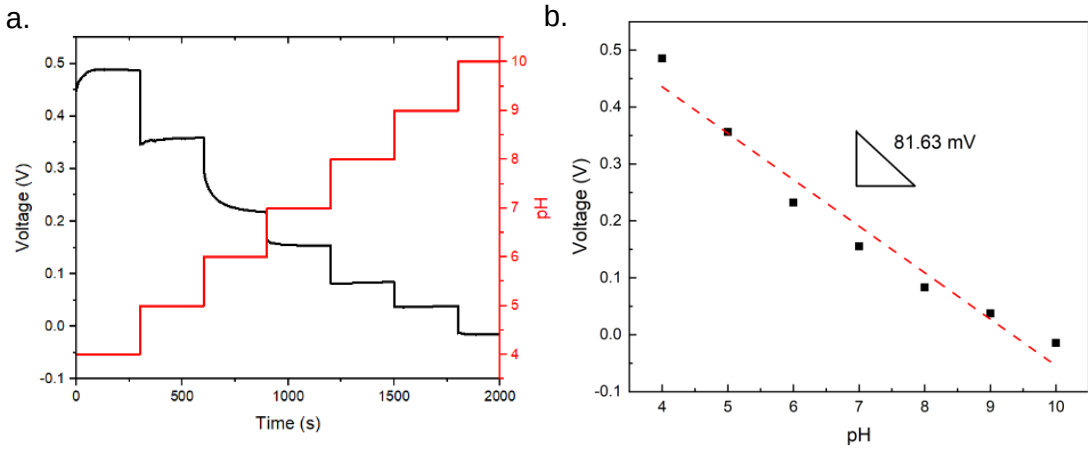

Figure 5.2. a. open circuit potential response of a pH sensor as a function of varying pH (5, 6, 7, 7.8, and 9). b. Calibration curve of the pH sensor. The sensitivity of the sensor was found to be 81.63 mV pH^{-1}.

Mathematical correlation models establishing the relationship between the UA response and change in pH can help in obtaining accurate sensor data. In order to achieve that, UA sensor calibration curves were recorded in different pH buffers (Figure 5.3a), and the data was further utilized to develop a regression model (Equation 5.1).

$$Current = (-0.0026 * Conc.) - (0.1924 * pH) - 1.6251 \quad \text{(Equation 5.1)}$$

Next, pH and UA measurements were made simultaneously, and the model was used to correct for the sensor response. The calibration equation developed at a pH of 7.8 was used for standard UA calculations, and the UA level was calculated to be 150 µM (Figure 5.3b). On calculating the UA response using the model, it was observed that the model did not result in accurate estimation of the actual UA level (i.e. 200 µM),

but the error was reduced from ±21% to ±7% (Figure 5.3b). In the future, an extensive study will be carried out with more sensor data to improve the accuracy of the developed model. Furthermore, more complex mathematical model needs to developed taking all the parameters into consideration at the same time.

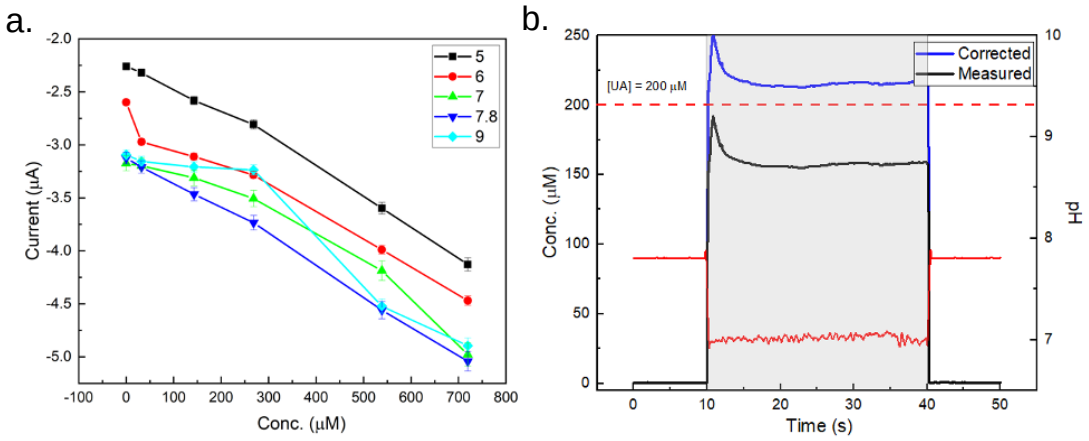

Figure 5.3. a. Calibration curves of the UA sensor in buffers of varying pH (5, 6, 7, 7.8, and 9). The highest current density and sensitivity was found at a pH of 7.8. Each experiment was carried out in triplicate (n = 3) and the data is represented as mean ± SD b. Simultaneous measurement of pH and UA levels. The black curve shows the estimated UA concentration on using the standard calibration curve obtained at pH 7.8 and the red curve shows the measured pH. The blue curve represents the corrected UA concentration as obtained from the developed regression model by taking the environmental pH (7.0 in this case) into consideration.

Similarly, the thermostability of a wearable sensor is considered an important and useful criterion especially for continuous monitoring applications. Any localized changes in the blood flow rate in the wound milieu can lead to an increase or decrease in the local temperature.[139,229] A decrease in the protein helical content and complete loss of tertiary structure at elevated temperatures results in the inactivation of UOx enzyme.[217] The rate of enzyme degradation at elevated temperatures is reported to be higher than at room temperature. The sensor response is thus expected to degrade at a higher rate at elevated temperatures. The change in sensor response after subjecting the sensor to elevated temperatures was recorded, and a 10% lower current was observed at 40^0C compared to a sensor placed at 25^0C (Figure 5.4).

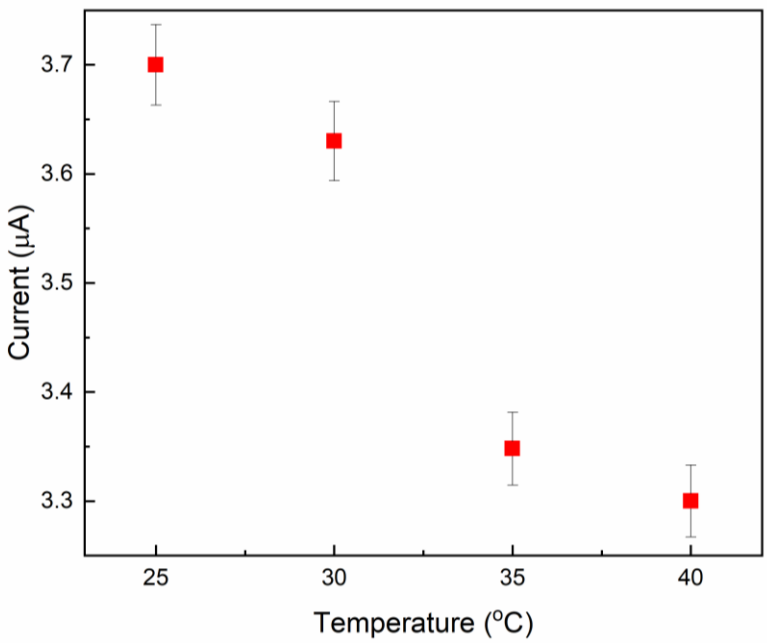

Figure 5.4. Change in UA sensor response of a MWCNT/Au/HRP/UOx functionalized electrode as a function of temperature (25°C, 30°C, 35°C, and 40°C) of the sensor environment. A linear degradation in the sensor response was observed with an increase in the temperature of the sensor's environment. Each experiment was carried out in triplicate (n = 3) and the data is represented as mean ± SD.

Similar to pH, calibration curves for the UA sensor were obtained at different temperatures. It was seen that the sensor response and the sensor sensitivity at higher temperatures was lower, which can be attributed to the deactivation of the enzyme (Figure 5.5a). Using the obtained data, a regression model was developed establish a correlation between the sensor's environmental temperature, sensor response and the corresponding UA concentration (Equation 5.2).

$$Current = (-0.0018 * Conc.) + (0.0283 * temp) - 4.0492 \quad \text{(Equation 5.2)}$$

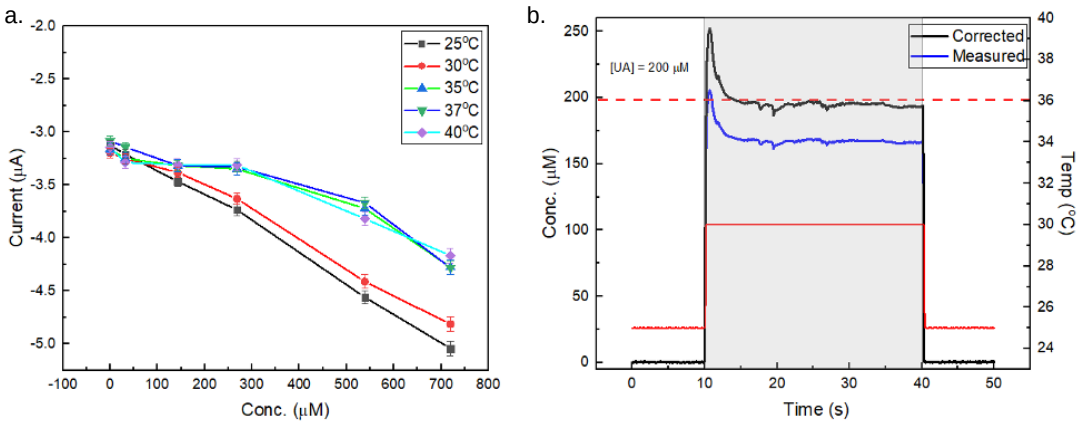

Figure 5.5. a. Calibration curves of the UA sensor in buffers of varying temperatures (25°C, 30°C, 35°C, and 40°C). The highest current density and sensitivity was found at a temperature of 25°C. Each experiment was carried out in triplicate (n = 3) and the data is represented as mean ± SD b. Simultaneous measurement of temperature and UA levels. The blue curve shows the estimated UA concentration on using the standard calibration curve obtained at temperature 25°C and the red curve represents the measured temperature. The black curve represents the corrected UA concentration as obtained from the developed regression model by taking the environmental temperature (30°C in this case) into consideration.

The developed model was further validated by making simultaneous temperature and UA measurements. As seen from Figure 5.5b, the model estimated the UA level with an error of ±3%. As mentioned earlier, a larger sensor dataset will aid in further improvement of the model accuracy. The obtained correlations between the pH, temperature and sensor response can thus be utilized to correct for the calculated UA levels. Moreover, these models can be used in the future to develop an edge IoT-based approach to correct for the sensor response in real-time.

5.3.2 Effect of sample volume and evaporation

One of the fundamental requirements of an electrochemical sensor is that a sufficient amount of sample volume is required to facilitate ion transport between the electrodes. Low exuding chronic wounds pose a major challenge for electrochemical measurements owing to insufficient wetting of the sensor to produce accurate response. The effect of sample volume on the sensor response is thus necessary to be assessed to

determine the volume required for optimal sensor functioning. In a real setting, a dressing is placed in between the sensor and wound to prevent any occlusion effects on the wound. Thus, a small piece of wound dressing (d: 5 mm) was placed over the UA sensor and different volumes of the UA solution were drop casted to allow for uniform distribution of the solution over the sensor surface. Results indicated a 6.8% decrease in the current response from 5 µl to 0.5 µl (Figure 5.6a), while current response for 5 µl or above was seen to be the same. While the sensor was functional at a low volume of 0.5 µl, the results implied that a minimum sample volume of 5 µl was required for accurate UA measurements. Chronic wounds are typically not expected to be completely dry and thus the study established the practical applicability of the sensor for UA measurement in low exuding wounds as well.

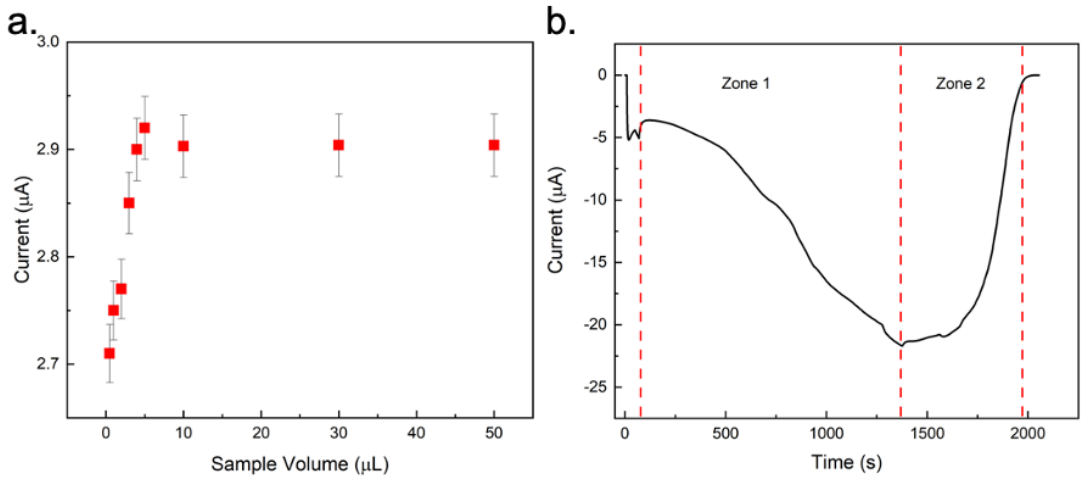

Figure 5.6. a. Change in UA current response of a MWCNT/Au/HRP/UOx functionalized electrode as a function of sample volume (0.5 µl, 1 µl, 2 µl, 3 µl, 4 µl, 5 µl, 10 µl, 30 µl and 50 µl). The minimal sample volume for accurate sensor functioning was found to be 5 µl. Each experiment was carried out in triplicate (n = 3) and the data is represented as mean ± SD b. Change in UA current response of a MWCNT/Au/HRP/UOx functionalized electrode to a 10 µl UA droplet (250 µM) evaporating with time under constant environmental conditions (25ºC and 50% RH). Zone 1 represents the evaporating stage of the droplet, with an increase in the current observed due to the evaporation of the solvent. Zone 2 shows an insufficient coverage of ions over the electrode surface due to evaporation, resulting in a zero current.

Traditionally, wet-to-dry wound dressings are used for dressing chronic wounds since maintaining optimal moisture conditions in a wound is vital. They are designed to maintain a humid environment at the wound site to increase the rate of epithelialization while removing the excess wound exudate. These dressings thus continually evaporate the wicked exudate from the dressing to allow for continued absorption for extended periods of time. While sensing in low sample volumes is challenging due to insufficient sensor wetting, evaporation of these low volumes further adds to the sensing complexity. Additionally, the substrate properties of the wound dressings also play a major role in sample transport. The mass transport dynamics of the UA from the wound environment to the sensor surface is primarily governed by the wicking properties of the dressing. Similar to the volume study, in order to study the effect of evaporation on the sensor response, a 10 µl droplet of UA solution (250 µM) was dropped onto a piece of dressing (d:5 mm) placed on the sensor. The solution was allowed to evaporate under maintained environmental conditions of 25^{o}C and 50% RH while monitoring the current response in real-time. As the sample evaporates, an increase in the current response was observed (Zone 1) due to an increase in the ionic concentration associated with the decreasing sample volume (Figure 5.6b). Subsequently, owing to the complete evaporation of the sample volume after 33 min, insufficient coverage on the sensor surface resulted in a zero-current response (Zone 2). The changes in the ion concentrations in the sample as a result of evaporation thus governs the sensor response and a theoretical model is desirable to map these changes in real-time. Such a model will require to take the substrate properties and UA transport mechanics into consideration to accurately predict the sensor response.

5.3.3 Adsorption of wound debris on active area

Wound exudate is a complex biofluid consisting of proteins, extracellular matrices, blood components and several electrolytes.[230,231] The adsorption of wound debris over the active area of the sensor can lead to the phenomenon of electrode fouling; which can be referred to as the accumulation of unwanted material on the surface, detrimental to the sensor performance. Sensor fouling is one of the critical factors in wound monitoring sensors that can affect the measurements under a continuous time period reducing the reliability of the sensors. When the sensor is placed directly over the wound bed, the different components of the wound exudate can adsorb over the electrode and may start crosslinking. This can result in blocking of a substantial portion of the active area, thereby fouling the electrode and resulting in a low sensor recovery. The change in UA sensor response with fouling was characterized as a function of the dried volume of wound exudate or biofluid extract from perilesional skin. Figure 5.7 illustrates the percentage decrease in current observed over 5 sequential depositions of buffer in absence of biofluid, wound exudate or biofluid extract from perilesional skin. While in the latter two cases, a continuous attenuation of the current response was observed with increasing volume, the degree of fouling of the sensor with adsorbed wound exudate was seen to be 1.5 times higher than the sensor with adsorbed biofluid extract from perilesional skin. The sensor with adsorbed biofluid from perilesional skin showed a similar current degradation rate as the sensor with no biofluid adsorbed. The peak current was observed to reduce by 68.6% after 5 depositions of the wound exudate, while only a 48.5% reduction was seen for the biofluid from perilesional skin adsorbed sensor. After three depositions, the diffusion of UA from the blk solution to electrode surface becomes extremely difficult as reflected in the 20% decrease in the sensor response. While sweat is a complex biofluid, a higher heterogeneity and matrix

complexity is expected in a wound exudate which in turn results in a greater response degradation. The lower degradation rate of the sensor adsorbed with only biofluid extract from perilesional skin can enable the sensor application for long-term monitoring purposes. These results can serve as models for the design and calibration of sensors for accurate response estimation.

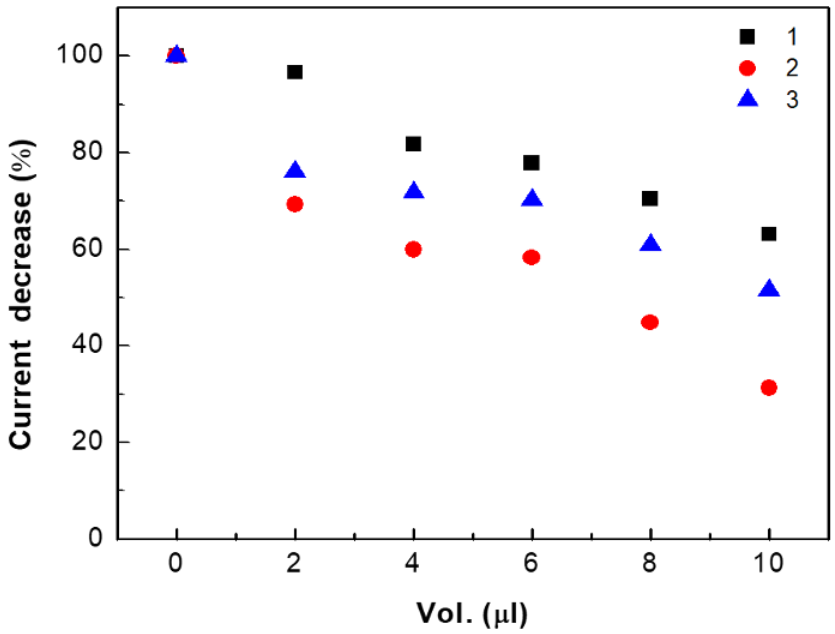

Figure 5.7. Change in current response of the UA sensor as a function of the volume of the buffer (0 µl, 2 µl, 4 µl, 6 µl, 8 µl and 10 µl) in the absence of biofluid (1), wound exudate (2) or perilesional skin extract (3) dried on the nanocomposite-enzyme functionalized electrodes. The higher degradation rate of electrode fouling with wound exudate showed the presence of non-specific adhering compounds present in the biofluid matrix.

Such sensors when placed in an *in vivo* environment especially on a wound bed, produce low recovery values compared to conventional testing, which can be ascribed to the demonstrated fouling effect. A sensor placed in the wound vicinity rather than directly over the wound bed can help reduce the electrode fouling issues. Hence, the measurement of UA levels in the biofluid from perilesional skin may present a promising sensing approach more suitable for continuous wound monitoring.

5.4 Conclusion

In this work, the effect of dynamic variability in the wound biofluid on UA sensor response has been investigated. The parameters under consideration included pH, temperature, sample volume, evaporation, and sensor fouling. In particular, the dynamic variability of these parameters with different wound healing stages is discussed and their effect on the UA sensor response is assessed. The sensor response was seen to be highest at a pH of 7.8, with a decrease in the response observed for both a more alkaline (pH > 8.0) and a more acidic environment (5 > pH > 8.0). The results agreed with the general optimal pH range for the uricase enzyme to be known between 7.5 and 8.5. Similarly, a direct correlation was observed between the sensor response and the operational temperature. A linear decrease in the current was seen as a function of increasing temperature. The results confirmed that as a consequence of these parameters temporally changing in the wound environment, the sensor response will be altered. The established correlations were utilized to develop mathematical models to correct for the real time sensor response obtained when placed in an *in vivo* environment and validated through simultaneous measurements. An optimal sample volume of 5 µl was determined from the sample volume studies. The current was seen to decrease as a function of decreasing volume owing to the insufficient fluid coverage over the electrodes. Further, as result of evaporation the UA concentration was seen to increase reflected as an increase in the current, with zero current observed subsequently due to complete evaporation of the sample volume. Deposition of extracellular proteins on the sensor surface resulted in a degraded sensor response. Physical adsorption of the wound exudate on the sensor surface was seen to result in an impeded UA diffusion to the sensor surface. The results show that changes in environmental parameters of the wound such as, pH and temperature need to be accounted for, in order to obtain accurate

UA sensor response. An integrated platform monitoring these parameters simultaneously may allow for real-time calibration of the UA sensor to obtain reliable *in vivo* measurements.

6 Toxicity Assessment of Wearable Wound Sensor and its Constituents

6.1 Introduction

In an emerging age of wearable medical devices, the health risk from exposure to the active materials incorporated in these devices is a topic of concern. Wearable sensors that monitor biological activity, disease, and metabolism, integrate biochemical sensors in their sensor suite that interface directly with the human body. These biochemical sensors are comprised of a combination of materials to sense the target biological analytes. These materials can be classified into different categories: active sensing materials or reaction catalysts, electron mediators, binders, and crosslinkers. Owing to the unique properties offered by nanoparticles, they are increasingly being used in biochemical sensors as reaction catalysts for improving sensor sensitivity. Biorecognition elements such as enzymes, antibodies, and aptamers fall under the active sensing materials category. While these biorecognition elements may not pose any major biocompatibility issues, questions have been raised about the biocompatibility of several nanoparticles. Previous studies have shown that the toxicity of nanoparticles is dependent on several factors, such as their material, size, shape, stabilizing agent, and concentration. For example, a previously reported study on screening of one such active sensing material, silver nanoparticles (AgNPs), showed that they are toxic to both dermal and epidermal cells at high concentrations.[232,233] It was further shown that given the smaller size of Ag ions, they induced higher toxicity as compared to AgNPs. Another study, on AgNPs, revealed that both the morphology and the stabilizing agent used in nanoparticle synthesis influenced their cytotoxic behavior.[234,235] Exposure to certain nanoparticles (NPs) can also lead to morphological

changes in the cellular structure by altering the shape of the cells to fusiform.[236–238] Carbon nanotubes have been extensively used as an electron mediator and have been reported to exhibit a time and dose-dependent toxicity.[239] A study showed that altering the surface chemistry of the carbon nanotubes leads to morphological changes in the cell.[240] Studies have further shown that some materials not only affect the cell viability but also lead to damage of subcellular organelles, like mitochondria and lysosomes. The damage to these subcellular organelles leads to increased levels of reactive oxygen species (ROS). Mitochondrial disruption has been seen as a result of cellular uptake of silica (SiO_2),[241] iron (Fe) NPs[242] and, multiwalled carbon nanotubes (MWCNTs)[243]. Studies have also shown that a high concentration of NPs can decrease the cellular ATP content, leading to a damaged mitochondrion.[244] Another study showed that the surface charge on gold nanoparticles (AuNPs) regulated their apoptotic inducing nature, wherein a charged AuNP expressed a higher number of apoptotic cells compared to an uncharged NP.[237] Similarly, several other NPs such as TiO_2, CuO, and AgNPs have been shown to induce apoptosis at certain concentrations.[245–247] The above-mentioned studies thus suggest that assessing the toxicity of any material being used in these wearable devices is of utmost importance.

One such example of wearable monitoring sensing systems is wearable wound sensors, which incorporate biochemical sensors that are placed in direct contact with the tissue and wound fluid. An open wound exposes the underlying human tissue, potentially subjecting it directly to the sensor and the active materials integrated within the sensor. Thus, the leaching of any toxic material into an open wound may induce an inflammatory response resulting in a hindered healing process. Therefore, toxicological screening of the active materials used in these wound sensors is highly imperative. *In vitro* human cell culture studies have emerged as an excellent tool for carrying out

preliminary toxicity studies. Based on the target human organ, a relevant cell line can be chosen to determine the toxic effects of the test material(s) under *in vitro* conditions. For instance, keratinocytes and fibroblasts can be used as model cell lines to understand the effect of sensing materials on open wounds. Keratinocytes constitute 90% of the human epidermis, with their primary function being protecting the skin against any environmental damage. They play a critical role in wound healing by participating in the epithelization process. In response to an injury, keratinocytes proliferate and migrate to form the epidermal barrier layer of the skin.[248] On the other hand, fibroblasts are the main connective tissue cells present in the body. They play a major role in the proliferation and remodeling stage of wound healing. These cells create a new extracellular matrix (ECM) and collagen structures that provide support for cell proliferation, thus facilitating wound contraction.[249] Any material toxic to these keratinocytes and fibroblasts may lead to significant impairing of the wound healing process. Thus, for this work, keratinocytes and fibroblasts were cultured *in vitro* to study the toxicity profiles of the active sensing materials used in our sensor. Through these studies, a comprehensive understanding of the toxicity effects and the ability of the cells to tolerate active materials can be developed to build biocompatible sensing systems.

In this chapter, the toxicity profile of the wound monitoring enzymatic sensor is investigated on human keratinocytes and fibroblasts. The sensor incorporates a combination of active sensing materials (biorecognition elements) and reaction catalysts (nanomaterials).[250,251] To assess the toxicity profile, the individual active materials and the fabricated sensor were investigated at different concentrations using the gold standard MTT assay. Furthermore, the mitochondrial and apoptotic effects of these materials was investigated. This was achieved by conducting *in vitro* assays on

an epidermal cell line (HaCaT) and a dermal cell line (HDFa). The chapter details the time and concentration-dependent changes in the cell viability, mitochondrial activity, and apoptotic activity of the cells on treatment with the entire wound sensing system.

6.2 Experimental

6.2.1 Materials and Apparatus

AuNPs (ø: 20 nm) and MWCNTs (9.5 nm × 1.5 μm) were purchased from Sigma Aldrich, USA. Uricase enzyme, horseradish peroxidase (HRP) enzyme, 3-(4, 5-dimethyl thiazolyl-2)-2, 5-diphenyltetrazolium bromide (MTT), and dimethyl sulfoxide (DMSO), Dulbecco's Phosphate Buffered Saline (DPBS) were purchased from Sigma Aldrich and ThermoFisher Scientific, USA respectively. alamarBlue was obtained from ThermoFisher Scientific, USA. Cell culture media, antibiotics, and other cell culture reagents were purchased from Gibco, ThermoFisher. The human epidermal keratinocyte cell line (HaCaT) was kindly provided by Dr. Marcus Cooke at the FIU Department of Environmental Health Sciences, Miami, Florida, and dermal fibroblast cell line (HDFa) was purchased from ATCC.

Fluorescence microscopy of the cells was carried out using a fluorescent microscope (Axio Scope.A1, Zeiss). The fluorescence intensity measurement was performed using a Synergy HTX Multi-Mode microplate reader (BioTek Instruments, USA). A Multiskan™ FC microplate reader (ThermoFisher Sc., USA) was used for absorbance measurements.

6.2.2 Exposure of keratinocytes and fibroblasts to the treatment groups

Cells (keratinocytes and fibroblasts) were maintained in Dulbecco's Modified Eagle's Medium (DMEM) and supplemented with a 10% fetal bovine serum (FBS) and 1%

antibiotics (penicillin/streptomycin). The cells were maintained in an atmosphere of 5% CO_2 at 37^{o}C and 70% RH until 70% confluency and then introduced to the different treatment groups. Five different treatment groups were selected for our study namely, gold nanoparticles (AuNPs), multiwalled carbon nanotubes (MWCNTs), uricase enzyme (UOx), horseradish peroxidase enzyme (HRP), and the biosensor. The toxicity profile of these treatment groups was assessed at different concentrations and different treatment periods as provided in Table 6.1. Three concentrations of each treatment group were tested for their toxicity at two different time points: 12 and 24 h. Concentration C2 in the table represents the concentrations of the materials as immobilized on the sensor, and C1 and C3 were taken as ten times lower and higher than C2.

Table 6.1. The treatment groups and the respective test concentrations used for assessing their cytotoxicity on epidermal (HaCaT) and dermal (HDFa) cell lines. In the table C1, C2, C3 represent concentration, and G1, G2, G3, G4, and G5 represent the test groups. Concentration C2 in the table represents the concentrations of the materials as immobilized on the sensor, and C1 and C3 were taken as ten times lower and higher than C2.

Treatment group	**Test concentrations**
G1: AuNPs	**C1**:0.5, **C2**:5 and **C3**:50 µg/ml
G2: MWCNTs	**C1**:0.001, **C2**:0.01 and **C3**:0.1 µg/ml
G3: UOx	**C1**:0.2, **C2**:2 and **C3**:20 µg/ml
G4: HRP	**C1**:0.02, **C2**:0.2 and **C3**:2 µg/ml
G5: Biosensor	**C1**: Unfunctionalized sensor **C2**: Functionalized sensor (AuNPs: 5 µg/ml, MWCNTs: 0.01 µg/ml, UOx: 2 µg/ml and HRP: 0.2 µg/ml)

6.2.3 Assessment of cell toxicity using MTT assay

The cell viability of keratinocytes and fibroblasts exposed to the different treatment groups was probed using the MTT assay. This assay is a colorimetric assay widely used for assessing cell viability. In living cells, the yellow-colored tetrazole gets converted to purple formazan crystals. The insoluble formazan crystals are then dissolved using a solubilization solution (DMSO) and the color intensity of the solution can be quantified at 570 nm using a plate reader to determine the cell viability.[252] The NAD(P)H-dependent oxidoreductase enzymes present in the cytosol of the cell catalyze this reaction, thus reflective of the cellular activity.[253] To evaluate the toxicity profile of the treatment groups IC70 values were taken into consideration in our study.[254]

HaCaT/HDFa cells were seeded in a 96-well plate with 10,000 cells per well and cultured until 70% confluency was reached. Subsequently, the original medium was replaced by medium containing a treatment group at different concentrations and incubated for varying time points (12 and 24 h). A volume of 20 μl (5 mg ml^{-1}) of MTT was added to each well and incubated at 37°C for 4 h. Finally, the medium was removed and 200 μl of dimethylsulfoxide (DMSO) was added to each well. Absorbance was measured at 570 nm using a microplate reader. Cells not exposed to any treatment group served as a set of negative control for the experiments and cells exposed to 70% ethanol for 15 min served as a set of positive control.[255,256]

6.2.4 Assessment of cell viability using live/dead assay

To assess the cell viability through imaging as a result of exposure to the different treatment groups, time-lapse fluorescent microscopic images were captured. A live/dead viability/cytotoxicity kit (ThermoFisher Sc., USA) was used for tagging the live/dead cells. Calcein AM and ethidium homodimer are the two dye molecules used to indicate live and dead cells, respectively. In live cells, calcein AM diffuses within

the cytoplasm via the plasma membrane and hydrolyzes to produce green fluorescent calcein.[257] This reaction is the result of the esterase activity of cells trapped within the cytosol. If the cell is dead, ethidium homodimer, a membrane impermeant dye molecule intercalates to the free nucleic acids indicating a compromised cell membrane integrity by exhibiting a red fluorescence.[258]

HaCaT/HDFa cells were seeded in a 96-well plate with 10,000 cells per well and cultured until 70% confluency was reached. Subsequently, the original medium was replaced by medium containing the treatment group at different concentrations and incubated for varying time points (12 and 24 h). After exposure to the treatment groups, the cells in the 96-well plate were incubated with the fluorescent dyes at optimal concentrations in dark at 25°C for 30 min following which the cells were imaged under a fluorescent microscope at 20x magnification of the objective lens. Cells not exposed to any treatment group served as a set of negative control for the experiments and cells exposed to 70% ethanol for 15 min served as a set of positive control.[259,260] Five images were taken per well to obtain statistically relevant data. The obtained images were further used to calculate the cell viability by manually counting the number of green and red cells in each image.

6.2.5 Assessment of mitochondrial activity

The mitochondrial activity of the cells exposed to the treatment groups was investigated using the resazurin assay. The cellular dehydrogenases present inside the mitochondria reduce resazurin (pink color) to form resorufin (red color) resulting in a colorimetric change. The resulting color intensity can then be correlated to the number of respiring cells (Eq. 1). The reduction of resazurin is carried out by different oxidoreductase enzymes present within the mitochondria, thus indicating the cellular mitochondrial activity.[261]

$$resazurin_{ox} + 2H^+ + 2e^- \leftrightarrow resazurin_{red}$$ Equation 1

HaCaT cells/HDFa cells were seeded in a 96-well plate with 10,000 cells per well and cultured until 70% confluency was reached. Subsequently, the original medium was replaced by medium containing the treatment group at different concentrations and incubated for 24 h. Alamar Blue was added (10% final volume) to the treated cells and incubated at 37°C. Following an incubation time of 4 h, the absorbance levels were measured using a microplate reader at 570 nm excitation and 600 nm reference wavelengths. A subtraction analysis of the dual wavelength was performed to obtain accurate measurements. Cells not exposed to any treatment group served as a set of negative control for the experiments and cells exposed to carbonyl cyanide m-chlorophenyl hydrazone (CCCP) served as a set of positive control.[262–264]

6.2.6 Assessment of apoptotic activity

The apoptotic activity of the cells exposed to the treatment groups was investigated using the Caspase 3/7 assay. Caspase-3 and caspase-7 are major and early indicators of apoptosis; these caspases are activated following the leakage of cytochrome C from the mitochondria.[265] The Caspase-3/7 assay is a fluorogenic substrate, consisting of a four amino acid peptide (DEVD) conjugated to a DNA binding dye. On activation of Caspase-3/7 in the apoptotic cell, the DEVD peptide is cleaved and the dye binds to DNA, producing a bright fluorescence response.[266]

HaCaT cells/HDFa cells were seeded in a 96-well plate with 10,000 cells per well and cultured until 70% confluency was reached. Subsequently, the original DMEM was replaced by DMEM containing the treatment group at different

concentrations and incubated for 24 h. Next, the medium was removed and 100 µl of Caspase 3/7 reagent (5 µM) was added to the wells. Following this, the cells were incubated at 37°C for 30 min and fluorescence was measured at excitation/emission wavelengths of 502/530 nm. Cells not exposed to any treatment group served as a set of negative control for the experiments and cells exposed to 10 µM camptothecin for 8 h served as a set of positive control.[267,268]

6.3 Results and Discussion

6.3.1 Assessment of cell toxicity using MTT assay

As discussed in the earlier chapters, the wound monitoring sensor used in this study was fabricated using screen-printing and is constituted of active materials that include AuNPs, and MWCNTs as electron transport substrates, and UOx, and HRP as the biorecognition elements. In vitro testing has been widely employed as the first step in assessing the biocompatibility of a certain material. The cytotoxicity of the above materials was determined using an MTT assay, to understand their effect on dermal and epidermal cells.

For both the cell lines, a time and dose-dependent decrease in cell viability was seen when treated with AuNPs. It was observed that at a lower concentration (effective concentration on the sensor, < 5 µg/ml) the cell viability was higher than 70% (IC70), confirming no cytotoxic effect (Figure 6.1a and Figure 6.2a). Beyond 5 µg/ml concentration of AuNPs, the cell viability decreased <50%, probably due to the generation of reactive oxygen species or toxicity of AuNPs[269] (Figure 6.1a and Figure 6.2a). The cytotoxic nature of the nanoparticles at higher concentrations can also be attributed to the surfactants used for stabilizing the NPs.[270] Contrary to AuNPs, in the case of MWCNTs no cytotoxic nature for both the cell lines was observed. At

concentrations > 0.1 µg/ml, the cell viability was observed to be >80% after exposure for 24 h (Figure 6.1b and Figure 6.2b). The biocompatible nature of MWCNTs is the reason they have been widely employed as catalysts especially in wearable applications.[271,272] As opposed to single-walled CNTs, multi-walled CNTs have been seen to exhibit no cytotoxic effects. Cell viability was observed to be 80% on treatment with UOx at the highest concentration for both the cells after a 24 h exposure. The higher cell viability (>70%) indicated that both the enzymes were non-toxic (Figure 6.1c,d and Figure 6.2c,d). The slight decrease in the viability on exposure to the UOx enzyme may be attributed to the presence of uric acid in the bovine serum present in the growth media. The production of hydrogen peroxide (H_2O_2) produced by the enzymatic reaction between the two materials (UOx and UA) may result in cell viability reduction.[273] It is well known that high concentrations of H_2O_2 result in cytotoxic behavior.[274] Since our results show reduced cell viability at higher UOx concentrations, it could be inferred as a result of increased H_2O_2 production.

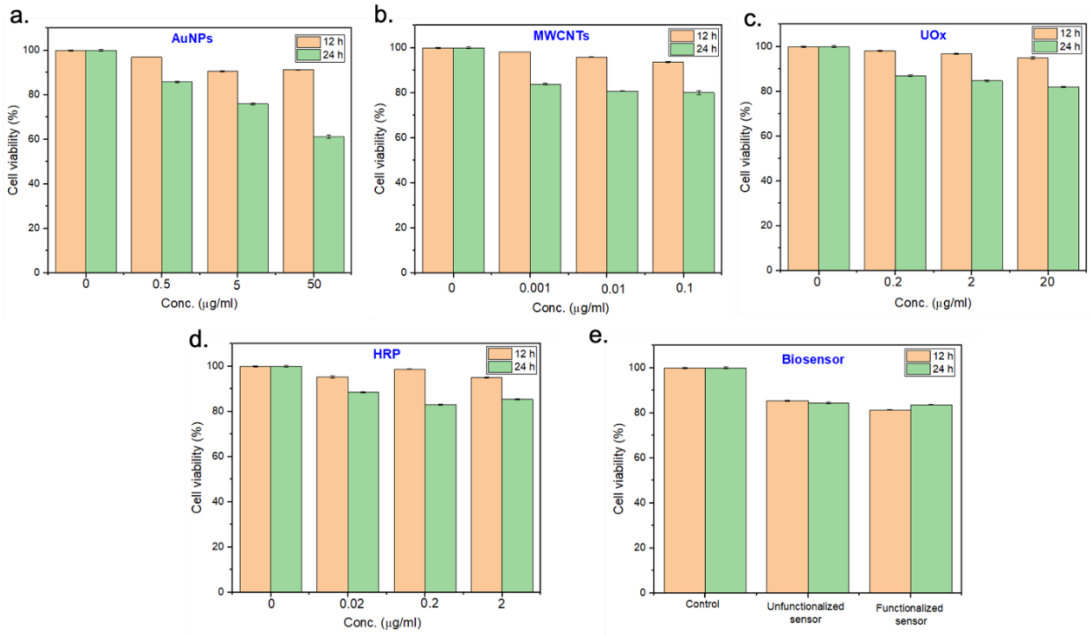

Figure 6.1. Cytotoxicity assessment of the active materials and sensor on the epidermal cell line, HaCaT. The x-axis represents the concentration of the test compound (µg/ml) and the y-axis represents the cell viability (%). Bar graphs depict the cell viability assessed by MTT assay in response to the treatment group a. AuNPs, b. MWCNTs, c.

UOx, d. HRP and e. sensor at varying concentrations and time points. All the data is depicted as mean ± SD from three (n = 3) independent experiments.

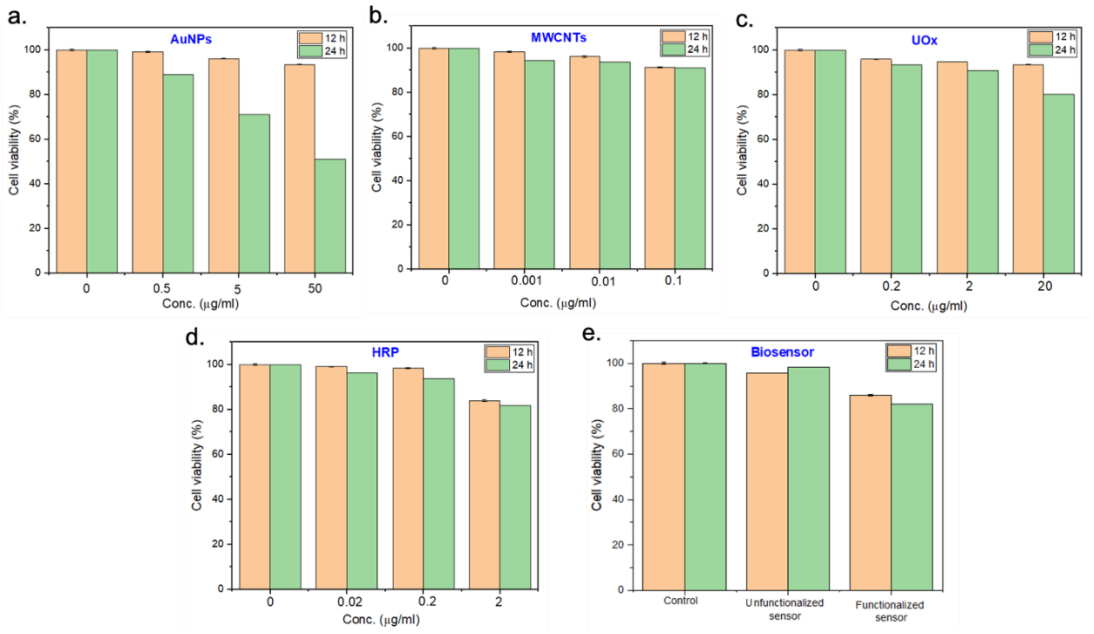

Figure 6.2. Cytotoxicity assessment of the active materials and sensor on the dermal cell line, HDFa. The x-axis represents the concentration of the test compound (µg/ml) and the y-axis represents the cell viability (%). Bar graphs depict the cell viability assessed by MTT assay in response to the treatment group a. AuNPs, b. MWCNTs, c. UOx, d. HRP and e. sensor at varying concentrations and time points. All the data is depicted as mean ± SD from three (n = 3) independent experiments.

Since the sensor utilizes screen-printed inks for its fabrication, we hypothesized that the inks may result in leaching of material which may induce a cytotoxic response. Thus, to evaluate the toxicity profile of the sensor/ink, we carried out an MTT assay on an unfunctionalized and functionalized sensor. The cell viabilities for an unfunctionalized sensor were recorded to be 85% and 98% for epidermal and dermal cell lines respectively (Figure 6.1e and Figure 6.2e). The higher % viability (>70%) suggested insignificant toxicity to either of the cells. On the other hand, cell viabilities of 83% and 82% were observed for a functionalized sensor after a 24 h treatment of the cells to the functionalized sensor for epidermal and dermal cell lines respectively (Figure 6.1e and Figure 6.2e). This slight decrease in the viability observed for the functionalized sensor can be owed to the immobilized active materials. It was observed

that the cell viability for the functionalized sensor was higher than that for the individual materials. This cell viability can be attributed to the enzyme casting over the nanomaterials. The enzyme matrix acts as a biocompatible coating over the biosensor resulting in reduced leaching of the sensor materials. Thus, our results (i) confirm that all the active materials used in the sensor exhibit no significant toxicity with cell viabilities being above 70% for the concentrations as used in the sensor and (ii) suggest that a functionalized sensor elicits only marginal effects on epidermal and dermal cell proliferation and viability.

6.3.2 Assessment of cell viability using live/dead assay

Fluorescent microscopy was carried out to assess the cell viability on exposure to the different treatment groups (AuNPs, MWCNTs, UOx, HRP, and sensor) at varying concentrations and time points (Figure 6.3 and Figure 6.4) for the dermal and epidermal cell lines. A live/dead staining protocol was used which distinguishes cells with a compromised cell membrane by tagging them red. Cells (HDFa and HaCaT) when treated with AuNPs at a concentration >5 µg/ml for 24 h revealed a higher number of dead cells, indicated by the red fluorescent dye (Figure 6.3b and Figure 6.4b) as compared to the negative control (Figure 6.3a and Figure 6.4a). In the case of MWCNT, UOx, and HRP enzyme a high number of live cells were observed for both HDFa and HaCaT cells (Figure 6.3c,d,e and Figure 6.4c,d,e). However, epidermal cells were observed to be more sensitive compared to the dermal cells (Figure 6.4c, d and e). In addition, treatment of both the cell lines with an unfunctionalized and functionalized sensor showed a lesser number of dead cells. As mentioned before, this can be attributed to the protective layer offered by the enzyme matrix over the AuNPs and MWCNTs (Figure 6.3f and Figure 6.4f). To corroborate the cell viability obtained from the MTT assay, image analysis was carried out using the captured fluorescence images by

manually counting the number of live and dead cells to calculate the cell viability (Appendix 1).

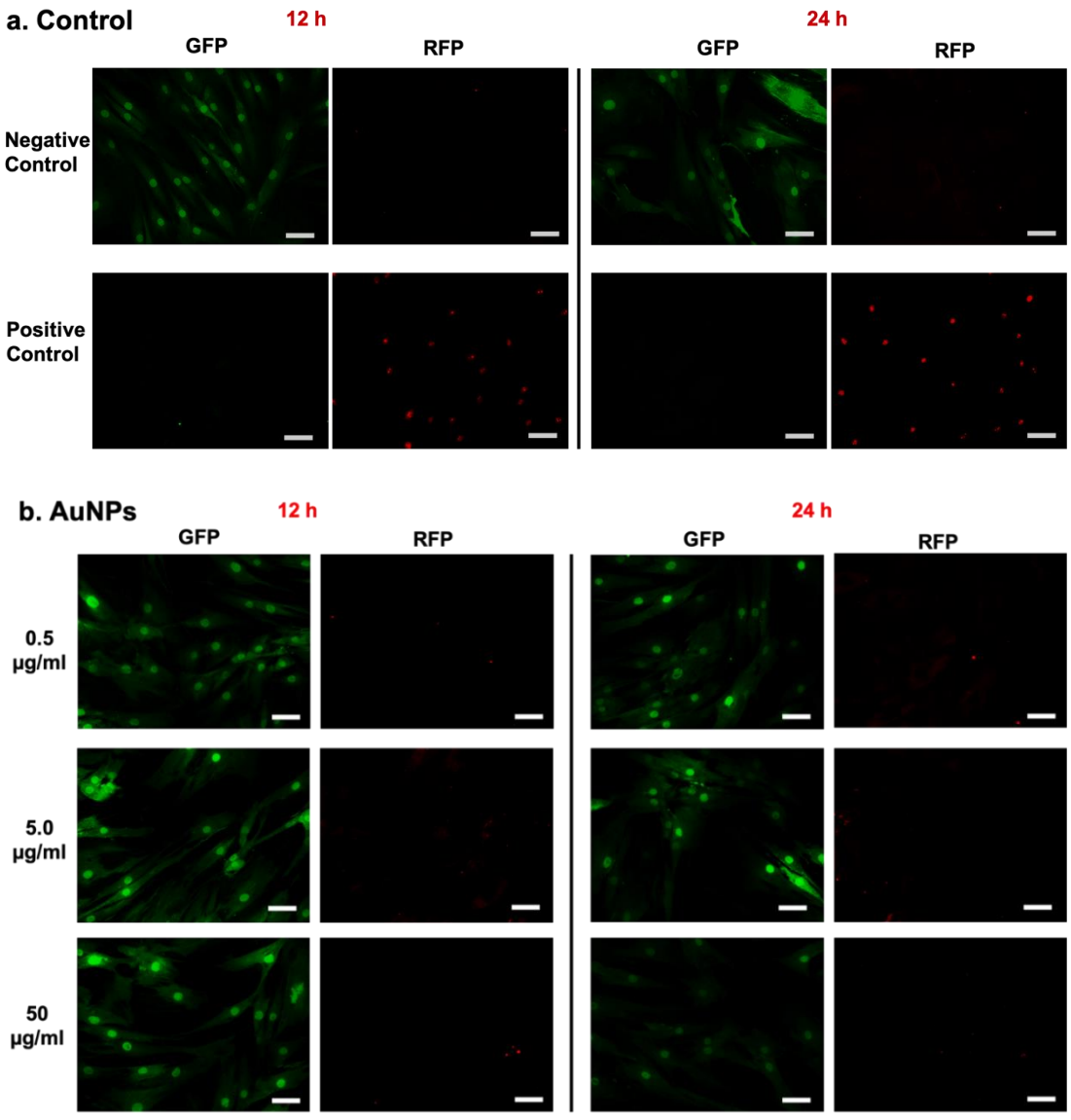

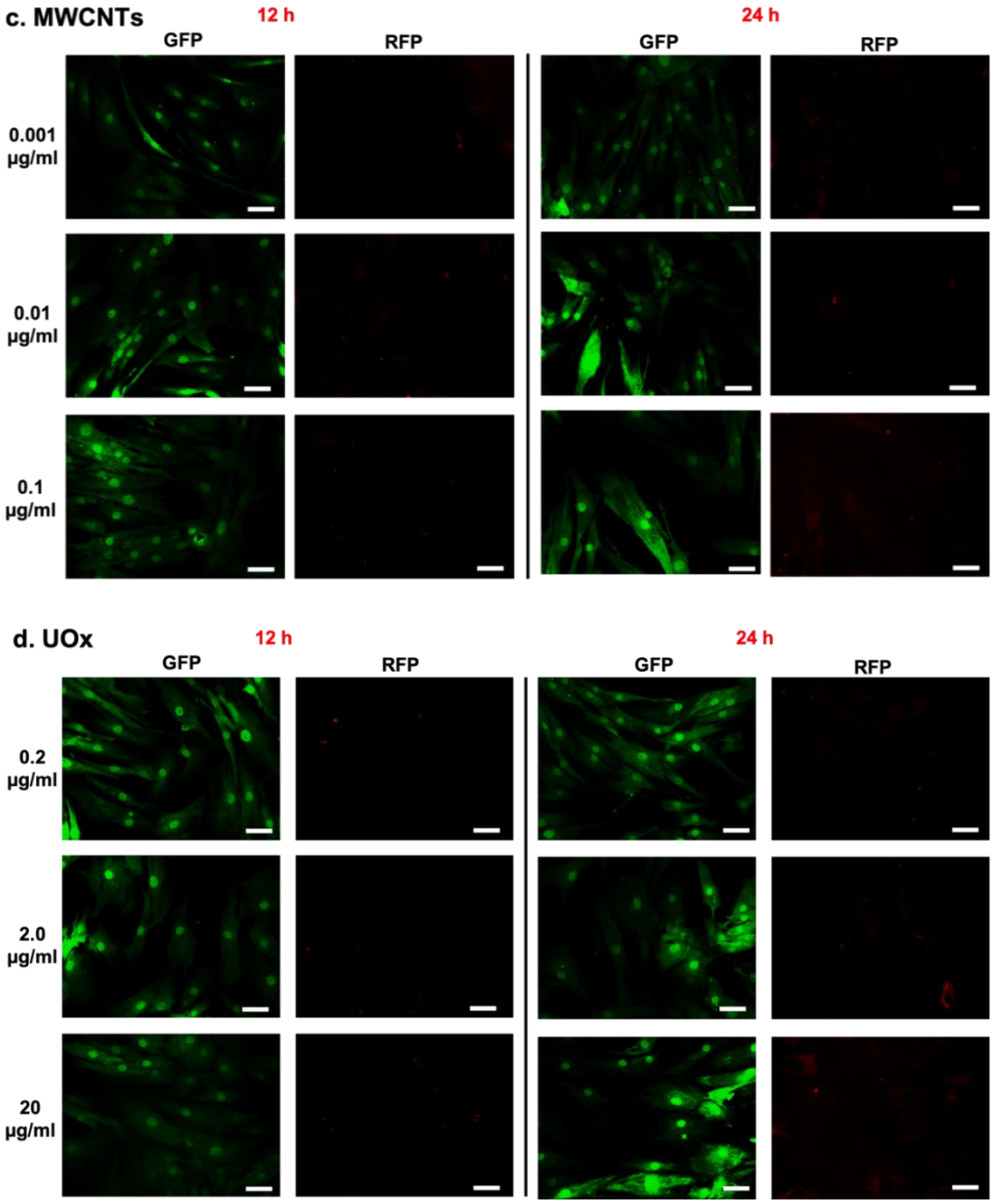
c. MWCNTs
12 h
24 h
GFP
RFP
GFP
RFP
0.001 µg/ml
0.01 µg/ml
0.1 µg/ml
d. UOx
12 h
24 h
GFP
RFP
GFP
RFP
0.2 µg/ml
2.0 µg/ml
20 µg/ml

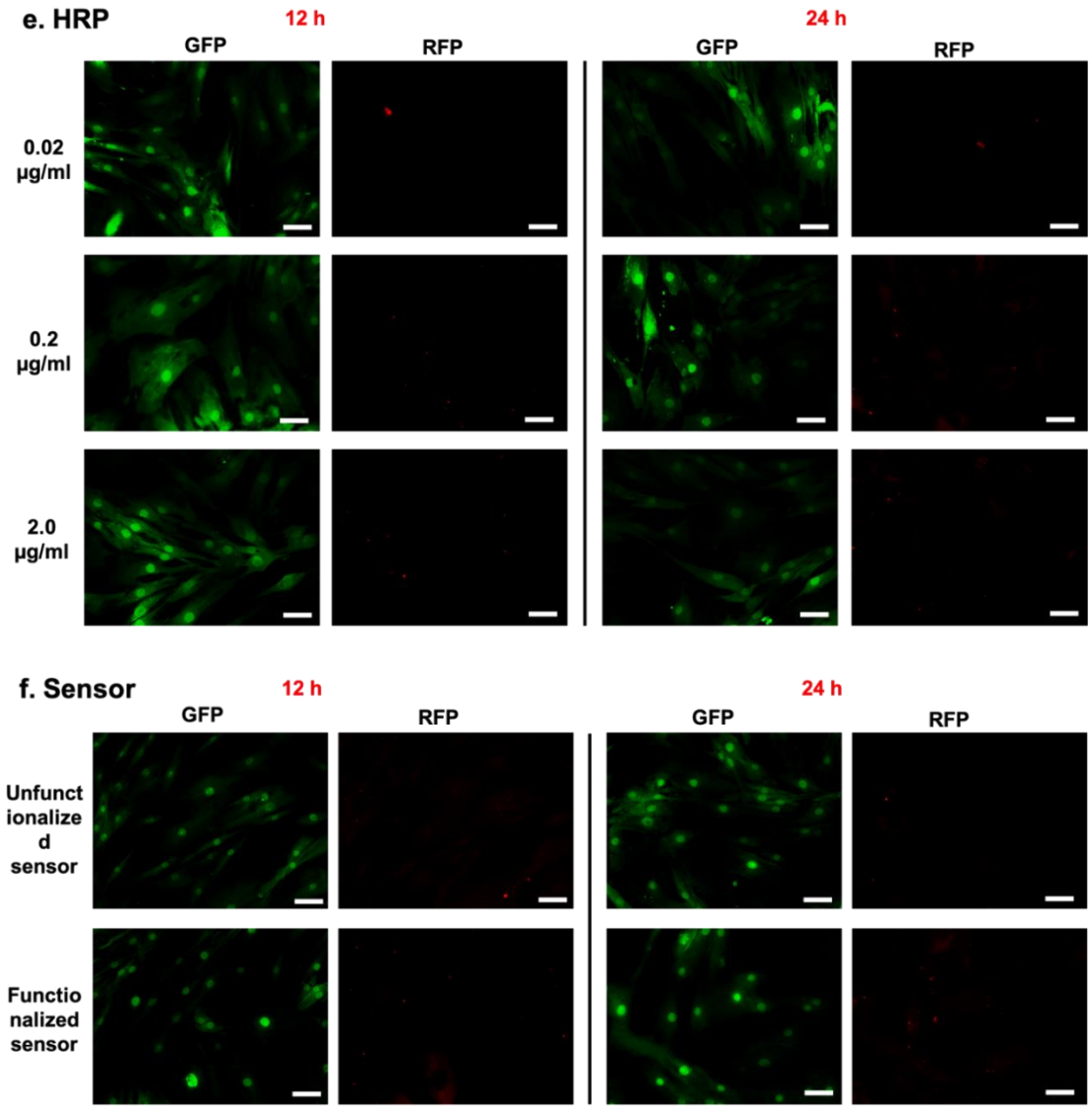

Figure 6.3. Live/Dead stained fluorescent images of HDFa (fibroblasts) when exposed to the different treatment groups. Representative fluorescent images captured after treatment with a. Control group (cells exposed to no treatment served as the negative control and the cells treated with 70% ethanol for 15 min served as the positive control) b. AuNPs (0.5, 5 and 50 µg ml^{-1}), c. MWCNTs (0.001, 0.01 and 0.1 µg ml^{-1}), d. UOx (0.0005, 0.005 and 0.05 U ml-1), e. HRP (0.0005, 0.005 and 0.05 U ml-1) and the f. sensor (functionalized and unfunctionalized), respectively at different time points (12 h and 24 h). In the images, the green color (calcein dye) represents the live cells while the red color (ethidium homodimer dye) represents the dead cells. Each experiment was carried out in triplicate (n=3) and five images were captured per well to account for spatial distribution. Magnification: 20x, Scale bars: 50 µm.

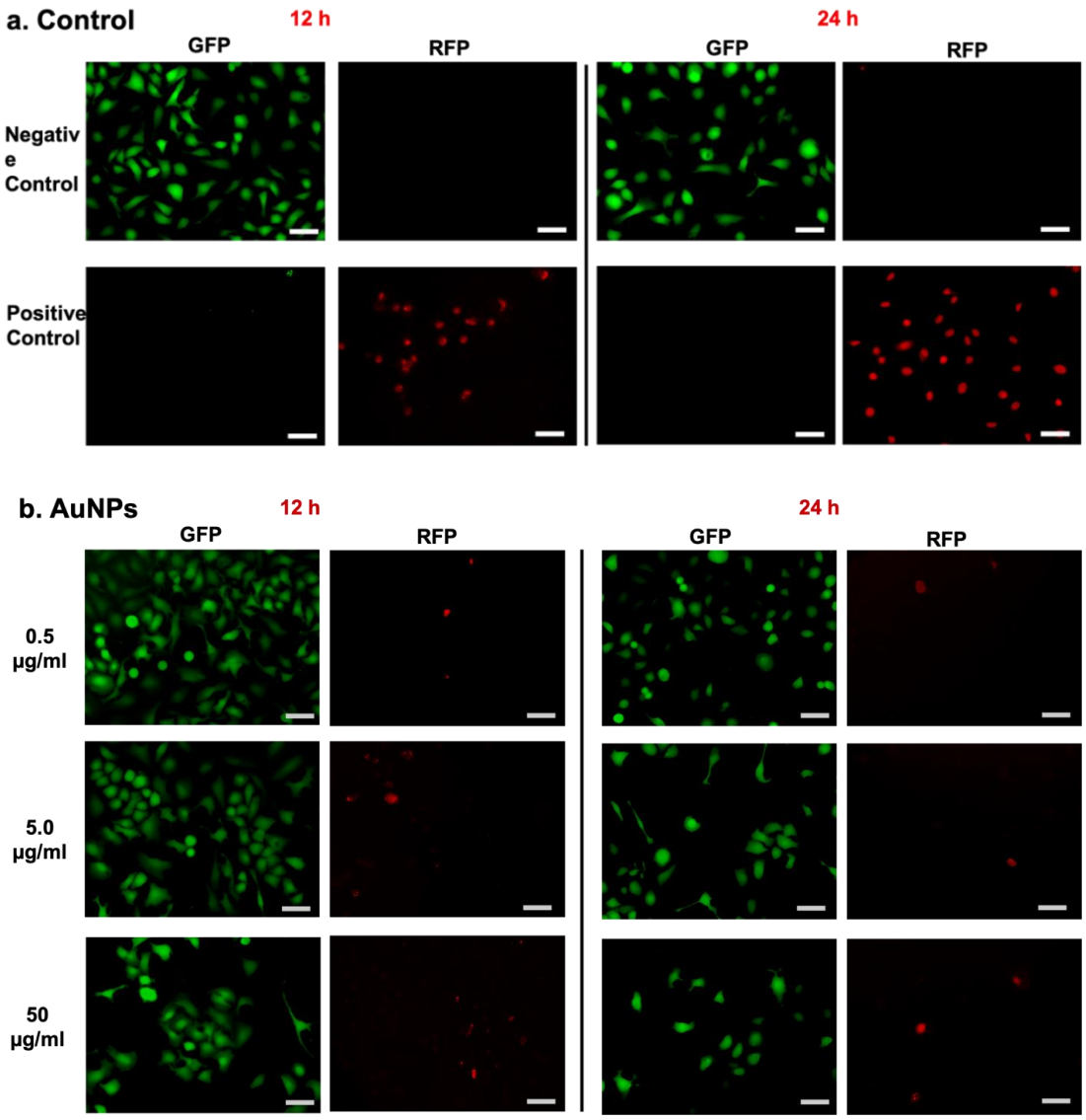
a. Control
12 h
24 h
GFP
RFP
GFP
RFP
Negative Control
Positive Control
b. AuNPs
12 h
24 h
GFP
RFP
GFP
RFP
0.5 µg/ml
5.0 µg/ml
50 µg/ml

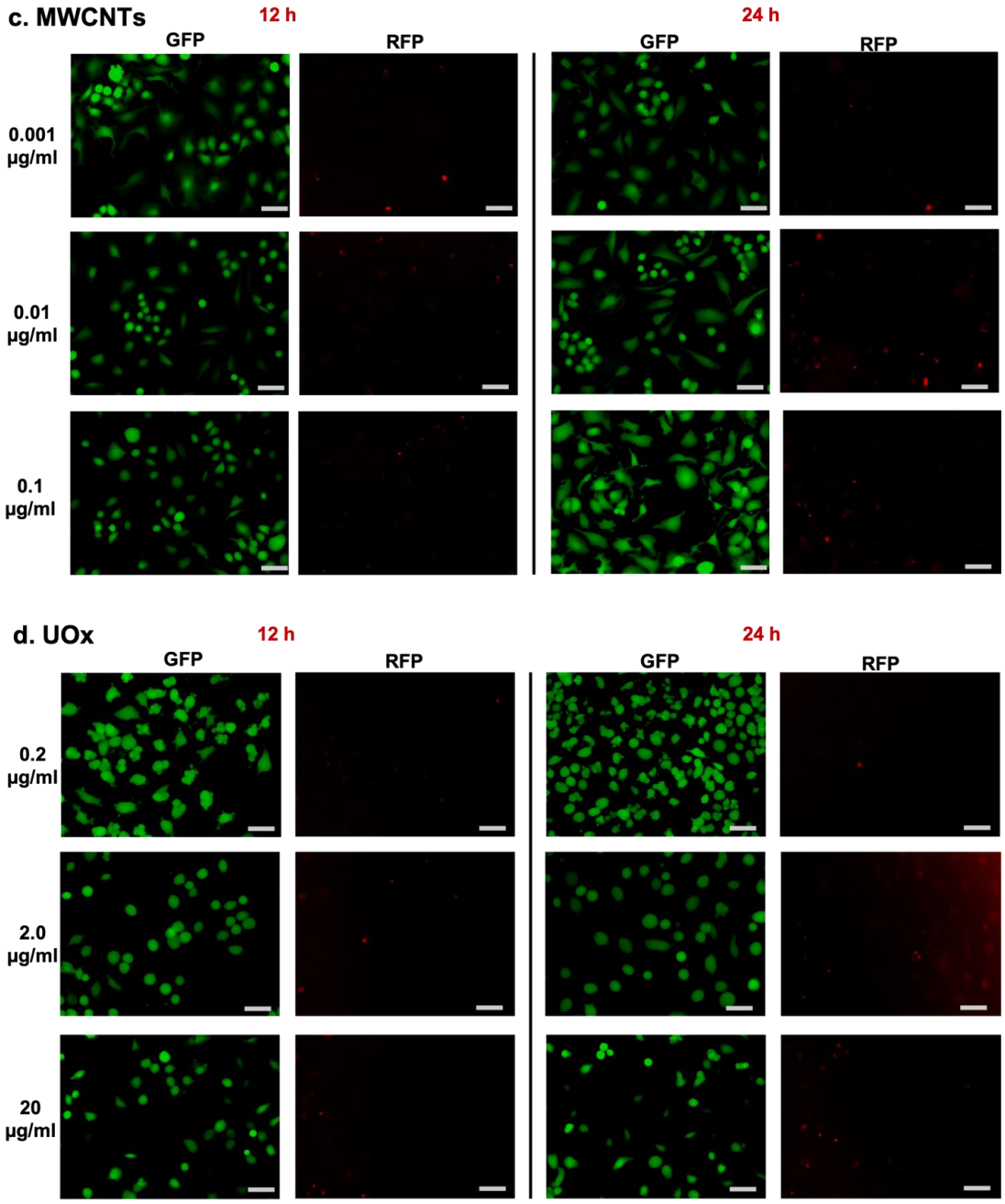
c. MWCNTs
12 h
24 h
GFP
RFP
GFP
RFP
0.001 µg/ml
0.01 µg/ml
0.1 µg/ml
d. UOx
12 h
24 h
GFP
RFP
GFP
RFP
0.2 µg/ml
2.0 µg/ml
20 µg/ml

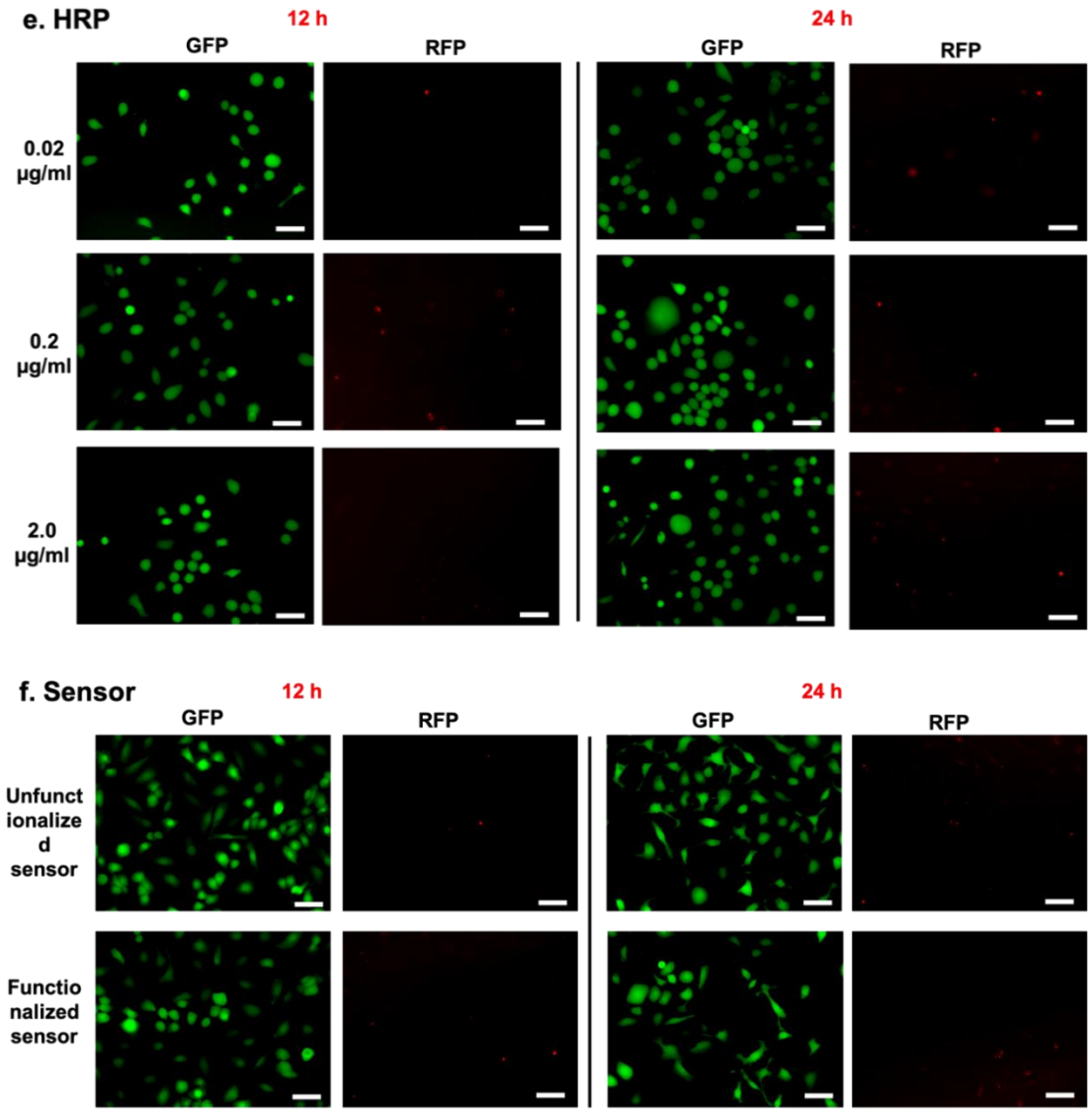

Figure 6.4. Live/Dead stained fluorescent images of HaCaT (keratinocytes) when exposed to the different treatment groups. Representative fluorescent images captured after treatment with a. Control group (cells exposed to no treatment served as the negative control and the cells treated with 70% ethanol for 15 min served as the positive control) b. AuNPs (0.5, 5 and 50 µg ml^{-1}), c. MWCNTs (0.001, 0.01 and 0.1 µg ml^{-1}), d. UOx (0.0005, 0.005 and 0.05 U ml-1), e. HRP (0.0005, 0.005 and 0.05 U ml-1) and the f. sensor (functionalized and unfunctionalized), respectively at different time points (12 h and 24 h). In the images, the green color (calcein dye) represents the live cells while the red color (ethidium homodimer dye) represents the dead cells. Each experiment was carried out in triplicate (n=3) and five images were captured per well to account for spatial distribution. Magnification: 20x, Scale bars: 50 µm.

6.3.3 Evaluation of mitochondrial activity

The metabolic activity of the epidermal and dermal cells after a 24 h exposure to the different treatment groups is provided in Table 6.2. The values demonstrate a minimal

decrease in the mitochondrial activity of the HaCaT cells after exposure to AuNPs, UOx, and HRP. The data further suggested a slight decrease in the activity to 0.87, at a higher concentration of MWNCTs. The functionalized sensor showed decreased activity (0.85) as compared to an unfunctionalized sensor (0.96), which is a result of the active materials immobilized on the sensor. On the contrary, the dermal cells, HDFa, showed higher sensitivity resulting in reduced mitochondrial activity in comparison to HaCaT cells. The cell activity on exposure to AuNPs reduced to 0.83 at a higher concentration, implying reduced cellular metabolic rate as Au interferes with the oxidative pathway in the mitochondria. Previous studies have shown that smaller NPs, result in the production of high superoxide levels resulting in mitochondrial dysfunction.[275] However, the cellular activity remained >0.85 for cells exposed to MWCNTs, UOx, and HRP enzyme. Similar to the epidermal cells, the dermal cells on exposure to an unfunctionalized sensor (0.91) showed higher activity levels compared to a functionalized sensor (0.86). The results for all the treatment groups demonstrated no effect on the metabolic activity of the dermal and epidermal cells at concentrations present in the sensor.

Table 6.2. Resazurin mitochondrial assay. Mitochondrial activity in epidermal (HaCaT) and dermal (HDFa) cells after a 24 h treatment with the different treatment groups, quantified using the AlamarBlue assay. The presented data shows the results of three independent experiments (n = 3). Values are presented as the mean ± SD.

Treatment Group	**Concentration (µg/ml)**	**Mitochondrial activity (Mean ± SD)**	
		Epidermal cell line (HaCaT)	**Dermal cell line (HDFa)**
AuNPs	0.5	0.99 ± 0.01	0.88 ± 0.01
	5	0.91 ± 0.02	0.83 ± 0.01

	50	0.99 ± 0.04	0.89 ± 0.05
MWCNTs	0.001	0.92 ± 0.04	0.85 ± 0.01
	0.01	0.89 ± 0.02	0.87 ± 0.01
	0.1	0.87 ± 0.02	0.87 ± 0.01
UOx	0.2	0.91 ± 0.04	0.90 ± 0.03
	2	0.92 ± 0.02	0.86 ± 0.01
	20	0.93 ± 0.01	0.87 ± 0.01
HRP	0.02	0.98 ± 0.02	0.94 ± 0.05
	0.2	0.96 ± 0.02	0.87 ± 0.01
	2	0.99 ± 0.01	0.76 ± 0.01
Sensor	Unfunctionalized	0.96 ± 0.02	0.91 ± 0.05
	Functionalized	0.85 ± 0.03	0.86 ± 0.01

6.3.4 Evaluation of apoptotic activity

The apoptotic effect of the active materials and the sensor on the epidermal and dermal cell lines after 24 h exposure was examined. All the treatment groups exhibited no apoptotic activity, probably suggesting an alternative cell death pathway (necrotic or induced due to ROS). For both the cell lines, exposure to AuNPs, MWCNTs, UOx and HRP showed ~2.3% cells expressing apoptotic activity at the concentrations present in the sensor (Table 6.3). A 2.67% and 3% of apoptotic cells were expressed on exposure to a higher concentration of AuNPs for epidermal and dermal cell lines respectively. Exposure to both the enzymes also resulted only in ~2% of apoptotic cells (Table 6.3). Furthermore, the low percentage of apoptotic cells of ~2% demonstrated that the sensor also showed no caspase-3/7 activity. The decreased apoptosis by the sensor may again

be attributed to the reduced percolation of the nanomaterials through the enzyme matrix. The obtained data indicate no apoptotic activity for any treatment group.

Table 6.3. Caspase 3/7 activity in epidermal (HaCaT) and dermal (HDFa) cells after a 24 h treatment with the different treatment groups, quantified using the Caspase-Glo 3/7 Assay. The presented data shows the results of three independent experiments (n = 3). Values are presented as the mean ± SD.

Treatment Group	**Concentration (µg/ml)**	**% Apoptotic cells (Mean ± SD)**	
		Epidermal cell line (HaCaT)	**Dermal cell line (HDFa)**
AuNPs	0.5	1.33 ± 1.11	2.00 ± 0.67
	5	2.33 ± 0.44	2.33 ± 0.88
	50	2.67 ± 1.11	3.00 ± 0.67
MWCNTs	0.001	1.00 ± 0.66	1.33 ± 0.88
	0.01	1.67 ± 0.44	1.67 ± 0.88
	0.1	2.33 ± 1.11	2.00 ± 0.67
UOx	0.2	1.33 ± 0.44	1.00 ± 0.67
	2	2.33 ± 1.55	1.00 ± 0.67
	20	2.33 ± 0.88	1.67 ± 0.88
HRP	0.02	1.00 ± 0.67	1.00 ± 0.67
	0.2	1.67 ± 0.44	1.67 ± 0.44
	2	2.00 ± 0.67	2.33 ± 0.88
Sensor	Unfunctionalized	1.33 ± 0.44	1.00 ± 0.67
	Functionalized	1.67 ± 0.44	2.00 ± 0.67

6.4 Conclusion

This chapter investigated the cytotoxicity profiles of the active materials used in the wound monitoring sensor and the sensor itself on human keratinocytes (HaCaT) and fibroblasts (HDFa). The cell viability studies indicated that all the active materials in the sensor and the sensor itself show no toxicity at IC70 dose at the concentrations present in the sensor. Higher cell viability was observed when the cells were subjected to functionalized sensors as compared to the individual active materials which was attributed to the protective layer offered by the enzyme matrix. The resazurin assay confirmed no impairment of the mitochondrial function induced by the active materials and the sensor. The results established that the active materials and the respective sensor incur a minimal loss in viability, mitochondrial damage, and showed no apoptotic cell death on exposure at concentrations present in the sensor to both the epidermal and dermal cell lines. The study confirmed that the fabricated sensor and its constituent active materials are not toxic in *in vitro* studies. The results from this investigation pave the way towards further testing on *in vivo* wound model systems.

7 Clinical Validation of the Uric Acid Monitoring Sensor

7.1 Introduction

Venous leg ulcers represent one of the most prevalent forms of chronic wounds especially in the US affecting 600,000 people annually.[276] They require a significant amount of healthcare resources with an estimated annual treatment cost of $2.5-3.5 billion.[277] Moreover, around one-third of the treated patients experience a recurrence of the ulcerations, resulting in a reduced quality of life.[278] The molecular biology of these wounds differs significantly from healing wounds, with various factors affecting the healing rate.[279–281] Treatment of these ulcers is costly and time consuming with patients requiring multiple clinical visits.[282] Standard clinical guidelines recommend color duplex ultrasonography or Doppler measurement to assess the outcomes of the wound treatments which requires expensive equipment and skilled personnel.[283,284] There is a need for technologies that can assess the healing efficacy of the provided treatments in real-time to allow for efficient wound care management.

Physical and chemical assessment parameters of the wound environment such as pH and pressure,[144,145,147,173] bacterial metabolites,[148,149], and purine metabolites[150–153] have provided alternatives to subjective measures like visual inspection, optical techniques[285] or, wound size measurements[142,143] enabling continuous wound monitoring. These sensing approaches offer significant advantages for longitudinal measurements providing real-time information about wound health. Sensors integrated directly onto wound dressings, also termed as “smart bandages”, allow for easy integration of the sensors on the wound without causing any patient discomfort. As mentioned in the earlier chapters, UA, a purine metabolite is known to have a direct correlation with the different stages of wound healing. It has been shown that UA

measurement can provide real-time assessment of the wound status enabling a way towards effective and timely therapeutic interventions for improved patient care at a personalized level.[251] Several smart bandages have been reported for electrochemical detection of UA in wound exudates on flexible sensor substrates. However, despite the advancements in the development of these smart bandages for UA detection, no human *in vivo* validation studies have been conducted with these sensors till date.

For the first time, this work aims to establish the feasibility of a wearable electrochemical sensor for UA measurement in wound exudates through both, *in vitro* and *in vivo* clinical validation studies. First, discarded wound dressings from venous leg ulcer patients were collected to determine the efficacy of the electrochemical sensor *in vitro*. The extracted biofluids from the dressings; wound exudate and sweat from the healthy skin, were analyzed for UA presence to determine its feasibility as a wound biomarker. An *in vivo* pilot study was then conducted, wherein the wearable sensor was placed on venous leg ulcers to record real-time changes in UA levels for multiple days. As an easy to apply and user compliant sensing system, the system may prove useful for better clinical decision making, especially for patients suffering from chronic wounds (e.g., venous leg ulcers). However, placing sensors in a complex environment like a wound bed is associated with multiple issues such as biofouling, biocompatibility, etc. especially for long-term measurements. We thus introduce a new approach for measurement of UA levels in sweat produced in the perilesional area. The proposed approach may provide a basis for near-wound sensing thus allowing for the development of a fully non-invasive wound monitoring system.

7.2 Experimental

7.2.1 Patients

Patients with an ulcer located in any extremity that attend the Wound Care Clinic at the University of Miami Hospital, Miami, Florida were approached to participate. Information from the patients that come for routine wound care and agree to participate was collected and de-identified in a data collection spreadsheet. Study patients were aged over 21 years of age and had a confirmed case of venous leg ulceration. For patients suffering from multiple venous leg ulcers, only the larger ulcer was considered as the target ulcer. A formal assessment was carried out by the doctors to determine the eligibility of a patient, after which the potential patient was provided with a study information sheet and asked to sign an informed consent form (ICF). After signing the ICF the patient's ulcer was treated with Standard of Care; i.e. standard compression therapy for a venous leg ulcer debridement.

Patient inclusion criteria

Patients of any gender or race that attend the Wound Care Clinic with a chronic ulcer who meet the below requirements could be asked to participate in the study:

1. Presence of a chronic venous leg ulcer as confirmed by the Clinical-Etiological-Anatomical-Pathophysiological (CEAP) clinical assessment that
    a. Has been present for over 4 weeks
    b. Ulcer located in any extremity
    c. Exudes a nominal amount of wound fluid for the sensor to function accurately
2. Over 21 years of age
3. Willing to apply the sensor over the wounds as directed

4. Able to provide an informed consent
5. Able to understand and comply with the requirements of the study

Patient exclusion criteria

1. Failure to satisfy ANY ONE of the inclusion criteria
2. History or active osteomyelitis
3. Has active cellulitis
4. Has gangrene
5. Has an ulcer located on the trunk
6. If the Ankle Brachial Index (ABI) is greater than 1.3, the investigator will use clinical judgment to determine if vascular insufficiency exists
7. Any experimental drugs taken or applied topically to the wound for 4 weeks preceding the study and for the duration of the study

Patient consent

Before the recruitment of any patient for the study, a detailed explanation of the nature and purpose of the study was provided. Patients were given enough time to read the consent carefully and were encouraged to ask questions. Once the essential information was provided and it was established that the patient understands the implications of participating in the study, the patients were asked to sign an informed consent. Once the patient signed the consent, we proceeded with the dressing placement.

Criteria for withdrawal

Patients were advised that they may withdraw from the study and remove the placed sensor at any time, for any reason or if necessary. On patient withdrawal, the reason was fully documented in the notes.

Screening evaluation

The study was designed to typically last for one week during which time the patients were required to wear the sensors along with the compression bandages. Prospective patients were fully informed about all the aspects and the intent of the study, including its procedures, risks, and benefits. Receipt of acknowledging the information provided was the signed informed consent provided by the patient.

7.2.2 Wound dressing collection and uric acid extraction

Discarded wound dressings from four de-identified subjects were collected from the Wound Care Center at the University of Miami for UA analysis. Allevyn hydrocellular foam dressings (10 cm x 10 cm) were placed on four de-identified subjects with varying etiologies. Two dressings were placed on each subject; one on the wound bed and another on the adjacent healthy skin for three days.

The dressings placed over the wound were used to extract two different biofluids; wound exudate and extract from perilesional skin. Samples of 4 cm × 4 cm area were cut from the dressings for UA extraction. As shown in Figure 7.1, the red boxes represent the wound exudate area, while the blue boxes represent the extract from the perilesional skin area. The perilesional skin areas were cut at a distance of 5 cm from the center of wound exudate areas to maintain a sufficient distance from the wound region. The dressings placed on the healthy skin were used to extract the biofluid (4 cm x 4 cm); as represented by the green boxes in Figure 7.1. These dressing samples were immersed in a NaOH buffer solution (0.1 M, pH 13.0), followed by a ramped heating from 37^{o}C to 60^{o}C at a rate of 5^{o}C min^{-1}. The solution was then ultrasonicated using a homogenizer for 60 s at 20 Hz and subsequently centrifuged at 2000G for 5 min to separate the debris from the solution. The extracted biofluids were used for

measuring UA concentrations using the electrochemical sensor and a standard colorimetric assay purchased from ThermoFisher Sc.

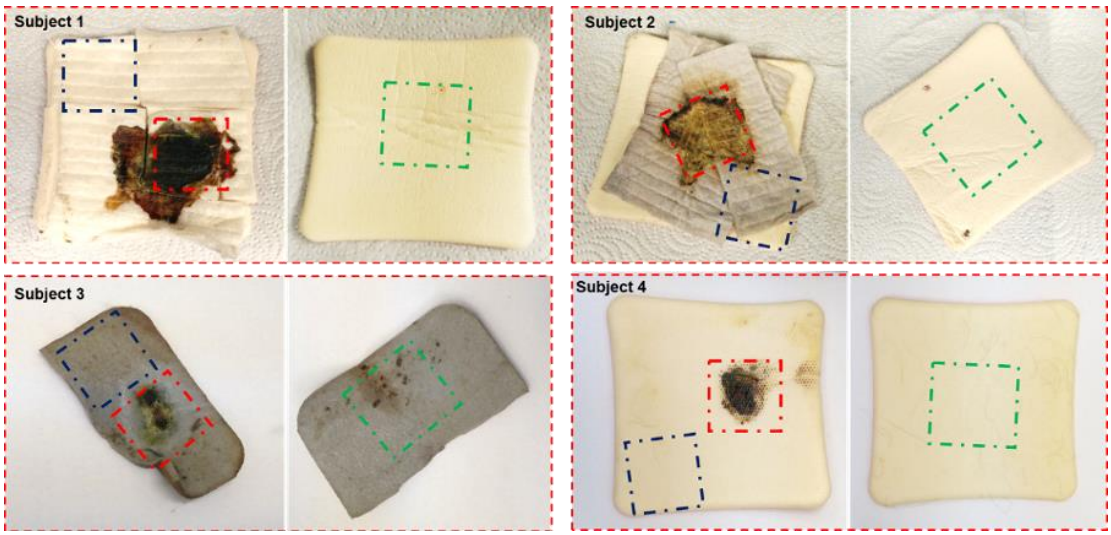

Figure 7.1 Images of discarded wound dressings from four de-identified subjects 1 to 4 respectively. The boxes in the figures represent the 4 cm x 4 cm sample areas. Red boxes represent the wound exudate region, and the blue boxes represent the extract from perilesional skin areas, while the green boxes are extracts from healthy skin.

7.2.3 Wound dimension measurements

The ruler method was used to record the physical measurements of the wound. The wound width and length were measured using a ruler, by recording the longest length and widest width across the wound edges. The wound depth was measured by applying a Q-tip at the deepest wound base region, while marking the level of the wound edge and measuring it using a ruler.

7.2.4 Uric acid sensor placement on wounds

The flexible wound monitoring sensor was placed on the wounds of two de-identified patients for three days. A multi-layer wrapping protocol was used for placing the sensor on a wound. A cotton dressing (10 cm x 10 cm) was placed on the wound as the first layer serving as a protective layer between the wound and the sensor surface. A cotton dressing (10 cm x 10 cm) with the incorporated sensors was placed next with the sensor

surface facing towards the wound bed. The third compression layer consisted of an Allevyn foam to absorb the excess wound exudate. A layer of high stretch fiber to provide a gradient of pressure across the calf muscles was wrapped next. The final layer was a short stretch fiber that was used to dynamically augment the pump action of the calf muscles to ensure proper blood flow in venous leg ulcer patients.

7.2.5 Ethical considerations

This study has been carried out according to the protocol approved by the Florida International University Institutional Review Board (IRB 20180305-IAA).

7.3 Results and discussion

7.3.1 *In vitro* sensor validation

Uric acid (UA), a product of the purine metabolic cycle, is considered to be an endogenous biomarker for wound healing assessment. As a consequence of cell rupture at the wound site, adenosine triphosphate (ATP) is released into the extracellular matrix, where the final reaction in the pathway is the conversion of xanthine to UA.[154] As a result of cell death there is local production of UA at the wound site, with the UA levels decreasing as the wound heals, hence serving as a diagnostic indicator for wound healing.[155] To establish the feasibility of UA measurement in a wound and determine the correlation between the wound physiology and the UA levels, four de-identified patients diagnosed with active venous leg ulcer (C6) were analyzed. Wound exudate and sweat collected from the patients were measured for the presence of UA. The UA levels in the wound exudates were seen to be 2-4 times higher than in sweat from the healthy skin (Table 7.1), confirming the localized production of UA in the wound milieu. The sample from a patient with a wound size of 4.0 cm x 3.5 cm (Figure 7.2a) was seen to have a UA concentration of 408.7 μM, while the subject with 2.5 cm x 2.1

cm wound size (Figure 7.2b) exhibited a UA concentration of 127.9 µM. The wound with a larger size was observed to have higher UA levels accumulated on the discarded dressing, suggesting a correlation may exist between the wound size and the UA concentration. However, further detailed validation is necessary with larger sample studies to confirm the correlation. The UA levels determined using the electrochemical sensor were further validated against a standard colorimetric UA assay. The average recovery of the wound exudate samples was seen to be 86.49%, compared to a recovery of 80% observed for the healthy sweat (Table 7.1); validating the high accuracy of the sensor to measure UA in real samples.

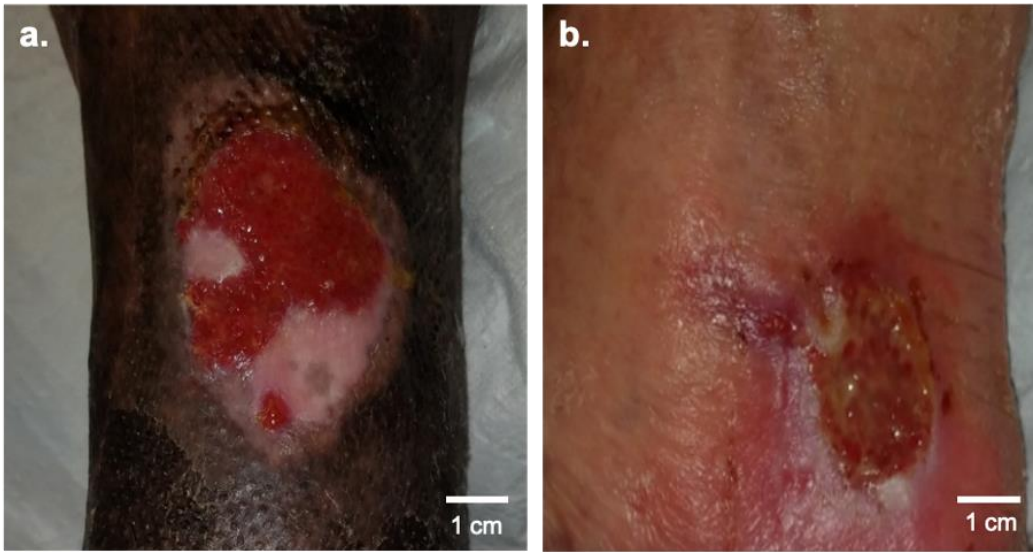

Figure 7.2 Wound images of two de-identified subjects a. Subject 1 and b. Subject 2 diagnosed with a venous leg ulcer. The larger wound of the Subject 1 correlated to a higher UA concentration, indicating a correlation between wound chronicity and UA levels.

Table 7.1. Electrochemical detection of UA in wound extracts vs. standard colorimetric UA assay. The high recovery values obtained confirmed the high efficacy of the sensor to measure UA in real wound exudate samples. Each experiment was carried out in triplicate (n = 3).

Subject	**Sample**	**UA assay (µM)**	**Biosensor (µM)**	**Recovery (%)**	**RSD (%)**
1	Wound exudate	413.80	408.69	98.77	3.7

	Perilesional skin	114.30	155.43	135.99	1.3
	Healthy skin	101.30	95.65	94.42	5.7
2	Wound exudate	231.50	166.30	71.84	1.5
	Perilesional skin	154.80	54.35	35.11	5.8
	Healthy skin	96.30	44.19	45.89	4.7
3	Wound exudate	337.23	230.42	68.33	2.5
	Perilesional skin	111.42	170.50	153.03	3.5
	Healthy skin	89.36	67.81	75.89	1.5
4	Wound exudate	119.48	127.87	107.03	4.5
	Perilesional skin	38.65	34.72	89.83	2.9
	Healthy skin	35.02	23.00	65.68	2.5

7.3.2 *In vivo* sensor validation

After establishing the feasibility of UA measurement in wound extracts, the fabricated sensors were validated through a pilot *in vivo* study. An array of four UA sensors integrated onto a single dressing enabled us to map the UA levels across the wound area, with each sensor programmed to collect data once per hour for one minute at 1.3 Hz. To map the UA levels across the wound area, two sensors were placed on the center of the wound bed, while the other two were positioned on the wound edges (Figure 7.3a and Figure 7.4a). The initially recorded low temperature (~25^{o}C) values from the sensor for both the subjects can be attributed to the time for while the sensor was run before being placed on the patient. All the sensors placed on both the subjects exhibited a flat line over the entire period of time (Figure 7.3b and Figure 7.4b).

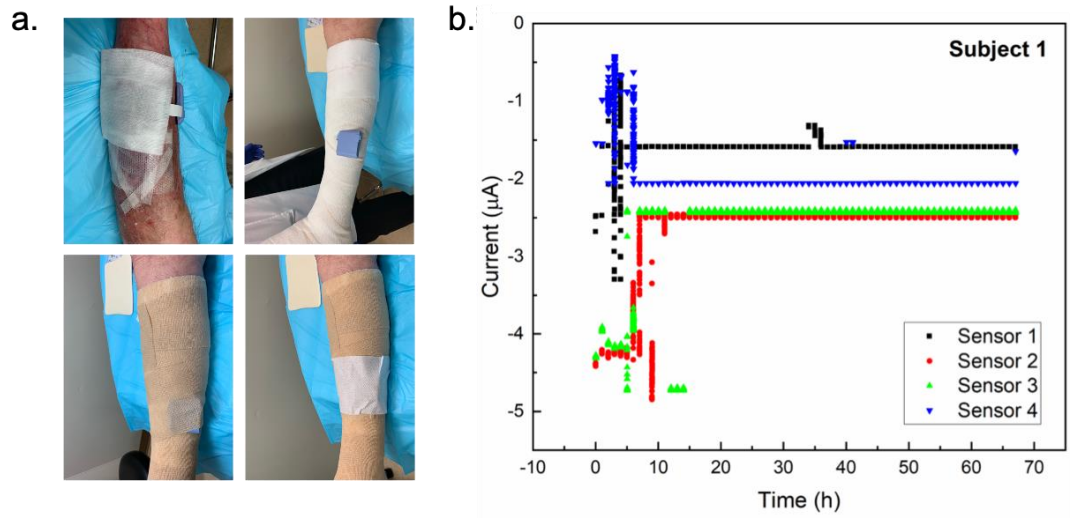

Figure 7.3 a. Photographs illustrating sensor placement steps on Subject 1. The wound size of the patient was recorded to be 12.0 cm x 4.0 cm x 0.2 cm. b. Longitudinal current response obtained from the four UA sensors placed on the subject for 72 h. An array of four UA sensors integrated onto a single dressing was placed on the subjects to map UA levels across the wound area. Sensors 1 and 4 were placed on the wound edges while sensors 2 and 3 were placed in the center of the wound for both the subjects.

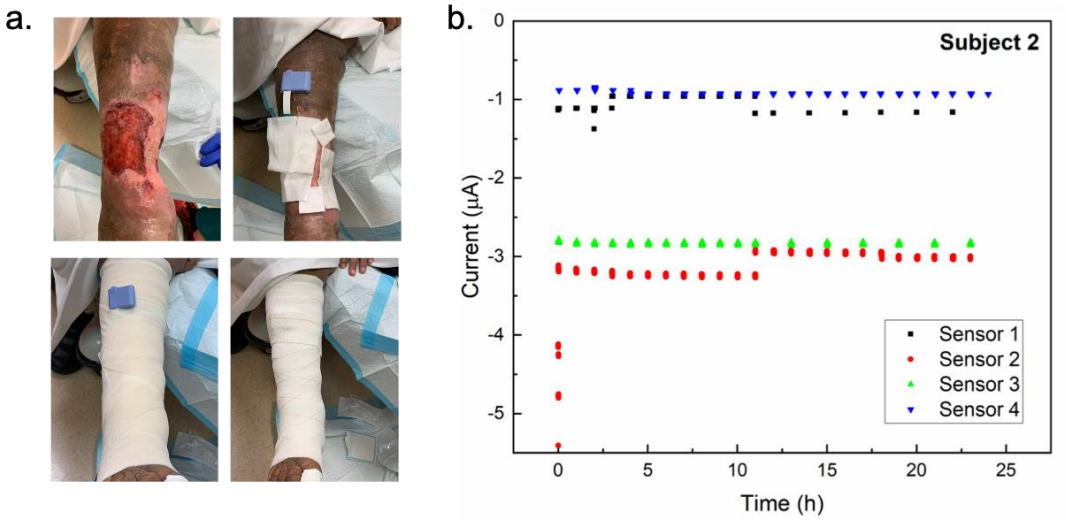

Figure 7.4 a. Photographs illustrating sensor placement steps on Subject 2. The wound size of the patient was recorded to be 7.5 cm x 5.6 cm x 0.5 cm. b. Longitudinal current response obtained from the four UA sensors placed on the subject for 24 h. An array of four UA sensors integrated onto a single dressing was placed on the subjects to map UA levels across the wound area. Sensors 1 and 4 were placed on the wound edges while sensors 2 and 3 were placed in the center of the wound for both the subjects.

Wound microenvironment is highly dynamic and complex with several unknown factors adding to the ambiguity of the sensor environment. The results

obtained from the pilot study suggested several potential reasons that may affect the sensor functionality when placed *in vivo*. As discussed in the earlier chapters, a change in parameters like pH and temperature of the biofluid can result in a loss of enzymatic activity. The *in vitro* stability studies confirmed this effect showing a decrease in the sensor functionality after two days. Although a higher rate of activity degradation of the enzyme maybe assumed when placed *in vivo*, an immediate loss is unexpected. A wound microenvironment contains a myriad of proteins and chemicals, of which some may exhibit a competitive inhibition towards the uricase enzyme,[286,287] with a possible effect of such inhibition being loss of sensor functionality. But, since the developed sensor was able to successfully detect UA in the collected wound exudates, it may be possibly concluded that these compounds are unlikely to cause significant interferences in the sensor signal. A probable reason for the observed loss in sensor functionality was thus hypothesized to be sensor biofouling. Whilst further clinical validation studies are required in order to derive conclusive results, the biofouling phenomenon and its consequent effect on the sensor functionality was explored further.

7.3.3 Sensor biofouling through biofilm growth on active area

Apart from the extracellular components present in a wound exudate, a wound milieu tends to develop a biofilm within 24 hours[288,289] due to manifestation of infections, hampering the wound healing significantly. As discussed earlier, the sensing of complex matrices such as a wound exudate is challenging due to sensor fouling resulting from adsorption of wound debris. However, formation of these biofilms (Figure 7.5) on the active surface area of the electrode can further compromise the sensor response and its long-term stability. Most knowledge of biofilms developed in chronic wounds has been derived from studies of *Pseudomonas aeruginosa (P.*

aeruginosa) and *Staphylococcus aureus*.[290,291] *In vitro* studies were carried out wherein the *P. aeruginosa* bacterial strain (PA01) was grown over the sensor surface to study the growth of biofilm with time. It was hypothesized that growth of such biofilms will foul the sensor and result in a degraded UA response from the sensor.

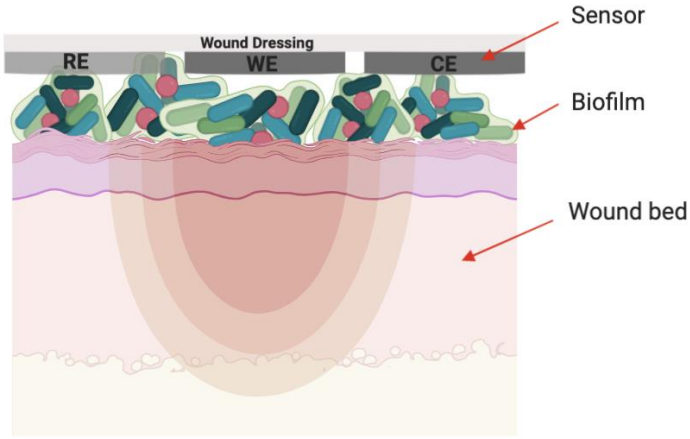

Figure 7.5. Schematic illustration of biofilm formation on the wound bed and the sensor surface. The biofilm layer formed on the sensor surface will act as a physical barrier impeding the diffusion of UA from the wound exudate to the active area of the sensor surface, thus resulting in sensor fouling over time.

The scanning electron micrographs recorded at different time points revealed a complete surface coverage by the biofilm after 3 days (Figure 7.6). The growth of biofilm over the sensor surface was further validated by the decrease in current response as a function of time. The electrode with the growing biofilm was seen to exhibit a 20% higher sensor fouling rate compared to the control electrode (no biofilm growth) after a period of seven days (Figure 7.7). The biofilm acts as a passivating layer on the electrode, impeding the diffusion of UA from the wound fluid to the electrode surface. The resulting concentration gradient of UA (lower at the electrode surface) thus results in a decreased sensor response. Additionally, the change in pH in the wound environment due to biofilm formation, can also affect the catalytic activity of the uricase enzyme further resulting in a sensor drift. This study ascertained that biofouling

has a significant effect on the sensor response and must be taken into consideration when the sensor is placed on the wound.

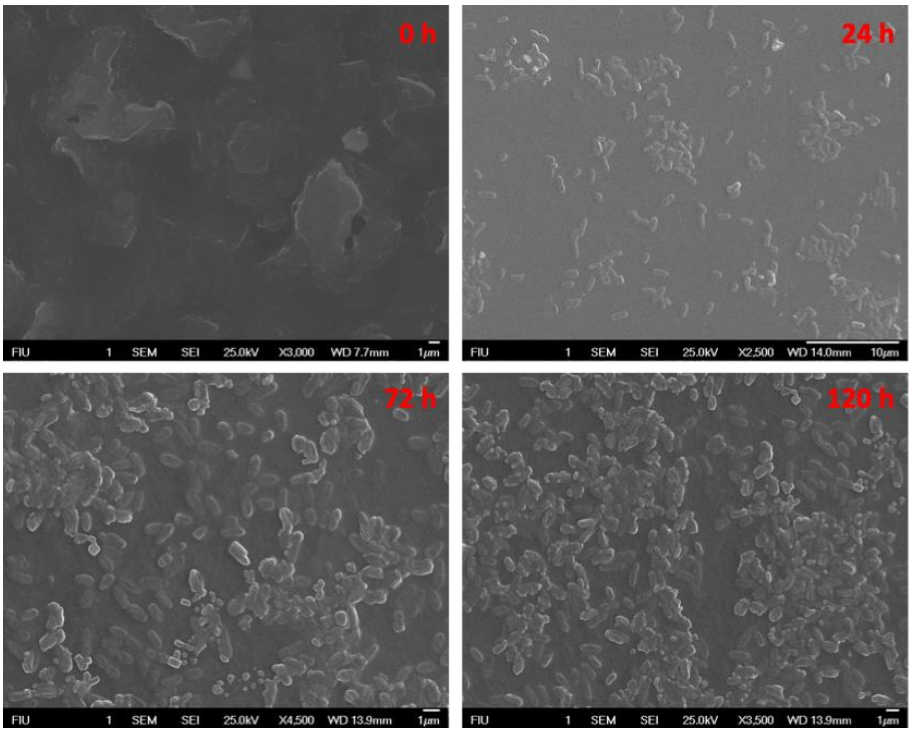

Figure 7.6. SEM images of biofilm growth on a MWCNT/Au/HRP/UOx functionalized sensor surface at different time points (0 h, 24 h, 72 h and 120 h). The biofilm was seen to completely cover the active area of the sensor surface after 72 h, hindering diffusion of UA to the sensor surface.

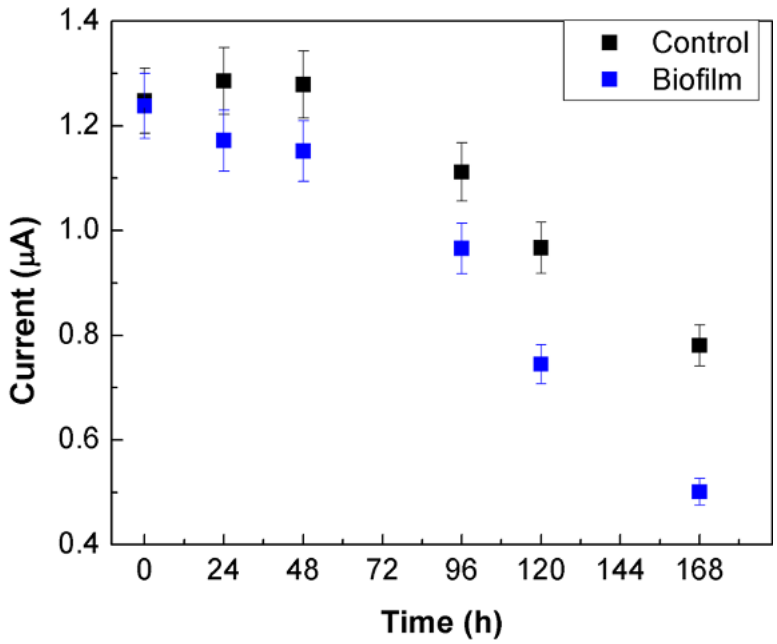

Figure 7.7. Current response of a MWCNT/Au/HRP/UOx functionalized sensor as a function of time when subjected to media with (biofilm) and without (control) a

growing biofilm. The higher degradation rate of the sensor response observed for the sensor with growing biofilm, showed the hindered diffusion of UA to the sensor. Each experiment was carried out in triplicate (n = 3) and the data is represented as mean ± SD.

7.3.4 Electrochemical monitoring of biofilm growth

In view of the fact that biofouling significantly impedes the sensor functionality, real time monitoring of these biofilms is essential. Previous literature suggests that biofilms produce lactic acid (LA)[292] in the wound environment resulting in a relatively acidic environment. Measurement of parameters like LA and pH may thus be utilized to assess the temporal growth of these biofilms in chronic wounds. The same bacterial model used in the biofouling study showed a proportional increase in the lactic acid levels as a function of biofilm growth, implying a direct correlation between the biofilm growth and LA production (Figure 7.8a). Additionally, the pH levels were also seen to decrease from 7.0 to 6.0 confirming the acidic environment as a result of the increasing bacterial count in the environment (Figure 7.8a and b).

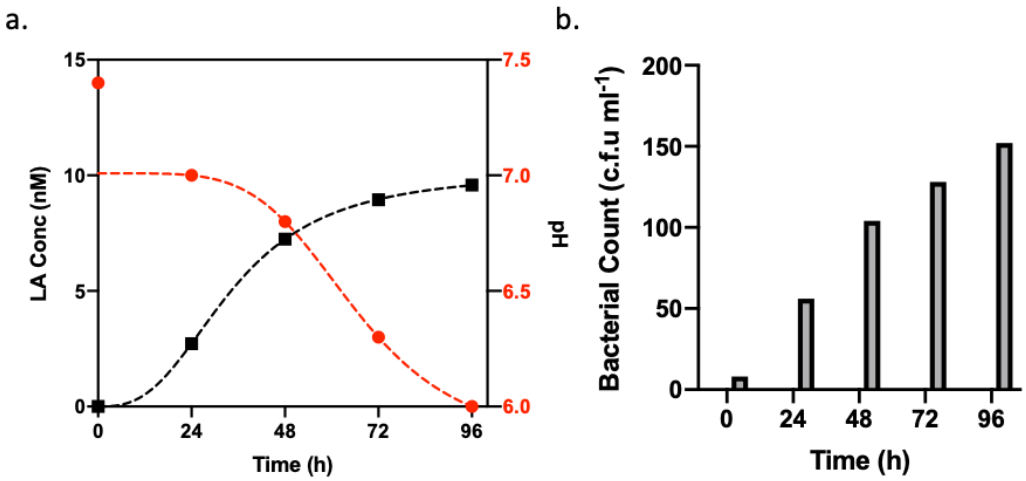

Figure 7.8. a. Change in lactic acid levels and pH levels and b. bacterial count as a function of biofilm growth at different time points (0 h, 24 h, 48 h, 72 h and 96 h).

This led to a sensor redesign wherein an enzymatic lactic sensor was developed and added to the wound sensing suite to monitor the growth of these biofilms (Figure 7.9a

and b). For the first time, this study reports a wound monitoring sensing platform that can measure UA for monitoring the wound healing progression in conjunction with a LA sensor for monitoring sensor biofouling.

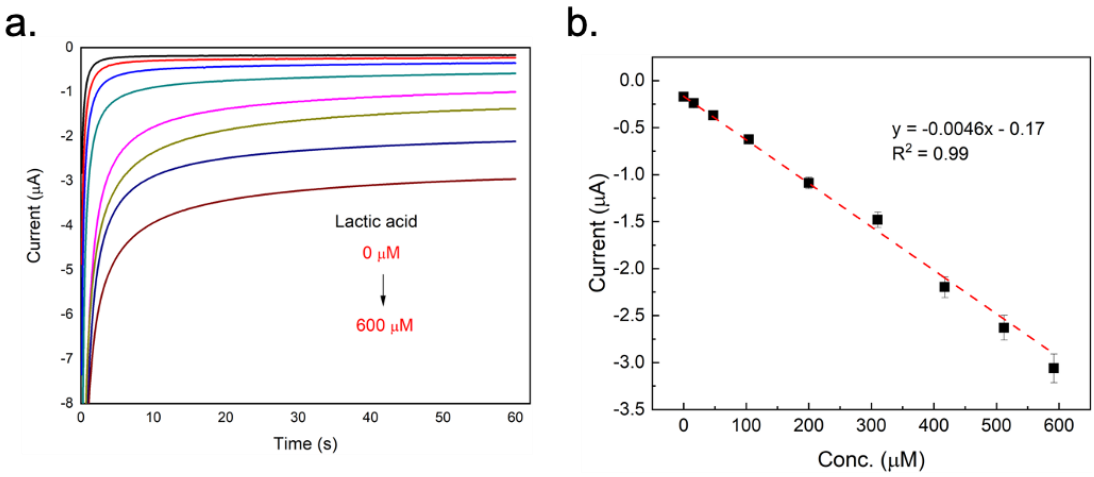

Figure 7.9. a. Amperometric response of the developed lactic acid sensor to varying levels of lactic acid. and b. Calibration curve showing a linear correlation between the current and the lactic acid concentration.

This multimodal sensing platform monitoring the wound healing and biofilm development can be leveraged in the future to develop a better understanding of the wound microenvironment and its effect on the electrochemical sensor response. The developed correlation between lactic acid production and biofilm growth could be further utilized to monitor the development of infections in the wound milieu to provide timely therapeutic assessment.

7.3.5 Feasibility of UA measurement in wound proximity

The positioning of the biosensor directly over the wound bed can lead to a lower sensor accuracy owing to occlusion of the active surface by the wound debris. An approach towards UA sensing in the wound proximity could open up a potential way for continuous wound monitoring. When an injury occurs, the cells begin to die resulting in the production of UA in the wound milieu. With the accumulation of UA at the

wound site, some UA passively diffuses from the extracellular fluid to the blood serum. The generated electrochemical gradient further facilitates the diffusion of serum UA to the eccrine sweat glands present in the wound vicinity. UA concentration in three different biological fluids; namely, wound exudate, sweat from perilesional skin, and sweat from healthy skin was evaluated using the standard addition method. The concentration trend in these biofluids for each patient is depicted in Figure 7.10.

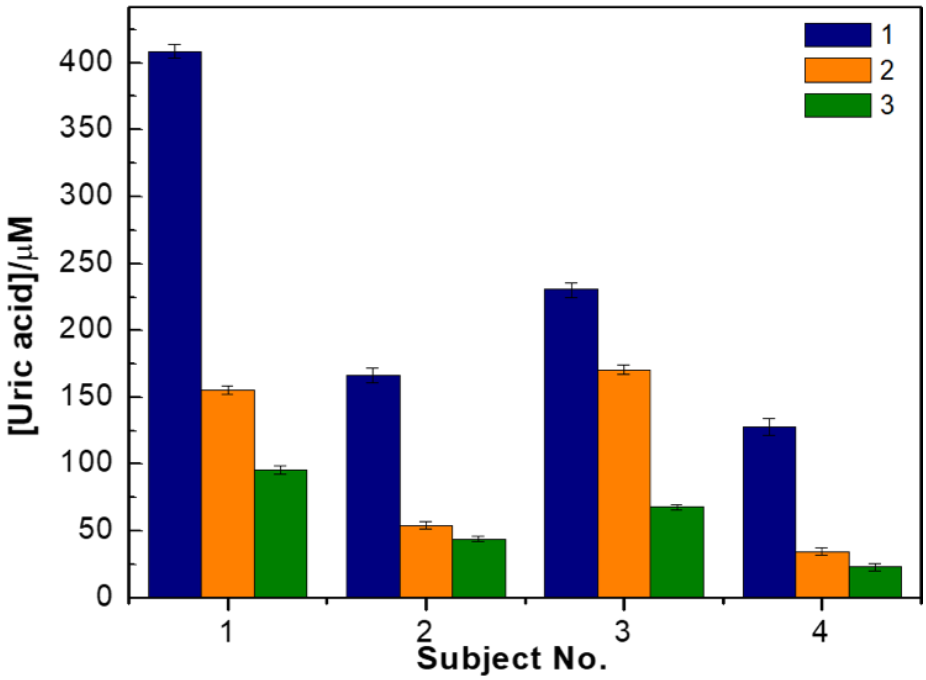

Figure 7.10 Trend in UA concentrations found in the wound exudate (1), perilesional skin extract (2), and healthy skin extract (3). The higher UA levels in the perilesional skin extract can be used for a non-invasive near-wound sensing approach. Each experiment was carried out in triplicate (n = 3) and the data is represented as mean ± SD.

As observed from the real samples, the wound exudate showed the highest UA concentration, followed by the biofluid extracts from perilesional skin and healthy skin for all the subjects. The higher levels of UA observed in the biofluid from the perilesional skin as compared to the healthy skin can be ascribed to the passive transport of UA in the surrounding sweat glands. The presence of elevated UA levels in the biofluid extract from perilesional skin can be used as a potential biomarker paving the

way towards a new near-wound sensing approach. It can help prevent occlusion and electrode fouling effects, and biocompatibility issues that result from embedding the sensor directly over the wound bed. The measured UA levels were validated against a standard colorimetric UA assay, and an average recovery of ~103% was observed for the biofluid extracts from perilesional skin (Table 7.1).

7.4 Conclusion

A clinical validation has been conducted to determine the feasibility of UA detection in chronic venous leg ulcers using a wearable wound monitoring system. Preliminary *in vitro* studies involved the extraction of wound exudates from discarded wound dressings. The collected dressings tested positive for UA presence, establishing the feasibility of using UA as a biomarker for wound monitoring. The UA levels in wound exudate were found to be 2-5 times higher than the levels found in sweat, confirming the local production of UA in the wounded area. The developed sensor exhibited a recovery of >85% showing the high accuracy of the electrochemical detection mechanism used by the sensor. Subsequently, an integrated flexible wound monitoring system was placed on venous leg ulcer patients for real-time UA monitoring. An optimized wrapping protocol for the placement of the sensors on the wounds was established. The studies indicated a loss of sensor functionality when placed on real wounds, where biofouling was attributed to be a major factor. A new sensing platform was developed for the first time that can monitor the wound progression and biofilm development simultaneously. Further, a new near-wound sensing approach has been presented, where the biofluid extracted from the perilesional skin was seen to have elevated levels of UA compared to the healthy skin extract. Based on this, biofluid extract from perilesional skin can be utilized for biosensing within the wound proximity, preventing electrode fouling and biocompatibility issues, simultaneously

improving the lifetime of the biosensor. The real sample results from the biosensor correlated well with the conventional colorimetric UA assay, establishing the practical usability of the sensor. The near-wound sensing methodology can enable a new approach towards long-term wound monitoring. Future clinical studies focused on healing wounds could help determine a more precise correlation between the UA levels, the wound chronicity and the wound healing progress.

8 Summary and Outlook for the Future of Wearable Sensing Systems

8.1 Summary

The present doctoral thesis studies how the dynamic sensor environment affects the sensor response and develops correlations between them to acquire accurate actionable data. In particular, the research investigates the dynamic parameters in the sensor environment and correlates them with experimentally measured behavior exploiting wound monitoring as a use case. The thesis first reviews the importance of wearable chemical sensing, with particular emphasis on enzymatic electrochemical sensors. Chapter 1 discusses the challenges of the current wearable chemical sensors and how the dynamic variability offered by the biofluid affects the sensor response. The wound bed is considered to be a classic example of a dynamic environment with several parameters (e.g., pH, temperature, analyte flux, evaporation) changing as a function of the wound healing status. The following chapter presents an enzymatic electrochemical sensing approach towards continuous wound monitoring through sensing of a purine metabolite, uric acid. The sensor utilizes a nanocomposite-based architecture coupled with a bi-enzymatic system to facilitate faster reaction kinetics. The sensor response at low overpotentials allowed for specific detection of UA with negligible effect from interfering compounds. Furthermore, the high stability of the sensor exhibited at physiological conditions demonstrated the applicability of the sensing architecture in a wearable setting.

The thesis further discusses a novel fabrication approach for highly flexible textile-based wearable electrochemical sensors. The chapter presents a facile and inexpensive process for the integration of flexible electrochemical sensors on textiles

to ensure user comfort and wearability. Such sensors can be easily integrated onto any garment ensuring no skin irritation while vigilantly monitoring the chemical parameters of the wearer. The mechanical characterization of the sensors revealed that a tensile strain of up to 100% and flexural strain of up to 180^{o} has a negligible effect on the mechanical properties of the fabricated sensor. The sensors were also shown to have a minimal impact (~3% deviation) on the electrochemical characteristics of the sensor when under mechanical deformation. The fabricated sensors were heat transferred to wound dressings for enzymatic electrochemical sensing of uric acid in a steady-state environment using the reaction mechanism established earlier. The high sensitivity of the flexible sensors enabled measurement of uric acid in the clinically relevant range. Owing to the mediator-free enzymatic approach, the sensor achieved stable and accurate measurements over a period of seven days under physiological conditions. The flexible sensors were further integrated with a backend wearable system-on-chip to allow for real-time data collection and transfer to realize an integrated wound monitoring system. While the UA sensing through this system exhibited a lower sensitivity owing to the poor noise filtration mechanism of the miniature potentiostat, the sensor was capable of UA detection in the medically relevant range. The variations in the wound fluid composition among individuals, leads to an uncertain environment in which the sensor is placed. The dynamic variability offered by these biofluids in any wearable construct can result in a confounded sensor response. The effect of potential dynamic environmental parameters like pH, temperature, sample volume and evaporation on the sensor response is discussed in the following chapter. The effect of these parameters on the mass transport kinetics of UA has been elaborated upon and calibration models have been developed. The sensor was observed to behave optimally in a pH range of 7.5 – 8, with the sensor response being higher at lower temperatures

owing to the higher enzymatic activity. Biofouling was identified as another major factor affecting the sensor response especially in complex biomatrix like wound exudate. The confounding of sensor response as a result of biofouling was explored further. It was observed that as a result of biofilm formation on the active area of the sensor surface, UA diffusion was inhibited, reflected as a decrease in the current response as a function of time.

On establishing the feasibility of UA measurement on the flexible sensors, the sensor materials and the sensor itself were investigated for their cytotoxicity. The wound sensor incorporates biochemical sensors that are placed in direct contact with the tissue and wound fluids. An open wound exposes the underlying human tissue, potentially subjecting it directly to the materials integrated within the sensor. The effect of the sensor and the constituent materials were investigated on human keratinocytes and fibroblasts to elucidate the toxicity mechanisms of each material. The time-lapse studies indicated that the materials in the sensor show minimal toxicity at the concentrations present in the sensor both at a cellular and intracellular level (mitochondrial and DNA damage). Likewise, the materials and the sensor exhibited no considerable impairment of the mitochondrial function or apoptotic activity on exposure at concentrations present in the sensor. The functionalized sensor was seen to exhibit lower toxicity compared to material mixtures. This improved biocompatibility of the sensor was attributed to the biocompatible protective layer offered by the enzyme matrix resulting in reduced leaching of the nanomaterials.

The work then presents the first ever demonstration of an *in vivo* study carried out on patients suffering from chronic wounds using a wearable wound sensor. A pilot trial is conducted to determine the feasibility of UA detection in chronic venous leg ulcers through both *in vitro* and *in vivo* clinical studies. The *in vitro* studies revealed

the concentration of UA in wound exudates to be 2-5 times higher than the levels found in sweat, establishing the feasibility of UA as a biomarker for wound monitoring. Subsequently, the integrated flexible wound monitoring system was placed on venous leg ulcer patients for real-time UA monitoring. The measurements led to the redesigning of the sensor, where a sensor platform capable of simultaneously monitoring wound health and sensor biofouling is reported for the first time. A near-wound sensing approach is further presented in the chapter, where the biofluid extracted from the perilesional skin was seen to have elevated levels of UA compared to the healthy skin extract. Based on this, biofluid extract from perilesional skin can be utilized for biosensing within the wound proximity, preventing electrode fouling thus improving the lifetime of the biosensor. The thesis overall presents the feasibility of stable UA measurement using the presented wound monitoring system both in laboratory (*in vitro)* and *in vivo* scenarios. The work elaborates on the transition of electrochemical sensing platforms from rigid to flexible and from steady-state to a dynamic-state environment. All the above parameters are taken into consideration to develop a robust sensing system providing accurate real-time data.

8.2 Future Outlook

The wearable technology market has been evolving at a rapid rate. This technology has proven potential to alter the future of medical industry and healthcare providers. Continuous monitoring of a person's vitals provides an opportunity for improved healthcare management. Easy access to a personalized database of a patient's medical history can enable the doctors to provide efficient treatments especially for patients with restricted medical facilities. Moreover, with the advent of artificial intelligence and machine learning techniques the data collected from these wearable devices can allow for predictive analytics for timely medical interventions. In the recent years, apart

from wearable physical sensors, significant progress has been made in the field of wearable electrochemical sensors. However, several fundamental and technological challenges still remain to fully realize their potential. A deeper understanding of the underlying biological relationships between the analyte concentrations found in biofluids like sweat and saliva to blood analyte concentrations are required to establish accurate correlations. The dependency of these analyte levels on the physiological processes should also be investigated for biologically relevant measurements.

Fabrication of these sensors on different substrates based on the wound type should be explored in the future. Mimicking the wound fluid dynamics and understanding the flow as a function of the substrate properties and its impact on the sensor response may help improve the sensor functionality when placed in vivo. Fundamental theoretical frameworks should be developed in order to elucidate the effects of the dynamic parameters on the sensor response and study the interdependency of these parameters. Technologies to measure these parametric values in an *in vivo* setting and on-chip feedback correction for the sensor response can result in improved sensing systems. In addition, core analytical sensing challenges such as sensitivity, selectivity and reproducibility of the sensors require to be addressed. Levels of certain analyte in biofluids like sweat are in the nanomolar range and novel sensing mechanisms are essential to enable sensing at a molecular level. Quantum technology has enabled the development of highly sensitive optical sensors and perhaps translational of such concepts to electrochemical sensing could lead to a new generation of wearable chemical sensing devices. Interdisciplinary solutions are required to address the above issues and enable the development of next-generation wearable technology. In particular, for wound monitoring sensors, the sensing systems need to be incorporated in conjunction with therapeutic systems to provide an active feedback

to control the drug release profile based on the wound status. This will enable the development of self-sufficient bandages reducing the need for multiple hospital visits especially for patients suffering from chronic wounds. Apart from the core sensing challenges, strategies for seamless integration of the sensing systems to other subsystems such as backend electronics for data collection is vital. As a result of the body movement, mechanical stress on the interface is likely to happen rendering the system susceptible to failure. Flawless integration of these subsystems is extremely crucial to facilitate the development of such sensing systems. It is evident that wearable electrochemical sensors hold considerable promise to revolutionize personalized healthcare, however innovative interdisciplinary solutions are required to realize these systems.

REFERENCES

(1) Heymann, D. L.; Shindo, N. COVID-19: What Is next for Public Health? *The Lancet*. Lancet Publishing Group February 22, 2020, pp 542–545. https://doi.org/10.1016/S0140-6736(20)30374-3.

(2) Hollander, J. E.; Carr, B. G. Virtually Perfect? Telemedicine for Covid-19. *N. Engl. J. Med.* **2020**, *382* (18), 1679–1681. https://doi.org/10.1056/NEJMp2003539.

(3) Vashist, S. K.; Luppa, P. B.; Yeo, L. Y.; Ozcan, A.; Luong, J. H. T. Emerging Technologies for Next-Generation Point-of-Care Testing. *Trends in Biotechnology*. Elsevier Ltd November 1, 2015, pp 692–705. https://doi.org/10.1016/j.tibtech.2015.09.001.

(4) Takeda, R.; Tadano, S.; Todoh, M.; Morikawa, M.; Nakayasu, M.; Yoshinari, S. Gait Analysis Using Gravitational Acceleration Measured by Wearable Sensors. *J. Biomech.* **2009**, *42* (3), 223–233. https://doi.org/10.1016/j.jbiomech.2008.10.027.

(5) Zhang, Z. Q.; Wong, W. C.; Wu, J. K. Ubiquitous Human Upper-Limb Motion Estimation Using Wearable Sensors. *IEEE Trans. Inf. Technol. Biomed.* **2011**, *15* (4), 513–521. https://doi.org/10.1109/TITB.2011.2159122.

(6) Rigas, G.; Tzallas, A. T.; Tsipouras, M. G.; Bougia, P.; Tripoliti, E. E.; Baga, D.; Fotiadis, D. I.; Tsouli, S. G.; Konitsiotis, S. Assessment of Tremor Activity in the Parkinsons Disease Using a Set of Wearable Sensors. *IEEE Trans. Inf. Technol. Biomed.* **2012**, *16* (3), 478–487. https://doi.org/10.1109/TITB.2011.2182616.

(7) Hong, Y. J.; Kim, I. J.; Ahn, S. C.; Kim, H. G. Activity Recognition Using Wearable Sensors for Elder Care. In *Proceedings of the 2008 2nd International Conference on Future Generation Communication and Networking, FGCN 2008*; 2008; Vol. 2, pp 302–305. https://doi.org/10.1109/FGCN.2008.165.

(8) Patterson, J. A. C.; McIlwraith, D. G.; Yang, G. Z. A Flexible, Low Noise Reflective PPG Sensor Platform for Ear-Worn Heart Rate Monitoring. In *Proceedings - 2009 6th International Workshop on Wearable and Implantable Body Sensor Networks, BSN 2009*; 2009; pp 286–291. https://doi.org/10.1109/BSN.2009.16.

(9) Zhang, Q.; Zhou, D.; Zeng, X. Highly Wearable Cuff-Less Blood Pressure and Heart Rate Monitoring with Single-Arm Electrocardiogram and Photoplethysmogram Signals. *Biomed. Eng. Online* **2017**, *16* (1), 23. https://doi.org/10.1186/s12938-017-0317-z.

(10) Phan, D.; Siong, L. Y.; Pathirana, P. N.; Seneviratne, A. Smartwatch: Performance Evaluation for Long-Term Heart Rate Monitoring. In *4th International Symposium on Bioelectronics and Bioinformatics, ISBB 2015*; Institute of Electrical and Electronics Engineers Inc., 2015; pp 144–147. https://doi.org/10.1109/ISBB.2015.7344944.

(11) Shin, K. Y.; Lee, J. S.; Jang, J. Highly Sensitive, Wearable and Wireless Pressure Sensor Using Free-Standing ZnO Nanoneedle/PVDF Hybrid Thin Film for Heart Rate Monitoring. *Nano Energy* **2016**, *22*, 95–104. https://doi.org/10.1016/j.nanoen.2016.02.012.

(12) Yang, H.; Qi, D.; Liu, Z.; Chandran, B. K.; Wang, T.; Yu, J.; Chen, X. Soft Thermal Sensor with Mechanical Adaptability. *Adv. Mater.* **2016**, *28* (41), 9175–9181. https://doi.org/10.1002/adma.201602994.

(13) Yang, J.; Wei, D.; Tang, L.; Song, X.; Luo, W.; Chu, J.; Gao, T.; Shi, H.; Du, C. Wearable Temperature Sensor Based on Graphene Nanowalls. *RSC Adv.* **2015**, *5* (32), 25609–25615. https://doi.org/10.1039/c5ra00871a.

(14) Yan, C.; Wang, J.; Lee, P. S. Stretchable Graphene Thermistor with Tunable Thermal Index. *ACS Nano* **2015**, *9* (2), 2130–2137. https://doi.org/10.1021/nn507441c.

(15) Trung, T. Q.; Ramasundaram, S.; Hwang, B.-U.; Lee, N.-E. An All-Elastomeric Transparent and Stretchable Temperature Sensor for Body-Attachable Wearable Electronics. *Adv. Mater.* **2016**, *28* (3), 502–509. https://doi.org/10.1002/adma.201504441.

(16) Xuan, X.; Yoon, H. S.; Park, J. Y. A Wearable Electrochemical Glucose Sensor Based on Simple and Low-Cost Fabrication Supported Micro-Patterned Reduced Graphene Oxide Nanocomposite Electrode on Flexible Substrate. *Biosens. Bioelectron.* **2018**, *109*, 75–82. https://doi.org/10.1016/j.bios.2018.02.054.

(17) Gao, W.; Emaminejad, S.; Nyein, H. Y. Y.; Challa, S.; Chen, K.; Peck, A.; Fahad, H. M.; Ota, H.; Shiraki, H.; Kiriya, D.; Lien, D. H.; Brooks, G. A.; Davis, R. W.; Javey, A. Fully Integrated Wearable Sensor Arrays for Multiplexed in Situ Perspiration Analysis. *Nature* **2016**, *529* (7587), 509–514. https://doi.org/10.1038/nature16521.

(18) Bandodkar, A. J.; Jeerapan, I.; You, J. M.; Nuñez-Flores, R.; Wang, J. Highly Stretchable Fully-Printed CNT-Based Electrochemical Sensors and Biofuel Cells: Combining Intrinsic and Design-Induced Stretchability. *Nano Lett.* **2016**, *16* (1), 721–727. https://doi.org/10.1021/acs.nanolett.5b04549.

(19) Lee, H.; Choi, T. K.; Lee, Y. B.; Cho, H. R.; Ghaffari, R.; Wang, L.; Choi, H. J.; Chung, T. D.; Lu, N.; Hyeon, T.; Choi, S. H.; Kim, D. H. A Graphene-Based Electrochemical Device with Thermoresponsive Microneedles for Diabetes Monitoring and Therapy. *Nat. Nanotechnol.* **2016**, *11* (6), 566–572. https://doi.org/10.1038/nnano.2016.38.

(20) Labroo, P.; Cui, Y. Flexible Graphene Bio-Nanosensor for Lactate. *Biosens. Bioelectron.* **2013**, *41* (1), 852–856. https://doi.org/10.1016/j.bios.2012.08.024.

(21) Currano, L. J.; Sage, F. C.; Hagedon, M.; Hamilton, L.; Patrone, J.; Gerasopoulos, K. Wearable Sensor System for Detection of Lactate in Sweat. *Sci. Rep.* **2018**, *8* (1), 1–11. https://doi.org/10.1038/s41598-018-33565-x.

(22) Imani, S.; Bandodkar, A. J.; Mohan, A. M. V.; Kumar, R.; Yu, S.; Wang, J.; Mercier, P. P. A Wearable Chemical-Electrophysiological Hybrid Biosensing System for Real-Time Health and Fitness Monitoring. *Nat. Commun.* **2016**, *7* (1), 1–7. https://doi.org/10.1038/ncomms11650.

(23) Anastasova, S.; Crewther, B.; Bembnowicz, P.; Curto, V.; Ip, H. M.; Rosa, B.; Yang, G. Z. A Wearable Multisensing Patch for Continuous Sweat Monitoring. *Biosens. Bioelectron.* **2017**, *93*, 139–145. https://doi.org/10.1016/j.bios.2016.09.038.

(24) Fensli, R.; Gunnarson, E.; Gundersen, T. A Wearable ECG-Recording System for Continuous Arrhythmia Monitoring in a Wireless Tele-Home-Care Situation. In *18th IEEE Symposium on Computer-Based Medical Systems (CBMS'05)*; IEEE; pp 407–412. https://doi.org/10.1109/CBMS.2005.22.

(25) Nemati, E.; Deen, M. J.; Mondal, T. A Wireless Wearable ECG Sensor for Long-Term Applications. In *IEEE Communications Magazine*; 2012; Vol. 50, pp 36–43. https://doi.org/10.1109/MCOM.2012.6122530.

(26) Li, G.; Lee, B. L.; Chung, W. Y. Smartwatch-Based Wearable EEG System for Driver Drowsiness Detection. *IEEE Sens. J.* **2015**, *15* (12), 7169–7180. https://doi.org/10.1109/JSEN.2015.2473679.

(27) Lin, C. T.; Chuang, C. H.; Huang, C. S.; Tsai, S. F.; Lu, S. W.; Chen, Y. H.; Ko, L. W. Wireless and Wearable EEG System for Evaluating Driver Vigilance. *IEEE Trans. Biomed. Circuits Syst.* **2014**, *8* (2), 165–176. https://doi.org/10.1109/TBCAS.2014.2316224.

(28) Lim, G. H.; Kwak, S. S.; Kwon, N.; Kim, T.; Kim, H.; Kim, S. M.; Kim, S. W.; Lim, B. Fully Stretchable and Highly Durable Triboelectric Nanogenerators Based on Gold-Nanosheet Electrodes for Self-Powered Human-Motion Detection. *Nano Energy* **2017**, *42*, 300–306. https://doi.org/10.1016/j.nanoen.2017.11.001.

(29) Sun, Q.; Seung, W.; Kim, B. J.; Seo, S.; Kim, S.-W.; Cho, J. H. Active Matrix Electronic Skin Strain Sensor Based on Piezopotential-Powered Graphene Transistors. *Adv. Mater.* **2015**, *27* (22), 3411–3417. https://doi.org/10.1002/adma.201500582.

(30) Liao, Q.; Mohr, M.; Zhang, X.; Zhang, Z.; Zhang, Y.; Fecht, H. J. Carbon Fiber-ZnO Nanowire Hybrid Structures for Flexible and Adaptable Strain Sensors. *Nanoscale* **2013**, *5* (24), 12350–12355. https://doi.org/10.1039/c3nr03536k.

(31) Kim, T.; Park, J.; Sohn, J.; Cho, D.; Jeon, S. Bioinspired, Highly Stretchable, and Conductive Dry Adhesives Based on 1D-2D Hybrid Carbon Nanocomposites for All-in-One ECG Electrodes. *ACS Nano* **2016**, *10* (4), 4770–4778. https://doi.org/10.1021/acsnano.6b01355.

(32) Hou, C.; Wang, H.; Zhang, Q.; Li, Y.; Zhu, M. Highly Conductive, Flexible, and Compressible All-Graphene Passive Electronic Skin for Sensing Human Touch. *Adv. Mater.* **2014**, *26* (29), 5018–5024. https://doi.org/10.1002/adma.201401367.

(33) Trung, T. Q.; Lee, N.-E. Flexible and Stretchable Physical Sensor Integrated Platforms for Wearable Human-Activity Monitoringand Personal Healthcare. *Adv. Mater.* **2016**, *28* (22), 4338–4372. https://doi.org/10.1002/adma.201504244.

(34) Gao, W.; Nyein, H. Y. Y.; Shahpar, Z.; Fahad, H. M.; Chen, K.; Emaminejad, S.; Gao, Y.; Tai, L. C.; Ota, H.; Wu, E.; Bullock, J.; Zeng, Y.; Lien, D. H.; Javey, A. Wearable Microsensor Array for Multiplexed Heavy Metal Monitoring of Body Fluids. *ACS Sensors* **2016**, *1* (7), 866–874. https://doi.org/10.1021/acssensors.6b00287.

(35) Keene, S. T.; Fogarty, D.; Cooke, R.; Casadevall, C. D.; Salleo, A.; Parlak, O. Wearable Organic Electrochemical Transistor Patch for Multiplexed Sensing of Calcium and Ammonium Ions from Human Perspiration. *Adv. Healthc. Mater.* **2019**, *8* (24), 1901321. https://doi.org/10.1002/adhm.201901321.

(36) Harada, S.; Honda, W.; Arie, T.; Akita, S.; Takei, K. Fully Printed, Highly Sensitive Multifunctional Artificial Electronic Whisker Arrays Integrated with Strain and Temperature Sensors. *ACS Nano* **2014**, *8* (4), 3921–3927. https://doi.org/10.1021/nn500845a.

(37) Kanao, K.; Harada, S.; Yamamoto, Y.; Honda, W.; Arie, T.; Akita, S.; Takei, K. Highly Selective Flexible Tactile Strain and Temperature Sensors against Substrate Bending for an Artificial Skin. *RSC Adv.* **2015**, *5* (38), 30170–30174. https://doi.org/10.1039/c5ra03110a.

(38) Yang, Y.; Song, Y.; Bo, X.; Min, J.; Pak, O. S.; Zhu, L.; Wang, M.; Tu, J.; Kogan, A.; Zhang, H.; Hsiai, T. K.; Li, Z.; Gao, W. A Laser-Engraved Wearable Sensor for Sensitive Detection of Uric Acid and Tyrosine in Sweat. *Nat. Biotechnol.* **2020**, *38* (2), 217–224. https://doi.org/10.1038/s41587-019-0321-x.

(39) Bruulsema, J. T.; Hayward, J. E.; Farrell, T. J.; Patterson, M. S.; Heinemann, L.; Berger, M.; Koschinsky, T.; Sandahl-Christiansen, J.; Orskov, H.; Essenpreis, M.; Schmelzeisen-Redeker, G.; Böcker, D. Correlation between Blood Glucose Concentration in Diabetics and Noninvasively Measured Tissue Optical Scattering Coefficient. *Opt. Lett.* **1997**, *22* (3), 190. https://doi.org/10.1364/ol.22.000190.

(40) Cichota, L. C.; Moresco, R. N.; Duarte, M. M. M. F.; Silva, J. E. P. da. Evaluation of Ischemia-Modified Albumin in Anemia Associated to Chronic Kidney Disease. *J. Clin. Lab. Anal.* **2008**, *22* (1), 1–5. https://doi.org/10.1002/jcla.20226.

(41) Wichmann, S.; Kirschbaum, C.; Böhme, C.; Petrowski, K. Cortisol Stress Response in Post-Traumatic Stress Disorder, Panic Disorder, and Major Depressive Disorder Patients. *Psychoneuroendocrinology* **2017**, *83*, 135–141. https://doi.org/10.1016/j.psyneuen.2017.06.005.

(42) Han, D.; Khan, Y.; Ting, J.; King, S. M.; Yaacobi-Gross, N.; Humphries, M. J.; Newsome, C. J.; Arias, A. C. Flexible Blade-Coated Multicolor Polymer Light-Emitting Diodes for Optoelectronic Sensors. *Adv. Mater.* **2017**, *29* (22), 1606206. https://doi.org/10.1002/adma.201606206.

(43) Lee, H.; Kim, E.; Lee, Y.; Kim, H.; Lee, J.; Kim, M.; Yoo, H. J.; Yoo, S. Toward All-Day Wearable Health Monitoring: An Ultralow-Power, Reflective Organic Pulse Oximetry Sensing Patch. *Sci. Adv.* **2018**, *4* (11), eaas9530. https://doi.org/10.1126/sciadv.aas9530.

(44) Madhan Mohan, P.; Nagarajan, V.; Das, S. R. Stress Measurement from Wearable Photoplethysmographic Sensor Using Heart Rate Variability Data. In *International Conference on Communication and Signal Processing, ICCSP 2016*; Institute of Electrical and Electronics Engineers Inc., 2016; pp 1141–1144. https://doi.org/10.1109/ICCSP.2016.7754331.

(45) Li, J.; Chen, J.; Xu, F. Sensitive and Wearable Optical Microfiber Sensor for Human Health Monitoring. *Adv. Mater. Technol.* **2018**, *3* (12), 1800296. https://doi.org/10.1002/admt.201800296.

(46) Chung, S. Y.; Lee, H. J.; Lee, T. Il; Kim, Y. S. A Wearable Piezoelectric Bending Motion Sensor for Simultaneous Detection of Bending Curvature and Speed. *RSC Adv.* **2017**, *7* (5), 2520–2526. https://doi.org/10.1039/C6RA25797F.

(47) Park, D. Y.; Joe, D. J.; Kim, D. H.; Park, H.; Han, J. H.; Jeong, C. K.; Park, H.; Park, J. G.; Joung, B.; Lee, K. J. Self-Powered Real-Time Arterial Pulse Monitoring Using Ultrathin Epidermal Piezoelectric Sensors. *Adv. Mater.* **2017**, *29* (37), 1702308. https://doi.org/10.1002/adma.201702308.

(48) Bandodkar, A. J.; Wang, J. Non-Invasive Wearable Electrochemical Sensors: A Review. *Trends in Biotechnology*. Elsevier Ltd 2014, pp 363–371. https://doi.org/10.1016/j.tibtech.2014.04.005.

(49) Sonner, Z.; Wilder, E.; Heikenfeld, J.; Kasting, G.; Beyette, F.; Swaile, D.; Sherman, F.; Joyce, J.; Hagen, J.; Kelley-Loughnane, N.; Naik, R. The Microfluidics of the Eccrine Sweat Gland, Including Biomarker Partitioning, Transport, and Biosensing Implications. *Biomicrofluidics* **2015**, *9* (3), 031301. https://doi.org/10.1063/1.4921039.

(50) Heikenfeld, J. Non-Invasive Analyte Access and Sensing through Eccrine Sweat: Challenges and Outlook circa 2016. *Electroanalysis* **2016**, *28* (6), 1242–1249. https://doi.org/10.1002/elan.201600018.

(51) Parrilla, M.; Ferré, J.; Guinovart, T.; Andrade, F. J. Wearable Potentiometric Sensors Based on Commercial Carbon Fibres for Monitoring Sodium in Sweat. *Electroanalysis* **2016**, *28* (6), 1267–1275. https://doi.org/10.1002/elan.201600070.

(52) Nyein, H. Y. Y.; Tai, L. C.; Ngo, Q. P.; Chao, M.; Zhang, G. B.; Gao, W.; Bariya, M.; Bullock, J.; Kim, H.; Fahad, H. M.; Javey, A. A Wearable Microfluidic Sensing Patch for Dynamic Sweat Secretion Analysis. *ACS Sensors* **2018**, *3* (5), 944–952. https://doi.org/10.1021/acssensors.7b00961.

(53) Schazmann, B.; Morris, D.; Slater, C.; Beirne, S.; Fay, C.; Reuveny, R.; Moyna, N.; Diamond, D. A Wearable Electrochemical Sensor for the Real-Time Measurement of Sweat Sodium Concentration. *Anal. Methods* **2010**, *2* (4), 342–348. https://doi.org/10.1039/b9ay00184k.

(54) Sempionatto, J. R.; Nakagawa, T.; Pavinatto, A.; Mensah, S. T.; Imani, S.; Mercier, P.; Wang, J. Eyeglasses Based Wireless Electrolyte and Metabolite Sensor Platform. *Lab Chip* **2017**, *17* (10), 1834–1842. https://doi.org/10.1039/c7lc00192d.

(55) Dam, V. A. T.; Zevenbergen, M. A. G.; Van Schaijk, R. Flexible Chloride Sensor for Sweat Analysis. In *Procedia Engineering*; Elsevier Ltd, 2015; Vol. 120, pp 237–240. https://doi.org/10.1016/j.proeng.2015.08.588.

(56) Choi, D. H.; Thaxton, A.; Jeong, I. cheol; Kim, K.; Sosnay, P. R.; Cutting, G. R.; Searson, P. C. Sweat Test for Cystic Fibrosis: Wearable Sweat Sensor vs. Standard Laboratory Test. *J. Cyst. Fibros.* **2018**, *17* (4), e35–e38. https://doi.org/10.1016/j.jcf.2018.03.005.

(57) Nyein, H. Y. Y.; Gao, W.; Shahpar, Z.; Emaminejad, S.; Challa, S.; Chen, K.; Fahad, H. M.; Tai, L. C.; Ota, H.; Davis, R. W.; Javey, A. A Wearable Electrochemical Platform for Noninvasive Simultaneous Monitoring of Ca2+ and PH. *ACS Nano* **2016**, *10* (7), 7216–7224. https://doi.org/10.1021/acsnano.6b04005.

(58) Kang, B. C.; Park, B. S.; Ha, T. J. Highly Sensitive Wearable Glucose Sensor Systems Based on Functionalized Single-Wall Carbon Nanotubes with Glucose Oxidase-Nafion Composites. *Appl. Surf. Sci.* **2019**, *470*, 13–18. https://doi.org/10.1016/j.apsusc.2018.11.101.

(59) Mohan, A. M. V.; Windmiller, J. R.; Mishra, R. K.; Wang, J. Continuous Minimally-Invasive Alcohol Monitoring Using Microneedle Sensor Arrays. *Biosens. Bioelectron.* **2017**, *91*, 574–579. https://doi.org/10.1016/j.bios.2017.01.016.

(60) Gamella, M.; Campuzano, S.; Manso, J.; Rivera, G. G. de; López-Colino, F.; Reviejo, A. J.; Pingarrón, J. M. A Novel Non-Invasive Electrochemical Biosensing Device for in Situ Determination of the Alcohol Content in Blood by Monitoring Ethanol in Sweat. *Anal. Chim. Acta* **2014**, *806*, 1–7. https://doi.org/10.1016/j.aca.2013.09.020.

(61) Kim, J.; Jeerapan, I.; Imani, S.; Cho, T. N.; Bandodkar, A.; Cinti, S.; Mercier, P. P.; Wang, J. Noninvasive Alcohol Monitoring Using a Wearable Tattoo-Based Iontophoretic-Biosensing System. *ACS Sensors* **2016**, *1* (8), 1011–1019. https://doi.org/10.1021/acssensors.6b00356.

(62) Lee, H.; Song, C.; Hong, Y. S.; Kim, M. S.; Cho, H. R.; Kang, T.; Shin, K.; Choi, S. H.; Hyeon, T.; Kim, D. H. Wearable/Disposable Sweat-Based Glucose Monitoring Device with Multistage Transdermal Drug Delivery Module. *Sci. Adv.* **2017**, *3* (3), e1601314. https://doi.org/10.1126/sciadv.1601314.

(63) Rose, D. P.; Ratterman, M. E.; Griffin, D. K.; Hou, L.; Kelley-Loughnane, N.; Naik, R. R.; Hagen, J. A.; Papautsky, I.; Heikenfeld, J. C. Adhesive RFID Sensor Patch for Monitoring of Sweat Electrolytes. *IEEE Trans. Biomed. Eng.* **2015**, *62* (6), 1457–1465. https://doi.org/10.1109/TBME.2014.2369991.

(64) Koh, A.; Kang, D.; Xue, Y.; Lee, S.; Pielak, R. M.; Kim, J.; Hwang, T.; Min, S.; Banks, A.; Bastien, P.; Manco, M. C.; Wang, L.; Ammann, K. R.; Jang, K. I.; Won, P.; Han, S.; Ghaffari, R.; Paik, U.; Slepian, M. J.; Balooch, G.; Huang, Y.; Rogers, J. A. A Soft, Wearable Microfluidic Device for the Capture, Storage, and Colorimetric Sensing of Sweat. *Sci. Transl. Med.* **2016**, *8* (366), 366ra165-366ra165. https://doi.org/10.1126/scitranslmed.aaf2593.

(65) Tierney, M. J.; Tamada, J. A.; Potts, R. O.; Jovanovic, L.; Garg, S. Clinical Evaluation of the GlucoWatch® Biographer: A Continual, Non-Invasive Glucose Monitor for Patients with Diabetes. In *Biosensors and Bioelectronics*; Elsevier, 2001; Vol. 16, pp 621–629. https://doi.org/10.1016/S0956-5663(01)00189-0.

(66) Bariya, M.; Nyein, H. Y. Y.; Javey, A. Wearable Sweat Sensors. *Nature Electronics*. Nature Publishing Group March 1, 2018, pp 160–171. https://doi.org/10.1038/s41928-018-0043-y.

(67) Aguirre, A.; Testa-Weintraub, L. A.; Banderas, J. A.; Haraszthy, G. G.; Reddy, M. S.; Levine, M. J. Sialochemistry: A Diagnostic Tool? *Crit. Rev. Oral Biol. Med.* **1993**, *4* (3), 343–350. https://doi.org/10.1177/10454411930040031201.

(68) Valdés-Ramírez, G.; Bandodkar, A. J.; Jia, W.; Martinez, A. G.; Julian, R.; Mercier, P.; Wang, J. Non-Invasive Mouthguard Biosensor for Continuous Salivary Monitoring of Metabolites. *Analyst* **2014**, *139* (7), 1632–1636. https://doi.org/10.1039/c3an02359a.

(69) Kim, J.; Imani, S.; de Araujo, W. R.; Warchall, J.; Valdés-Ramírez, G.; Paixão, T. R. L. C.; Mercier, P. P.; Wang, J. Wearable Salivary Uric Acid Mouthguard Biosensor with Integrated Wireless Electronics. *Biosens. Bioelectron.* **2015**, *74*, 1061–1068. https://doi.org/10.1016/j.bios.2015.07.039.

(70) Minamitani, H.; Suzuki, Y.; Iijima, A.; Nagao, T. A Denture Base Type of Sensor System for Simultaneous Monitoring of Hydrogen Ion Concentration PH and Tissue Temperature in the Oral Cavity. *IEICE Trans. Inf. Syst.* **2002**, *E85-D* (1), 22–29.

(71) Graf, H.; Mühlemann, H. R. Telemetry of Plaque PH from Interdental Area. *Helv. Odontol. Acta* **1966**, *10* (2), 94–101.

(72) Mannoor, M. S.; Tao, H.; Clayton, J. D.; Sengupta, A.; Kaplan, D. L.; Naik, R. R.; Verma, N.; Omenetto, F. G.; McAlpine, M. C. Graphene-Based Wireless Bacteria Detection on Tooth Enamel. *Nat. Commun.* **2012**, *3* (1), 1–9. https://doi.org/10.1038/ncomms1767.

(73) Tseng, P.; Napier, B.; Garbarini, L.; Kaplan, D. L.; Omenetto, F. G. Functional, RF-Trilayer Sensors for Tooth-Mounted, Wireless Monitoring of the Oral Cavity and Food Consumption. *Adv. Mater.* **2018**, *30* (18), 1703257. https://doi.org/10.1002/adma.201703257.

(74) Graf, H.; Mühlemann, H. R. Oral Telemetry of Fluoride Ion Activity. *Arch. Oral Biol.* **1969**, *14* (3). https://doi.org/10.1016/0003-9969(69)90228-3.

(75) Arakawa, T.; Kuroki, Y.; Nitta, H.; Chouhan, P.; Toma, K.; Sawada, S. ichi; Takeuchi, S.; Sekita, T.; Akiyoshi, K.; Minakuchi, S.; Mitsubayashi, K. Mouthguard Biosensor with Telemetry System for Monitoring of Saliva Glucose: A Novel Cavitas Sensor. *Biosens. Bioelectron.* **2016**, *84*, 106–111. https://doi.org/10.1016/j.bios.2015.12.014.

(76) Yang, Y.; Gao, W. Wearable and Flexible Electronics for Continuous Molecular Monitoring. *Chemical Society Reviews*. Royal Society of Chemistry March 21, 2019, pp 1465–1491. https://doi.org/10.1039/c7cs00730b.

(77) Gupta, S.; Nayak, M.; Sunitha, J.; Dawar, G.; Sinha, N.; Rallan, N. Correlation of Salivary Glucose Level with Blood Glucose Level in Diabetes Mellitus. *J. Oral Maxillofac. Pathol.* **2017**, *21* (3), 334–339. https://doi.org/10.4103/jomfp.JOMFP_222_15.

(78) Ljubijankić, N.; Popović-Javorić, R.; Šćeta, S.; Šapčanin, A.; Tahirović, I.; Sofić, E. Daily Fluctuation of Cortisol in the Saliva and Serum of Healthy Persons. *Bosn. J. Basic Med. Sci.* **2008**, *8* (2), 110–115. https://doi.org/10.17305/bjbms.2008.2962.

(79) Rantamäki, A. H.; Seppänen-Laakso, T.; Oresic, M.; Jauhiainen, M.; Holopainen, J. M. Human Tear Fluid Lipidome: From Composition to Function. *PLoS One* **2011**, *6* (5). https://doi.org/10.1371/journal.pone.0019553.

(80) Farandos, N. M.; Yetisen, A. K.; Monteiro, M. J.; Lowe, C. R.; Yun, S. H. Contact Lens Sensors in Ocular Diagnostics. *Advanced Healthcare Materials*. Wiley-VCH Verlag April 1, 2015, pp 792–810. https://doi.org/10.1002/adhm.201400504.

(81) Yan, Q.; Peng, B.; Su, G.; Cohan, B. E.; Major, T. C.; Meyerhoff, M. E. Measurement of Tear Glucose Levels with Amperometric Glucose Biosensor/Capillary Tube Configuration. *Anal. Chem.* **2011**, *83* (21), 8341–8346. https://doi.org/10.1021/ac201700c.

(82) Yao, H.; Shum, A. J.; Cowan, M.; Lähdesmäki, I.; Parviz, B. A. A Contact Lens with Embedded Sensor for Monitoring Tear Glucose Level. *Biosens. Bioelectron.* **2011**, *26* (7), 3290–3296. https://doi.org/10.1016/j.bios.2010.12.042.

(83) Park, J.; Kim, J.; Kim, S. Y.; Cheong, W. H.; Jang, J.; Park, Y. G.; Na, K.; Kim, Y. T.; Heo, J. H.; Lee, C. Y.; Lee, J. H.; Bien, F.; Park, J. U. Soft, Smart Contact Lenses with Integrations of Wireless Circuits, Glucose Sensors, and Displays. *Sci. Adv.* **2018**, *4* (1), eaap9841. https://doi.org/10.1126/sciadv.aap9841.

(84) van Haeringen, N. J.; Glasius, E. Collection Method Dependant Concentrations of Some Metabolites in Human Tear Fluid, with Special Reference to Glucose in Hyperglycaemic Conditions. *Albr. von Graefes Arch. für Klin. und Exp. Ophthalmol.* **1977**, *202* (1), 1–7. https://doi.org/10.1007/BF00496763.

(85) Choy, C. K. M.; Cho, P.; Chung, W. Y.; Benzie, I. F. F. Water-Soluble Antioxidants in Human Tears: Effect of the Collection Method. *Investig. Ophthalmol. Vis. Sci.* **2001**, *42* (13), 3130–3134.

(86) Chu, M. X.; Shirai, T.; Takahashi, D.; Arakawa, T.; Kudo, H.; Sano, K.; Sawada, S. I.; Yano, K.; Iwasaki, Y.; Akiyoshi, K.; Mochizuki, M.; Mitsubayashi, K. Biomedical Soft Contact-Lens Sensor for in Situ Ocular Biomonitoring of Tear Contents. *Biomed. Microdevices* **2011**, *13* (4), 603–611. https://doi.org/10.1007/s10544-011-9530-x.

(87) Iguchi, S.; Kudo, H.; Saito, T.; Ogawa, M.; Saito, H.; Otsuka, K.; Funakubo, A.; Mitsubayashi, K. A Flexible and Wearable Biosensor for Tear Glucose Measurement. *Biomed. Microdevices* **2007**, *9* (4), 603–609. https://doi.org/10.1007/s10544-007-9073-3.

(88) Kudo, H.; Sawada, T.; Kazawa, E.; Yoshida, H.; Iwasaki, Y.; Mitsubayashi, K. A Flexible and Wearable Glucose Sensor Based on Functional Polymers with Soft-MEMS Techniques. *Biosens. Bioelectron.* **2006**, *22* (4 SPEC. ISS.), 558–562. https://doi.org/10.1016/j.bios.2006.05.006.

(89) Iguchi, S.; Mitsubayashi, K.; Uehara, T.; Ogawa, M. A Wearable Oxygen Sensor for Transcutaneous Blood Gas Monitoring at the Conjunctiva. In *Sensors and Actuators, B: Chemical*; Elsevier, 2005; Vol. 108, pp 733–737. https://doi.org/10.1016/j.snb.2004.12.099.

(90) Thomas, N.; Lähdesmäki, I.; Parviz, B. A. A Contact Lens with an Integrated Lactate Sensor. *Sensors Actuators, B Chem.* **2012**, *162* (1), 128–134. https://doi.org/10.1016/j.snb.2011.12.049.

(91) Daeschlein, G.; Langner, I.; Wild, T.; Von Podewils, S.; Sicher, C.; Kiefer, T.; Jünger, M. Hyperspectral Imaging as a Novel Diagnostic Tool in Microcirculation of Wounds. *Clin. Hemorheol. Microcirc.* **2017**, *67* (3–4), 467–474. https://doi.org/10.3233/CH-179228.

(92) Jayachandran, M.; Rodriguez, S.; Solis, E.; Lei, J.; Godavarty, A. Critical Review of Noninvasive Optical Technologies for Wound Imaging. *Advances in Wound Care*. Mary Ann Liebert Inc. August 1, 2016, pp 349–359. https://doi.org/10.1089/wound.2015.0678.

(93) Sharp, D. Printed Composite Electrodes for In-Situ Wound PH Monitoring. *Biosens. Bioelectron.* **2013**, *50*, 399–405. https://doi.org/10.1016/j.bios.2013.06.042.

(94) Lyu, B.; Punjiya, M.; Matharu, Z.; Sonkusale, S. An Improved PH Mapping Bandage with Thread-Based Sensors for Chronic Wound Monitoring. In *Proceedings - IEEE International Symposium on Circuits and Systems*; Institute of Electrical and Electronics Engineers Inc., 2018; Vol. 2018-May. https://doi.org/10.1109/ISCAS.2018.8351878.

(95) Guinovart, T.; Valdés-Ramírez, G.; Windmiller, J. R.; Andrade, F. J.; Wang, J. Bandage-Based Wearable Potentiometric Sensor for Monitoring Wound PH. *Electroanalysis* **2014**, *26* (6), 1345–1353. https://doi.org/10.1002/elan.201300558.

(96) Rahimi, R.; Ochoa, M.; Parupudi, T.; Zhao, X.; Yazdi, I. K.; Dokmeci, M. R.; Tamayol, A.; Khademhosseini, A.; Ziaie, B. A Low-Cost Flexible PH Sensor Array for Wound Assessment. *Sensors Actuators, B Chem.* **2016**, *229*, 609–617. https://doi.org/10.1016/j.snb.2015.12.082.

(97) Najafabadi, A. H.; Tamayol, A.; Annabi, N.; Ochoa, M.; Mostafalu, P.; Akbari, M.; Nikkhah, M.; Rahimi, R.; Dokmeci, M. R.; Sonkusale, S.; Ziaie, B.; Khademhosseini, A. Biodegradable Nanofibrous Polymeric Substrates for Generating Elastic and Flexible Electronics. *Adv. Mater.* **2014**, *26* (33), 5823–5830. https://doi.org/10.1002/adma.201401537.

(98) Hattori, Y.; Falgout, L.; Lee, W.; Jung, S.-Y.; Poon, E.; Lee, J. W.; Na, I.; Geisler, A.; Sadhwani, D.; Zhang, Y.; Su, Y.; Wang, X.; Liu, Z.; Xia, J.; Cheng, H.; Webb, R. C.; Bonifas, A. P.; Won, P.; Jeong, J.-W.; Jang, K.-I.; Song, Y. M.; Nardone, B.; Nodzenski, M.; Fan, J. A.; Huang, Y.; West, D. P.; Paller, A. S.; Alam, M.; Yeo, W.-H.; Rogers, J. A. Multifunctional Skin-Like Electronics for Quantitative, Clinical Monitoring of Cutaneous Wound Healing. *Adv. Healthc. Mater.* **2014**, *3* (10), 1597–1607. https://doi.org/10.1002/adhm.201400073.

(99) Jarošová, R.; McClure, S. E.; Gajda, M.; Jović, M.; Girault, H. H.; Lesch, A.; Maiden, M.; Waters, C.; Swain, G. M. Inkjet-Printed Carbon Nanotube Electrodes for Measuring Pyocyanin and Uric Acid in a Wound Fluid Simulant and Culture Media. *Anal. Chem.* **2019**, *91* (14), 8835–8844. https://doi.org/10.1021/acs.analchem.8b05591.

(100) Liu, X.; Lillehoj, P. B. Embroidered Electrochemical Sensors on Gauze for Rapid Quantification of Wound Biomarkers. *Biosens. Bioelectron.* **2017**, *98*, 189–194. https://doi.org/10.1016/j.bios.2017.06.053.

(101) Sharp, D.; Davis, J. Integrated Urate Sensors for Detecting Wound Infection. *Electrochem. commun.* **2008**, *10* (5), 709–713. https://doi.org/10.1016/j.elecom.2008.02.025.

(102) Kassal, P.; Kim, J.; Kumar, R.; De Araujo, W. R.; Steinberg, I. M.; Steinberg, M. D.; Wang, J. Smart Bandage with Wireless Connectivity for Uric Acid Biosensing as an Indicator of Wound Status. *Electrochem. commun.* **2015**, *56*, 6–10. https://doi.org/10.1016/j.elecom.2015.03.018.

(103) Schreml, S.; Szeimies, R.-M.; Karrer, S.; Heinlin, J.; Landthaler, M.; Babilas, P. The Impact of the PH Value on Skin Integrity and Cutaneous Wound Healing. *J. Eur. Acad. Dermatology Venereol.* **2010**, *24* (4), 373–378. https://doi.org/10.1111/j.1468-3083.2009.03413.x.

(104) Percival, S. L.; McCarty, S.; Hunt, J. A.; Woods, E. J. The Effects of PH on Wound Healing, Biofilms, and Antimicrobial Efficacy. *Wound Repair Regen.* **2014**, *22* (2), 174–186. https://doi.org/10.1111/wrr.12125.

(105) Schneider, L. A.; Korber, A.; Grabbe, S.; Dissemond, J. Influence of PH on Wound-Healing: A New Perspective for Wound-Therapy? *Archives of Dermatological Research*. Springer February 8, 2007, pp 413–420. https://doi.org/10.1007/s00403-006-0713-x.

(106) Jones, E. M.; Cochrane, C. A.; Percival, S. L. The Effect of PH on the Extracellular Matrix and Biofilms. *Adv. Wound Care* **2015**, *4* (7), 431–439. https://doi.org/10.1089/wound.2014.0538.

(107) Rahimi, R.; Ochoa, M.; Tamayol, A.; Khalili, S.; Khademhosseini, A.; Ziaie, B. Highly Stretchable Potentiometric PH Sensor Fabricated via Laser Carbonization and Machining of Carbon−Polyaniline Composite. *ACS Appl. Mater. Interfaces* **2017**, *9* (10), 9015–9023. https://doi.org/10.1021/acsami.6b16228.

(108) Tamayol, A.; Akbari, M.; Zilberman, Y.; Comotto, M.; Lesha, E.; Serex, L.; Bagherifard, S.; Chen, Y.; Fu, G.; Ameri, S. K.; Ruan, W.; Miller, E. L.; Dokmeci, M. R.; Sonkusale, S.; Khademhosseini, A. Flexible PH-Sensing Hydrogel Fibers for Epidermal Applications. *Adv. Healthc. Mater.* **2016**, *5* (6), 711–719. https://doi.org/10.1002/adhm.201500553.

(109) Derakhshandeh, H.; Kashaf, S. S.; Aghabaglou, F.; Ghanavati, I. O.; Tamayol, A. Smart Bandages: The Future of Wound Care. *Trends in Biotechnology*. Elsevier Ltd December 1, 2018, pp 1259–1274. https://doi.org/10.1016/j.tibtech.2018.07.007.

(110) Tamayol, A.; Hassani Najafabadi, A.; Mostafalu, P.; Yetisen, A. K.; Commotto, M.; Aldhahri, M.; Abdel-Wahab, M. S.; Najafabadi, Z. I.; Latifi, S.; Akbari, M.; Annabi, N.; Yun, S. H.; Memic, A.; Dokmeci, M. R.; Khademhosseini, A. Biodegradable Elastic Nanofibrous Platforms with Integrated Flexible Heaters for On-Demand Drug Delivery. *Sci. Rep.* **2017**, *7* (1), 1–10. https://doi.org/10.1038/s41598-017-04749-8.

(111) Mostafalu, P.; Kiaee, G.; Giatsidis, G.; Khalilpour, A.; Nabavinia, M.; Dokmeci, M. R.; Sonkusale, S.; Orgill, D. P.; Tamayol, A.; Khademhosseini, A. A Textile Dressing for Temporal and Dosage Controlled Drug Delivery. *Adv. Funct. Mater.* **2017**, *27* (41), 1702399. https://doi.org/10.1002/adfm.201702399.

(112) Bagherifard, S.; Tamayol, A.; Mostafalu, P.; Akbari, M.; Comotto, M.; Annabi, N.; Ghaderi, M.; Sonkusale, S.; Dokmeci, M. R.; Khademhosseini, A. Dermal Patch with Integrated Flexible Heater for on Demand Drug Delivery. *Adv. Healthc. Mater.* **2016**, *5* (1), 175–184. https://doi.org/10.1002/adhm.201500357.

(113) Bagherifard, S.; Tamayol, A.; Mostafalu, P.; Akbari, M.; Comotto, M.; Annabi, N.; Ghaderi, M.; Sonkusale, S.; Dokmeci, M. R.; Khademhosseini, A. Dermal Patch with Integrated Flexible Heater for on Demand Drug Delivery. *Adv. Healthc. Mater.* **2016**, *5* (1), 175–184. https://doi.org/10.1002/adhm.201500357.

(114) Mostafalu, P.; Kiaee, G.; Giatsidis, G.; Khalilpour, A.; Nabavinia, M.; Dokmeci, M. R.; Sonkusale, S.; Orgill, D. P.; Tamayol, A.; Khademhosseini, A. A Textile Dressing for Temporal and Dosage Controlled Drug Delivery. *Adv. Funct. Mater.* **2017**, *27* (41), 1702399. https://doi.org/10.1002/adfm.201702399.

(115) WILLIAMS, R. W.; MASON, L. B.; BRADSHAW, H. H. Factors Affecting Wound Healing. *Surg. Forum* **1950**, *89* (3), 410–417. https://doi.org/10.1177/0022034509359125.

(116) Fromm, H. J. The Effect of Temperature and PH on Enzyme Activity; Springer, Berlin, Heidelberg, 1975; pp 201–235. https://doi.org/10.1007/978-3-642-80966-8_8.

(117) Larsen, M. J.; Jensen, A. F.; Madsen, D. M.; Pearce, E. I. F. Individual Variations of PH, Buffer Capacity, and Concentrations of Calcium and Phosphate in Unstimulated Whole Saliva. *Arch. Oral Biol.* **1999**, *44* (2), 111–117. https://doi.org/10.1016/S0003-9969(98)00108-3.

(118) Wang, S.; Zhang, G.; Meng, H.; Li, L. Effect of Exercise-Induced Sweating on Facial Sebum, Stratum Corneum Hydration, and Skin Surface Ph in Normal Population. *Ski. Res. Technol.* **2013**, *19* (1). https://doi.org/10.1111/j.1600-0846.2012.00645.x.

(119) Gerrett, N.; Amano, T.; Inoue, Y.; Havenith, G.; Kondo, N. The Effects of Exercise and Passive Heating on the Sweat Glands Ion Reabsorption Rates. *Physiol. Rep.* **2018**, *6* (5). https://doi.org/10.14814/phy2.13619.

(120) Jones, L. A.; Muhlfeld, C. C.; Hauer, F. R. Temperature. In *Methods in Stream Ecology: Third Edition*; Elsevier Inc., 2017; Vol. 1, pp 109–120. https://doi.org/10.1016/B978-0-12-416558-8.00006-8.

(121) Dak, P.; Ebrahimi, A.; Alam, M. A. Non-Faradaic Impedance Characterization of an Evaporating Droplet for Microfluidic and Biosensing Applications. *Lab Chip* **2014**, *14* (14), 2469–2479. https://doi.org/10.1039/c4lc00193a.

(122) Norouzi Rad, M.; Shokri, N. Nonlinear Effects of Salt Concentrations on Evaporation from Porous Media. *Geophys. Res. Lett.* **2012**, *39* (4), n/a-n/a. https://doi.org/10.1029/2011GL050763.

(123) Bazargan, V.; Stoeber, B. Effect of Substrate Conductivity on the Evaporation of Small Sessile Droplets. *Phys. Rev. E* **2016**, *94* (3), 033103. https://doi.org/10.1103/PhysRevE.94.033103.

(124) Sobac, B.; Brutin, D. Thermal Effects of the Substrate on Water Droplet Evaporation. *Phys. Rev. E - Stat. Nonlinear, Soft Matter Phys.* **2012**, *86* (2), 021602. https://doi.org/10.1103/PhysRevE.86.021602.

(125) Lopes, M. C.; Bonaccurso, E.; Gambaryan-Roisman, T.; Stephan, P. Influence of the Substrate Thermal Properties on Sessile Droplet Evaporation: Effect of Transient Heat Transport. *Colloids Surfaces A Physicochem. Eng. Asp.* **2013**, *432*, 64–70. https://doi.org/10.1016/j.colsurfa.2013.04.017.

(126) Yokota, M.; Berglund, L. G.; Gonzalez, J. A.; Blanchard, L. A. *Transient Sweat Rate Calculation from Humidity Measurements under Clothing*; 2006.

(127) Sato, K.; Sato, F. Individual Variations in Structure and Function of Human Eccrine Sweat Gland. *Am. J. Physiol. - Regul. Integr. Comp. Physiol.* **1983**, *14* (2). https://doi.org/10.1152/ajpregu.1983.245.2.r203.

(128) NIELSEN, B.; NIELSEN, M. On the Regulation of Sweat Secretion in Exercise. *Acta Physiol. Scand.* **1965**, *64* (4), 314–322. https://doi.org/10.1111/j.1748-1716.1965.tb04185.x.

(129) Buono, M. J.; Ball, K. D.; Kolkhorst, F. W. Sodium Ion Concentration vs. Sweat Rate Relationship in Humans. *J. Appl. Physiol.* **2007**, *103* (3), 990–994. https://doi.org/10.1152/japplphysiol.00015.2007.

(130) Van Andel, E.; De Bus, I.; Tijhaar, E. J.; Smulders, M. M. J.; Savelkoul, H. F. J.; Zuilhof, H. Highly Specific Binding on Antifouling Zwitterionic Polymer-Coated Microbeads as Measured by Flow Cytometry. *ACS Appl. Mater. Interfaces* **2017**, *9* (44), 38211–38221. https://doi.org/10.1021/acsami.7b09725.

(131) Walsh, T. R.; Knecht, M. R. Biointerface Structural Effects on the Properties and Applications of Bioinspired Peptide-Based Nanomaterials. *Chemical Reviews*. American Chemical Society October 25, 2017, pp 12641–12704. https://doi.org/10.1021/acs.chemrev.7b00139.

(132) Moulton, S. E.; Barisci, J. N.; Bath, A.; Stella, R.; Wallace, G. G. Studies of Double Layer Capacitance and Electron Transfer at a Gold Electrode Exposed to Protein Solutions. *Electrochim. Acta* **2004**, *49* (24), 4223–4230. https://doi.org/10.1016/j.electacta.2004.03.034.

(133) Hu, Y.; Liang, B.; Fang, L.; Ma, G.; Yang, G.; Zhu, Q.; Chen, S.; Ye, X. Antifouling Zwitterionic Coating via Electrochemically Mediated Atom Transfer Radical Polymerization on Enzyme-Based Glucose Sensors for Long-Time Stability in 37 °c Serum. *Langmuir* **2016**, *32* (45), 11763–11770. https://doi.org/10.1021/acs.langmuir.6b03016.

(134) Goda, T.; Tabata, M.; Sanjoh, M.; Uchimura, M.; Iwasaki, Y.; Miyahara, Y. Thiolated 2-Methacryloyloxyethyl Phosphorylcholine for an Antifouling Biosensor Platform. *Chem. Commun.* **2013**, *49* (77), 8683–8685. https://doi.org/10.1039/c3cc44357d.

(135) Roy, S.; Soh, J. H.; Ying, J. Y. A Microarray Platform for Detecting Disease-Specific Circulating MiRNA in Human Serum. *Biosens. Bioelectron.* **2016**, *75*, 238–246. https://doi.org/10.1016/j.bios.2015.08.039.

(136) Emilsson, G.; Schoch, R. L.; Feuz, L.; Höök, F.; Lim, R. Y. H.; Dahlin, A. B. Strongly Stretched Protein Resistant Poly(Ethylene Glycol) Brushes Prepared by Grafting-To. *ACS Appl. Mater. Interfaces* **2015**, *7* (14), 7505–7515. https://doi.org/10.1021/acsami.5b01590.

(137) Roberts, J. R.; Park, J.; Helton, K.; Wisniewski, N.; McShane, M. J. Biofouling of Polymer Hydrogel Materials and Its Effect on Diffusion and Enzyme-Based Luminescent Glucose Sensor Functional Characteristics. In *Journal of Diabetes Science and Technology*; Diabetes Technology Society, 2012; Vol. 6, pp 1267–1275. https://doi.org/10.1177/193229681200600605.

(138) Frykberg, R. G.; Banks, J. Management of Diabetic Foot Ulcers: A Review. *Fed. Pract.* **2016**, *33* (2), 16.

(139) Dini, V.; Salvo, P.; Janowska, A.; Di Francesco, F.; Barbini, A.; Romanelli, M. Correlation between Wound Temperature Obtained with an Infrared Camera and Clinical Wound Bed Score in Venous Leg Ulcers. *Wounds* **2015**, *27* (10), 274–278.

(140) Rice, J. B.; Desai, U.; Cummings, A. K. G.; Birnbaum, H. G.; Skornicki, M.; Parsons, N. Burden of Venous Leg Ulcers in the United States. *J. Med. Econ.* **2014**, *17* (5), 347–356.

(141) Lim, H. W.; Collins, S. A. B.; Resneck Jr, J. S.; Bolognia, J. L.; Hodge, J. A.; Rohrer, T. A.; Van Beek, M. J.; Margolis, D. J.; Sober, A. J.; Weinstock, M. A. The Burden of Skin Disease in the United States. *J. Am. Acad. Dermatol.* **2017**, *76* (5), 958-972. e2.

(142) Papazoglou, E. S.; Zubkov, L.; Mao, X.; Neidrauer, M.; Rannou, N.; Weingarten, M. S. Image Analysis of Chronic Wounds for Determining the Surface Area. *Wound repair Regen.* **2010**, *18* (4), 349–358.

(143) Cobb, M. J.; Chen, Y.; Underwood, R. A.; Usui, M. L.; Olerud, J.; Li, X. Noninvasive Assessment of Cutaneous Wound Healing Using Ultrahigh-Resolution Optical Coherence Tomography. *J. Biomed. Opt.* **2006**, *11* (6), 64002.

(144) Ono, S.; Imai, R.; Ida, Y.; Shibata, D.; Komiya, T.; Matsumura, H. Increased Wound PH as an Indicator of Local Wound Infection in Second Degree Burns. *Burns* **2015**, *41* (4), 820–824.

(145) Kassal, P.; Zubak, M.; Scheipl, G.; Mohr, G. J.; Steinberg, M. D.; Steinberg, I. M. Smart Bandage with Wireless Connectivity for Optical Monitoring of PH. *Sensors Actuators B Chem.* **2017**, *246*, 455–460.

(146) Guinovart, T.; Valdés-Ramírez, G.; Windmiller, J. R.; Andrade, F. J.; Wang, J. Bandage-Based Wearable Potentiometric Sensor for Monitoring Wound PH. *Electroanalysis* **2014**, *26* (6), 1345–1353.

(147) Farooqui, M. F.; Shamim, A. Low Cost Inkjet Printed Smart Bandage for Wireless Monitoring of Chronic Wounds. *Sci. Rep.* **2016**, *6*, 28949.

(148) Sharp, D.; Gladstone, P.; Smith, R. B.; Forsythe, S.; Davis, J. Approaching Intelligent Infection Diagnostics: Carbon Fibre Sensor for Electrochemical Pyocyanin Detection. *Bioelectrochemistry* **2010**, *77* (2), 114–119.

(149) Ciani, I.; Schulze, H.; Corrigan, D. K.; Henihan, G.; Giraud, G.; Terry, J. G.; Walton, A. J.; Pethig, R.; Ghazal, P.; Crain, J. Development of Immunosensors for Direct Detection of Three Wound Infection Biomarkers at Point of Care Using Electrochemical Impedance Spectroscopy. *Biosens. Bioelectron.* **2012**, *31* (1), 413–418.

(150) Kassal, P.; Kim, J.; Kumar, R.; de Araujo, W. R.; Steinberg, I. M.; Steinberg, M. D.; Wang, J. Smart Bandage with Wireless Connectivity for Uric Acid Biosensing as an Indicator of Wound Status. *Electrochem. commun.* **2015**, *56*, 6–10.

(151) Pal, A.; Goswami, D.; Cuellar, H. E.; Castro, B.; Kuang, S.; Martinez, R. V. Early Detection and Monitoring of Chronic Wounds Using Low-Cost, Omniphobic Paper-Based Smart Bandages. *Biosens. Bioelectron.* **2018**, *117*, 696–705.

(152) RoyChoudhury, S.; Umasankar, Y.; Hutcheson, J. D.; Lev-Tov, H. A.; Kirsner, R. S.; Bhansali, S. Uricase Based Enzymatic Biosensor for Non-Invasive Detection of Uric Acid by Entrapment in PVA-SbQ Polymer Matrix. *Electroanalysis* **2018**, *30* (10), 2374–2385.

(153) RoyChoudhury, S.; Umasankar, Y.; Jaller, J.; Herskovitz, I.; Mervis, J.; Darwin, E.; Hirt, P. A.; Borda, L. J.; Lev-Tov, H. A.; Kirsner, R. Continuous Monitoring of Wound Healing Using a Wearable Enzymatic Uric Acid Biosensor. *J. Electrochem. Soc.* **2018**, *165* (8), B3168–B3175.

(154) McCord, J. M. Oxygen-Derived Free Radicals in Postischemic Tissue Injury. *N. Engl. J. Med.* **1985**, *312* (3), 159–163.

(155) Fernandez, M. L.; Upton, Z.; Edwards, H.; Finlayson, K.; Shooter, G. K. Elevated Uric Acid Correlates with Wound Severity. *Int. Wound J.* **2012**, *9* (2), 139–149.

(156) Luo, J.; Jiang, S.; Zhang, H.; Jiang, J.; Liu, X. A Novel Non-Enzymatic Glucose Sensor Based on Cu Nanoparticle Modified Graphene Sheets Electrode. *Anal. Chim. Acta* **2012**, *709*, 47–53.

(157) Pedrosa, V. A.; Paliwal, S.; Balasubramanian, S.; Nepal, D.; Davis, V.; Wild, J.; Ramanculov, E.; Simonian, A. Enhanced Stability of Enzyme Organophosphate Hydrolase Interfaced on the Carbon Nanotubes. *Colloids Surfaces B Biointerfaces* **2010**, *77* (1), 69–74.

(158) Verma, M. L.; Naebe, M.; Barrow, C. J.; Puri, M. Enzyme Immobilisation on Amino-Functionalised Multi-Walled Carbon Nanotubes: Structural and Biocatalytic Characterisation. *PLoS One* **2013**, *8* (9), e73642.

(159) Jain, S.; Verma, S.; Singh, S. P.; Sharma, S. N. An Electrochemical Biosensor Based on Novel Butylamine Capped CZTS Nanoparticles Immobilized by Uricase for Uric Acid Detection. *Biosens. Bioelectron.* **2019**, *127*, 135–141.

(160) Rodríguez-López, J. N.; Lowe, D. J.; Hernández-Ruiz, J.; Hiner, A. N. P.; García-Cánovas, F.; Thorneley, R. N. F. Mechanism of Reaction of Hydrogen Peroxide with Horseradish Peroxidase: Identification of Intermediates in the Catalytic Cycle. *J. Am. Chem. Soc.* **2001**, *123* (48), 11838–11847.

(161) Le, T. X. H.; Esmilaire, R.; Drobek, M.; Bechelany, M.; Vallicari, C.; Nguyen, D. L.; Julbe, A.; Tingry, S.; Cretin, M. Design of a Novel Fuel Cell-Fenton System: A Smart Approach to Zero Energy Depollution. *J. Mater. Chem. A* **2016**, *4* (45), 17686–17693.

(162) Le, T. X. H.; Bechelany, M.; Engel, A. B.; Cretin, M.; Tingry, S. Gold Particles Growth on Carbon Felt for Efficient Micropower Generation in a Hybrid Biofuel Cell. *Electrochim. Acta* **2016**, *219*, 121–129.

(163) Both Engel, A.; Bechelany, M.; Fontaine, O.; Cherifi, A.; Cornu, D.; Tingry, S. One-Pot Route to Gold Nanoparticles Embedded in Electrospun Carbon Fibers as an Efficient Catalyst Material for Hybrid Alkaline Glucose Biofuel Cells. *ChemElectroChem* **2016**, *3* (4), 629–637.

(164) Fang, Y.; Umasankar, Y.; Ramasamy, R. P. A Novel Bi-Enzyme Electrochemical Biosensor for Selective and Sensitive Determination of Methyl Salicylate. *Biosens. Bioelectron.* **2016**, *81*, 39–45.

(165) Dai, M.; Huang, T.; Chao, L.; Xie, Q.; Tan, Y.; Chen, C.; Meng, W. Horseradish Peroxidase-Catalyzed Polymerization of l-DOPA for Mono-/Bi-Enzyme Immobilization and Amperometric Biosensing of H2O2 and Uric Acid. *Talanta* **2016**, *149*, 117–123.

(166) Castillo, J.; Gáspár, S.; Sakharov, I.; Csöregi, E. Bienzyme Biosensors for Glucose, Ethanol and Putrescine Built on Oxidase and Sweet Potato Peroxidase. *Biosens. Bioelectron.* **2003**, *18* (5–6), 705–714.

(167) Roşca, D. A.; Wright, J. A.; Hughes, D. L.; Bochmann, M. Gold Peroxide Complexes and the Conversion of Hydroperoxides into Gold Hydrides by Successive Oxygen-Transfer Reactions. *Nat. Commun.* **2013**, *4* (1), 1–7. https://doi.org/10.1038/ncomms3167.

(168) Wang, H.; Dong, Z.; Na, C. Hierarchical Carbon Nanotube Membrane-Supported Gold Nanoparticles for Rapid Catalytic Reduction of p-Nitrophenol. *ACS Sustain. Chem. Eng.* **2013**, *1* (7), 746–752.

(169) Georgakilas, V.; Gournis, D.; Tzitzios, V.; Pasquato, L.; Guldi, D. M.; Prato, M. Decorating Carbon Nanotubes with Metal or Semiconductor Nanoparticles. *J. Mater. Chem.* **2007**, *17* (26), 2679–2694.

(170) Bonneté, F. Macromolecular Crystallization Controlled by Colloidal Interactions: The Case of Urate Oxidase. In *Crystallization-Science and Technology*; InTech, 2012.

(171) Asuri, P.; Karajanagi, S. S.; Yang, H.; Yim, T.-J.; Kane, R. S.; Dordick, J. S. Increasing Protein Stability through Control of the Nanoscale Environment. *Langmuir* **2006**, *22* (13), 5833–5836.

(172) Asuri, P.; Karajanagi, S. S.; Sellitto, E.; Kim, D.; Kane, R. S.; Dordick, J. S. Water-soluble Carbon Nanotube-enzyme Conjugates as Functional Biocatalytic Formulations. *Biotechnol. Bioeng.* **2006**, *95* (5), 804–811.

(173) Trengove, N. J.; Langton, S. R.; Stacey, M. C. Biochemical Analysis of Wound Fluid from Nonhealing and Healing Chronic Leg Ulcers. *Wound repair Regen.* **1996**, *4* (2), 234–239.

(174) Omar, M. N.; Salleh, A. B.; Lim, H. N.; Tajudin, A. A. Electrochemical Detection of Uric Acid via Uricase-Immobilized Graphene Oxide. *Anal. Biochem.* **2016**, *509*, 135–141.

(175) Ahmad, R.; Tripathy, N.; Ahn, M.-S.; Hahn, Y.-B. Solution Process Synthesis of High Aspect Ratio ZnO Nanorods on Electrode Surface for Sensitive Electrochemical Detection of Uric Acid. *Sci. Rep.* **2017**, *7*, 46475.

(176) Ali, M.; Shah, I.; Kim, S. W.; Sajid, M.; Lim, J. H.; Choi, K. H. Quantitative Detection of Uric Acid through ZnO Quantum Dots Based Highly Sensitive Electrochemical Biosensor. *Sensors Actuators A Phys.* **2018**, *283*, 282–290.

(177) Verma, S.; Choudhary, J.; Singh, K. P.; Chandra, P.; Singh, S. P. Uricase Grafted Nanoconducting Matrix Based Electrochemical Biosensor for Ultrafast Uric Acid Detection in Human Serum Samples. *Int. J. Biol. Macromol.* **2019**, *130*, 333–341.

(178) Jung, M.; Jeon, S.; Bae, J. Scalable and Facile Synthesis of Stretchable Thermoelectric Fabric for Wearable Self-Powered Temperature Sensors. *RSC Adv.* **2018**, *8* (70), 39992–39999. https://doi.org/10.1039/C8RA06664G.

(179) Hughes-Riley, T.; Lugoda, P.; Dias, T.; Trabi, C.; Morris, R. A Study of Thermistor Performance within a Textile Structure. *Sensors* **2017**, *17* (8), 1804. https://doi.org/10.3390/s17081804.

(180) Paul, G.; Torah, R.; Beeby, S.; Tudor, J. Novel Active Electrodes for ECG Monitoring on Woven Textiles Fabricated by Screen and Stencil Printing. *Sensors Actuators, A Phys.* **2015**, *221*, 60–66. https://doi.org/10.1016/j.sna.2014.10.030.

(181) Coosemans, J.; Hermans, B.; Puers, R. Integrating Wireless ECG Monitoring in Textiles. *Sensors Actuators, A Phys.* **2006**, *130–131* (SPEC. ISS.), 48–53. https://doi.org/10.1016/j.sna.2005.10.052.

(182) Pani, D.; Dessi, A.; Saenz-Cogollo, J. F.; Barabino, G.; Fraboni, B.; Bonfiglio, A. Fully Textile, PEDOT:PSS Based Electrodes for Wearable ECG Monitoring Systems. *IEEE Trans. Biomed. Eng.* **2016**, *63* (3), 540–549. https://doi.org/10.1109/TBME.2015.2465936.

(183) Esfahani, M. I. M.; Nussbaum, M. A. A "Smart" Undershirt for Tracking Upper Body Motions: Task Classification and Angle Estimation. *IEEE Sens. J.* **2018**, *18* (18), 7650–7658. https://doi.org/10.1109/JSEN.2018.2859626.

(184) Liu, M.; Pu, X.; Jiang, C.; Liu, T.; Huang, X.; Chen, L.; Du, C.; Sun, J.; Hu, W.; Wang, Z. L. Large-Area All-Textile Pressure Sensors for Monitoring Human Motion and Physiological Signals. *Adv. Mater.* **2017**, *29* (41), 1703700. https://doi.org/10.1002/adma.201703700.

(185) Merritt, C. R.; Nagle, H. T.; Grant, E. Textile-Based Capacitive Sensors for Respiration Monitoring. *IEEE Sens. J.* **2009**, *9* (1), 71–78. https://doi.org/10.1109/JSEN.2008.2010356.

(186) Yang, X.; Chen, Z.; Elvin, C. S. M.; Janice, L. H. Y.; Ng, S. H.; Teo, J. T.; Wu, R. Textile Fiber Optic Microbend Sensor Used for Heartbeat and Respiration Monitoring. *IEEE Sens. J.* **2015**, *15* (2), 757–761. https://doi.org/10.1109/JSEN.2014.2353640.

(187) Guinovart, T.; Valdés-Ramírez, G.; Windmiller, J. R.; Andrade, F. J.; Wang, J. Bandage-Based Wearable Potentiometric Sensor for Monitoring Wound PH. *Electroanalysis* **2014**, *26* (6), 1345–1353. https://doi.org/10.1002/elan.201300558.

(188) Windmiller, J. R.; Bandodkar, A. J.; Parkhomovsky, S.; Wang, J. Stamp Transfer Electrodes for Electrochemical Sensing on Non-Planar and Oversized Surfaces. *Analyst* **2012**, *137* (7), 1570–1575. https://doi.org/10.1039/c2an35041f.

(189) Liu, X.; Lillehoj, P. B. Embroidered Electrochemical Sensors for Biomolecular Detection. *Lab Chip* **2016**, *16* (11), 2093–2098. https://doi.org/10.1039/c6lc00307a.

(190) Abadi, Z.; Mottaghitalab, V.; Bidoki, M.; Benvidi, A. Flexible Biosensor Using Inkjet Printing of Silver Nanoparticles. *Sens. Rev.* **2014**, *34* (4), 360–366. https://doi.org/10.1108/SR-07-2013-704.

(191) Afroj, S.; Karim, N.; Wang, Z.; Tan, S.; He, P.; Holwill, M.; Ghazaryan, D.; Fernando, A.; Novoselov, K. S. Engineering Graphene Flakes for Wearable Textile Sensors via Highly Scalable and Ultrafast Yarn Dyeing Technique. *ACS Nano* **2019**, *13* (4), 3847–3857. https://doi.org/10.1021/acsnano.9b00319.

(192) Yang, Y. L.; Chuang, M. C.; Lou, S. L.; Wang, J. Thick-Film Textile-Based Amperometric Sensors and Biosensors. *Analyst* **2010**, *135* (6), 1230–1234. https://doi.org/10.1039/b926339j.

(193) Parrilla, M.; Cánovas, R.; Jeerapan, I.; Andrade, F. J.; Wang, J. A Textile-Based Stretchable Multi-Ion Potentiometric Sensor. *Adv. Healthc. Mater.* **2016**, *5* (9), 996–1001. https://doi.org/10.1002/adhm.201600092.

(194) Yokus, M. A.; Foote, R.; Jur, J. S. Printed Stretchable Interconnects for Smart Garments: Design, Fabrication, and Characterization. *IEEE Sens. J.* **2016**, *16* (22), 7967–7976. https://doi.org/10.1109/JSEN.2016.2605071.

(195) Schrenk, W. J.; Alfrey, T. Some Physical Properties of Multilayered Films. *Polym. Eng. Sci.* **1969**, *9* (6), 393–399. https://doi.org/10.1002/pen.760090604.

(196) Yang, C.-H.; Chou, K.-T.; Chung, M.-B.; Chuang, K. S.; Huang, T.-C. Automatic Detection of Calcaneal-Fifth Metatarsal Angle Using Radiograph: A Computer-Aided Diagnosis of Flat Foot for Military New Recruits in Taiwan. *PLoS One* **2015**, *10* (6), e0131387. https://doi.org/10.1371/journal.pone.0131387.

(197) Liu, R.; Liu, J.; Lao, T. T.; Ying, M.; Wu, X. Determination of Leg Cross-Sectional Curvatures and Application in Pressure Prediction for Lower Body Compression Garments. *Text. Res. J.* **2019**, *89* (10), 1835–1852. https://doi.org/10.1177/0040517518779246.

(198) Bandodkar, A. J.; Nuñez-Flores, R.; Jia, W.; Wang, J. All-Printed Stretchable Electrochemical Devices. *Adv. Mater.* **2015**, *27* (19), 3060–3065. https://doi.org/10.1002/adma.201500768.

(199) Yin, L.; Lv, J.; Wang, J. Structural Innovations in Printed, Flexible, and Stretchable Electronics. *Adv. Mater. Technol.* **2020**, *5* (11), 2000694. https://doi.org/10.1002/admt.202000694.

(200) Krawczyk, K. K.; Groten, J.; Glushko, O.; Krivec, M.; Frühwirth, M.; Schulz, G.; Wolf, C.; Hartmann, D.; Moser, M.; Cordill, M. J.; Stadlober, B.; Griesser, T. Self-Reducing Silver Ink on Polyurethane Elastomers for the Manufacture of Thin and Highly Stretchable Electrical Circuits. *Chem. Mater.* **2021**. https://doi.org/10.1021/acs.chemmater.0c04025.

(201) Liu, Y. L.; Liu, R.; Qin, Y.; Qiu, Q. F.; Chen, Z.; Cheng, S. B.; Huang, W. H. Flexible Electrochemical Urea Sensor Based on Surface Molecularly Imprinted Nanotubes for Detection of Human Sweat. *Anal. Chem.* **2018**, *90* (21), 13081–13087. https://doi.org/10.1021/acs.analchem.8b04223.

(202) Nakata, S.; Arie, T.; Akita, S.; Takei, K. Wearable, Flexible, and Multifunctional Healthcare Device with an ISFET Chemical Sensor for Simultaneous Sweat PH and Skin Temperature Monitoring. *ACS Sensors* **2017**, *2* (3), 443–448. https://doi.org/10.1021/acssensors.7b00047.

(203) Khan, Y.; Garg, M.; Gui, Q.; Schadt, M.; Gaikwad, A.; Han, D.; Yamamoto, N. A. D.; Hart, P.; Welte, R.; Wilson, W.; Czarnecki, S.; Poliks, M.; Jin, Z.; Ghose, K.; Egitto, F.; Turner, J.; Arias, A. C. Flexible Hybrid Electronics: Direct Interfacing of Soft and Hard Electronics for Wearable Health Monitoring. *Adv. Funct. Mater.* **2016**, *26* (47), 8764–8775. https://doi.org/10.1002/adfm.201603763.

(204) Trung, T. Q.; Lee, N.-E. Flexible and Stretchable Physical Sensor Integrated Platforms for Wearable Human-Activity Monitoringand Personal Healthcare. *Adv. Mater.* **2016**, *28* (22), 4338–4372. https://doi.org/10.1002/adma.201504244.

(205) Jia, W.; Bandodkar, A. J.; Valdés-Ramírez, G.; Windmiller, J. R.; Yang, Z.; Ramírez, J.; Chan, G.; Wang, J. Electrochemical Tattoo Biosensors for Real-Time Noninvasive Lactate Monitoring in Human Perspiration. *Anal. Chem.* **2013**, *85* (14), 6553–6560. https://doi.org/10.1021/ac401573r.

(206) Kim, J.; Sempionatto, J. R.; Imani, S.; Hartel, M. C.; Barfidokht, A.; Tang, G.; Campbell, A. S.; Mercier, P. P.; Wang, J. Simultaneous Monitoring of Sweat and Interstitial Fluid Using a Single Wearable Biosensor Platform. *Adv. Sci.* **2018**, *5* (10), 1800880. https://doi.org/10.1002/advs.201800880.

(207) Yang, Y.; Song, Y.; Bo, X.; Min, J.; Pak, O. S.; Zhu, L.; Wang, M.; Tu, J.; Kogan, A.; Zhang, H.; Hsiai, T. K.; Li, Z.; Gao, W. A Laser-Engraved Wearable Sensor for Sensitive Detection of Uric Acid and Tyrosine in Sweat. *Nat. Biotechnol.* **2020**, *38* (2), 217–224. https://doi.org/10.1038/s41587-019-0321-x.

(208) Wang, Y.; Wang, X.; Lu, W.; Yuan, Q.; Zheng, Y.; Yao, B. A Thin Film Polyethylene Terephthalate (PET) Electrochemical Sensor for Detection of Glucose in Sweat. *Talanta* **2019**, *198*, 86–92. https://doi.org/10.1016/j.talanta.2019.01.104.

(209) Yamamoto, Y.; Harada, S.; Yamamoto, D.; Honda, W.; Arie, T.; Akita, S.; Takei, K. Printed Multifunctional Flexible Device with an Integrated Motion Sensor for Health Care Monitoring. *Sci. Adv.* **2016**, *2* (11). https://doi.org/10.1126/sciadv.1601473.

(210) Maier, D.; Laubender, E.; Basavanna, A.; Schumann, S.; Güder, F.; Urban, G. A.; Dincer, C. Toward Continuous Monitoring of Breath Biochemistry: A Paper-Based Wearable Sensor for Real-Time Hydrogen Peroxide Measurement in Simulated Breath. *ACS Sensors* **2019**, *4* (11), 2945–2951. https://doi.org/10.1021/acssensors.9b01403.

(211) Cao, Q.; Liang, B.; Tu, T.; Wei, J.; Fang, L.; Ye, X. Three-Dimensional Paper-Based Microfluidic Electrochemical Integrated Devices (3D-PMED) for Wearable Electrochemical Glucose Detection. *RSC Adv.* **2019**, *9* (10), 5674–5681. https://doi.org/10.1039/c8ra09157a.

(212) An, Q.; Gan, S.; Xu, J.; Bao, Y.; Wu, T.; Kong, H.; Zhong, L.; Ma, Y.; Song, Z.; Niu, L. A Multichannel Electrochemical All-Solid-State Wearable Potentiometric Sensor for Real-Time Sweat Ion Monitoring. *Electrochem. commun.* **2019**, *107*, 106553. https://doi.org/10.1016/j.elecom.2019.106553.

(213) He, W.; Wang, C.; Wang, H.; Jian, M.; Lu, W.; Liang, X.; Zhang, X.; Yang, F.; Zhang, Y. Integrated Textile Sensor Patch for Real-Time and Multiplex Sweat Analysis. *Sci. Adv.* **2019**, *5* (11), eaax0649. https://doi.org/10.1126/sciadv.aax0649.

(214) Pal, A.; Goswami, D.; Cuellar, H. E.; Castro, B.; Kuang, S.; Martinez, R. V. Early Detection and Monitoring of Chronic Wounds Using Low-Cost, Omniphobic Paper-Based Smart Bandages. *Biosens. Bioelectron.* **2018**, *117*, 696–705. https://doi.org/10.1016/j.bios.2018.06.060.

(215) Wu, R.; Ma, C.; Yong, Y. C.; Job Zhang, Y. H. P.; Zhu, Z. Composition and Distribution of Internal Resistance in an Enzymatic Fuel Cell and Its Dependence on Cell Design and Operating Conditions. *RSC Adv.* **2019**, *9* (13), 7292–7300. https://doi.org/10.1039/C8RA09147A.

(216) Asuri, P.; Karajanagi, S. S.; Yang, H.; Yim, T. J.; Kane, R. S.; Dordick, J. S. Increasing Protein Stability through Control of the Nanoscale Environment. *Langmuir* **2006**, *22* (13), 5833–5836. https://doi.org/10.1021/la0528450.

(217) Caves, M. S.; Derham, B. K.; Jezek, J.; Freedman, R. B. Thermal Inactivation of Uricase (Urate Oxidase): Mechanism and Effects of Additives. *Biochemistry* **2013**, *52* (3), 497–507. https://doi.org/10.1021/bi301334w.

(218) Lee, H.; Hong, Y. J.; Baik, S.; Hyeon, T.; Kim, D.-H. Enzyme-Based Glucose Sensor: From Invasive to Wearable Device. *Adv. Healthc. Mater.* **2018**, *7* (8), 1701150. https://doi.org/10.1002/adhm.201701150.

(219) Chen, C.; Ran, R.; Yang, Z.; Lv, R.; Shen, W.; Kang, F.; Huang, Z. H. An Efficient Flexible Electrochemical Glucose Sensor Based on Carbon Nanotubes/Carbonized Silk Fabrics Decorated with Pt Microspheres. *Sensors Actuators, B Chem.* **2018**, *256*, 63–70. https://doi.org/10.1016/j.snb.2017.10.067.

(220) Yokus, M. A.; Songkakul, T.; Pozdin, V. A.; Bozkurt, A.; Daniele, M. A. Wearable Multiplexed Biosensor System toward Continuous Monitoring of Metabolites. *Biosens. Bioelectron.* **2020**, *153*, 112038. https://doi.org/10.1016/j.bios.2020.112038.

(221) Moyer, J.; Wilson, D.; Finkelshtein, I.; Wong, B.; Potts, R. Correlation between Sweat Glucose and Blood Glucose in Subjects with Diabetes. *Diabetes Technol. Ther.* **2012**, *14* (5), 398–402. https://doi.org/10.1089/dia.2011.0262.

(222) Bijman, J.; Quinton, P. M. Lactate and Bicarbonate Uptake in the Sweat Duct of Cystic Fibrosis and Normal Subjects. *Pediatr. Res.* **1987**, *21* (1), 79–82. https://doi.org/10.1203/00006450-198701000-00017.

(223) Fellmann, N.; Labbe, A.; Gachon, A. M.; Coudert, J. Thermal Sweat Lactate in Cystic Fibrosis and in Normal Children. *Eur. J. Appl. Physiol. Occup. Physiol.* **1985**, *54* (5), 511–516. https://doi.org/10.1007/BF00422962.

(224) Derbyshire, P. J.; Barr, H.; Davis, F.; Higson, S. P. J. Lactate in Human Sweat: A Critical Review of Research to the Present Day. *Journal of Physiological Sciences*. BioMed Central November 8, 2012, pp 429–440. https://doi.org/10.1007/s12576-012-0213-z.

(225) Fierheller, M.; Sibbald, R. G. A Clinical Investigation into the Relationship between Increased Periwound Skin Temperature and Local Wound Infection in Patients with Chronic Leg Ulcers. *Adv. Skin Wound Care* **2010**, *23* (8), 369–379. https://doi.org/10.1097/01.ASW.0000383197.28192.98.

(226) Percival, S. L.; McCarty, S.; Hunt, J. A.; Woods, E. J. The Effects of PH on Wound Healing, Biofilms, and Antimicrobial Efficacy. *Wound Repair Regen.* **2014**, *22* (2), 174–186. https://doi.org/10.1111/wrr.12125.

(227) Fu, W.; Hu, S.; Zhou, X.; Long, X. Effect of Electrolyte on the Proton Transport through Graphane in the Electrochemical Cell: A First-Principles Study. *J. Phys. Chem. Lett.* **2020**, *11* (8), 3025–3031. https://doi.org/10.1021/acs.jpclett.9b03837.

(228) Cheng, L. J. Electrokinetic Ion Transport in Nanofluidics and Membranes with Applications in Bioanalysis and Beyond. *Biomicrofluidics* **2018**, *12* (2), 021502. https://doi.org/10.1063/1.5022789.

(229) Chanmugam, A.; Langemo, D.; Thomason, K.; Haan, J.; Altenburger, E. A.; Tippett, A.; Henderson, L.; Zortman, T. A. Relative Temperature Maximum in Wound Infection and Inflammation as Compared with a Control Subject Using Long-Wave Infrared Thermography. *Adv. Skin Wound Care* **2017**, *30* (9), 406–414. https://doi.org/10.1097/01.ASW.0000522161.13573.62.

(230) Cutting, K. F. Wound Exudate: Composition and Functions. *Br. J. Community Nurs.* **2003**, *8* (Sup3), S4–S9. https://doi.org/10.12968/bjcn.2003.8.sup3.11577.

(231) Trengove, N. J.; Langton, S. R.; Stacey, M. C. Biochemical Analysis of Wound Fluid from Nonhealing and Healing Chronic Leg Ulcers. *Wound Repair Regen.* **1996**, *4* (2), 234–239. https://doi.org/10.1046/j.1524-475X.1996.40211.x.

(232) Galandáková, A.; Frankova, J.; Ambrožová, N.; Habartova, K.; Pivodova, V.; Zálešák, B.; Šafářová, K.; Smekalova, M.; Ulrichova, J. Effects of Silver Nanoparticles on Human Dermal Fibroblasts and Epidermal Keratinocytes. *Hum. Exp. Toxicol.* **2016**, *35* (9), 946–957.

(233) Poon, V. K. M.; Burd, A. In Vitro Cytotoxity of Silver: Implication for Clinical Wound Care. *Burns* **2004**, *30* (2), 140–147.

(234) Bastos, V.; de Oliveira, J. M. P. F.; Brown, D.; Jonhston, H.; Malheiro, E.; Daniel-da-Silva, A. L.; Duarte, I. F.; Santos, C.; Oliveira, H. The Influence of Citrate or PEG Coating on Silver Nanoparticle Toxicity to a Human Keratinocyte Cell Line. *Toxicol. Lett.* **2016**, *249*, 29–41.

(235) Holmes, A. M.; Lim, J.; Studier, H.; Roberts, M. S. Varying the Morphology of Silver Nanoparticles Results in Differential Toxicity against Micro-Organisms, HaCaT Keratinocytes and Affects Skin Deposition. *Nanotoxicology* **2016**, *10* (10), 1503–1514.

(236) Arora, S.; Jain, J.; Rajwade, J. M.; Paknikar, K. M. Cellular Responses Induced by Silver Nanoparticles: In Vitro Studies. *Toxicol. Lett.* **2008**, *179* (2), 93–100.

(237) Schaeublin, N. M.; Braydich-Stolle, L. K.; Schrand, A. M.; Miller, J. M.; Hutchison, J.; Schlager, J. J.; Hussain, S. M. Surface Charge of Gold Nanoparticles Mediates Mechanism of Toxicity. *Nanoscale* **2011**, *3* (2), 410–420.

(238) Shvedova, A.; Castranova, V.; Kisin, E.; Schwegler-Berry, D.; Murray, A.; Gandelsman, V.; Maynard, A.; Baron, P. Exposure to Carbon Nanotube Material: Assessment of Nanotube Cytotoxicity Using Human Keratinocyte Cells. *J. Toxicol. Environ. Heal. Part A* **2003**, *66* (20), 1909–1926.

(239) Monteiro-Riviere, N. A.; Nemanich, R. J.; Inman, A. O.; Wang, Y. Y.; Riviere, J. E. Multi-Walled Carbon Nanotube Interactions with Human Epidermal Keratinocytes. *Toxicol. Lett.* **2005**, *155* (3), 377–384.

(240) Tian, F.; Cui, D.; Schwarz, H.; Estrada, G. G.; Kobayashi, H. Cytotoxicity of Single-Wall Carbon Nanotubes on Human Fibroblasts. *Toxicol. Vitr.* **2006**, *20* (7), 1202–1212.

(241) Kyung, O. Y.; Grabinski, C. M.; Schrand, A. M.; Murdock, R. C.; Wang, W.; Gu, B.; Schlager, J. J.; Hussain, S. M. Toxicity of Amorphous Silica Nanoparticles in Mouse Keratinocytes. *J. Nanoparticle Res.* **2009**, *11* (1), 15–24.

(242) Grudzinski, I. P.; Bystrzejewski, M.; Cywinska, M. A.; Kosmider, A.; Poplawska, M.; Cieszanowski, A.; Ostrowska, A. Cytotoxicity Evaluation of Carbon-Encapsulated Iron Nanoparticles in Melanoma Cells and Dermal Fibroblasts. *J. Nanoparticle Res.* **2013**, *15* (8), 1835.

(243) Ding, L.; Stilwell, J.; Zhang, T.; Elboudwarej, O.; Jiang, H.; Selegue, J. P.; Cooke, P. A.; Gray, J. W.; Chen, F. F. Molecular Characterization of the Cytotoxic Mechanism of Multiwall Carbon Nanotubes and Nano-Onions on Human Skin Fibroblast. *Nano Lett.* **2005**, *5* (12), 2448–2464.

(244) Burd, A.; Kwok, C. H.; Hung, S. C.; Chan, H. S.; Gu, H.; Lam, W. K.; Huang, L. A Comparative Study of the Cytotoxicity of Silver-based Dressings in Monolayer Cell, Tissue Explant, and Animal Models. *Wound repair Regen.* **2007**, *15* (1), 94–104.

(245) Carrola, J.; Bastos, V.; Jarak, I.; Oliveira-Silva, R.; Malheiro, E.; Daniel-da-Silva, A. L.; Oliveira, H.; Santos, C.; Gil, A. M.; Duarte, I. F. Metabolomics of Silver Nanoparticles Toxicity in HaCaT Cells: Structure–Activity Relationships and Role of Ionic Silver and Oxidative Stress. *Nanotoxicology* **2016**, *10* (8), 1105–1117.

(246) Alarifi, S.; Ali, D.; Verma, A.; Alakhtani, S.; Ali, B. A. Cytotoxicity and Genotoxicity of Copper Oxide Nanoparticles in Human Skin Keratinocytes Cells. *Int. J. Toxicol.* **2013**, *32* (4), 296–307. https://doi.org/10.1177/1091581813487563.

(247) Shukla, R. K.; Kumar, A.; Pandey, A. K.; Singh, S. S.; Dhawan, A. Titanium Dioxide Nanoparticles Induce Oxidative Stress-Mediated Apoptosis in Human Keratinocyte Cells. *J. Biomed. Nanotechnol.* **2011**, *7* (1), 100–101. https://doi.org/10.1166/jbn.2011.1221.

(248) Pastar, I.; Stojadinovic, O.; Tomic-Canic, M. Role of Keratinocytes in Healing of Chronic Wounds. *Surgical technology international*. January 2008, pp 105–112.

(249) desJardins-Park, H. E.; Foster, D. S.; Longaker, M. T. Fibroblasts and Wound Healing: An Update. *Regen. Med.* **2018**, *13* (5), 491–495. https://doi.org/10.2217/rme-2018-0073.

(250) RoyChoudhury, S.; Umasankar, Y.; Bhushan, P.; Hirt, P. A.; MacQuhae, F. E.; Borda, L. J.; Lev-Tov, H. A.; Kirsner, R.; Bhansali, S. Nanocomposite Bienzymatic Sensor for Monitoring Xanthine in Wound Diagnostics. *J. Electrochem. Soc.* **2019**, *166* (9), B3295–B3301. https://doi.org/10.1149/2.0401909jes.

(251) Bhushan, P.; Umasankar, Y.; RoyChoudhury, S.; Hirt, P. A.; MacQuhaec, F. E.; Borda, L. J.; Lev-Tov, H. A.; Kirsner, R. S.; Bhansali, S. Biosensor for Monitoring Uric Acid in Wound and Its Proximity: A Potential Wound Diagnostic Tool. *J. Electrochem. Soc.* **2019**, *166* (10), B830–B836. https://doi.org/10.1149/2.1441910jes.

(252) Vistica, D. T.; Skehan, P.; Scudiero, D.; Monks, A.; Pittman, A.; Boyd, M. R. Tetrazolium-Based Assays for Cellular Viability: A Critical Examination of Selected Parameters Affecting Formazan Production. *Cancer Res.* **1991**, *51* (10).

(253) Berridge, M. V.; Tan, A. S. Characterization of the Cellular Reduction of 3-(4,5-Dimethylthiazol-2- Yl)-2,5-Diphenyltetrazolium Bromide (MTT): Subcellular Localization, Substrate Dependence, and Involvement of Mitochondrial Electron Transport in MTT Reduction. *Arch. Biochem. Biophys.* **1993**, *303* (2), 474–482. https://doi.org/10.1006/abbi.1993.1311.

(254) ISO - ISO 10993-5:2009 - Biological evaluation of medical devices — Part 5: Tests for in vitro cytotoxicity https://www.iso.org/standard/36406.html (accessed Jan 30, 2021).

(255) Vybrant® MTT Cell Proliferation Assay Kit - US.

(256) Choi, S.; Han, S. I.; Jung, D.; Hwang, H. J.; Lim, C.; Bae, S.; Park, O. K.; Tschabrunn, C. M.; Lee, M.; Bae, S. Y.; Yu, J. W.; Ryu, J. H.; Lee, S. W.; Park, K.; Kang, P. M.; Lee, W. B.; Nezafat, R.; Hyeon, T.; Kim, D. H. Highly Conductive, Stretchable and Biocompatible Ag–Au Core–Sheath Nanowire Composite for Wearable and Implantable Bioelectronics. *Nat. Nanotechnol.* **2018**, *13* (11), 1048–1056. https://doi.org/10.1038/s41565-018-0226-8.

(257) Papadopoulos, N. G.; Dedoussis, G. V. Z.; Spanakos, G.; Gritzapis, A. D.; Baxevanis, C. N.; Papamichail, M. An Improved Fluorescence Assay for the Determination of Lymphocyte-Mediated Cytotoxicity Using Flow Cytometry. *J. Immunol. Methods* **1994**, *177* (1–2), 101–111. https://doi.org/10.1016/0022-1759(94)90147-3.

(258) Decherchi, P.; Cochard, P.; Gauthier, P. Dual Staining Assessment of Schwann Cell Viability within Whole Peripheral Nerves Using Calcein-AM and Ethidium Homodimer. *J. Neurosci. Methods* **1997**, *71* (2), 205–213. https://doi.org/10.1016/S0165-0270(96)00146-X.

(259) Jing, X.; Mi, H. Y.; Peng, X. F.; Turng, L. S. Biocompatible, Self-Healing, Highly Stretchable Polyacrylic Acid/Reduced Graphene Oxide Nanocomposite Hydrogel Sensors via Mussel-Inspired Chemistry. *Carbon N. Y.* **2018**, *136*, 63–72. https://doi.org/10.1016/j.carbon.2018.04.065.

(260) LIVE/DEAD Viability/Cytotoxicity Kit.

(261) Rampersad, S. N. Multiple Applications of Alamar Blue as an Indicator of Metabolic Function and Cellular Health in Cell Viability Bioassays. *Sensors (Switzerland)* **2012**, *12* (9), 12347–12360. https://doi.org/10.3390/s120912347.

(262) Measuring cytotoxicity or proliferation - alamarBlue Assay Protocol | Bio-Rad.

(263) Aleshin, V.; Artiukhov, A.; Oppermann, H.; Kazantsev, A.; Lukashev, N.; Bunik, V. Mitochondrial Impairment May Increase Cellular NAD(P)H: Resazurin Oxidoreductase Activity, Perturbing the NAD(P)H-Based Viability Assays. *Cells* **2015**, *4* (3), 427–451. https://doi.org/10.3390/cells4030427.

(264) CCCP (Carbonyl cyanide m-chlorophenyl hydrazone, NSC 88124, CAS Number: 555-60-2) | Cayman Chemical.

(265) Walsh, J. G.; Cullen, S. P.; Sheridan, C.; Lüthi, A. U.; Gerner, C.; Martin, S. J. Executioner Caspase-3 and Caspase-7 Are Functionally Distinct Proteases. *Proc. Natl. Acad. Sci. U. S. A.* **2008**, *105* (35), 12815–12819. https://doi.org/10.1073/pnas.0707715105.

(266) Shim, M. K.; Yoon, H. Y.; Lee, S.; Jo, M. K.; Park, J.; Kim, J. H.; Jeong, S. Y.; Kwon, I. C.; Kim, K. Caspase-3/-7-Specific Metabolic Precursor for Bioorthogonal Tracking of Tumor Apoptosis. *Sci. Rep.* **2017**, *7* (1), 1–15. https://doi.org/10.1038/s41598-017-16653-2.

(267) CellEvent™ Caspase-3/7 Green Detection Reagent.

(268) Huang, T. C.; Lee, J. F.; Chen, J. Y. Pardaxin, an Antimicrobial Peptide, Triggers Caspase-Dependent and ROS-Mediated Apoptosis in HT-1080 Cells. *Mar. Drugs* **2011**, *9* (10), 1995–2009. https://doi.org/10.3390/md9101995.

(269) Shang, L.; Nienhaus, K.; Nienhaus, G. U. Engineered Nanoparticles Interacting with Cells: Size Matters. *J. Nanobiotechnology* **2014**, *12* (1), 5.

(270) Goodman, C. M.; McCusker, C. D.; Yilmaz, T.; Rotello, V. M. Toxicity of Gold Nanoparticles Functionalized with Cationic and Anionic Side Chains. *Bioconjug. Chem.* **2004**, *15* (4), 897–900.

(271) Suzuki, K.; Yataka, K.; Okumiya, Y.; Sakakibara, S.; Sako, K.; Mimura, H.; Inoue, Y. Rapid-Response, Widely Stretchable Sensor of Aligned MWCNT/Elastomer Composites for Human Motion Detection. *ACS Sensors* **2016**, *1* (6), 817–825. https://doi.org/10.1021/acssensors.6b00145.

(272) Maity, D.; Kumar, R. T. R. Polyaniline Anchored MWCNTs on Fabric for High Performance Wearable Ammonia Sensor. *ACS Sensors* **2018**, *3* (9), 1822–1830. https://doi.org/10.1021/acssensors.8b00589.

(273) Honn, K. V.; Singley, J. A.; Chavin, W. Fetal Bovine Serum: A Multivariate Standard. *Exp. Biol. Med.* **1975**, *149* (2), 344–347. https://doi.org/10.3181/00379727-149-38804.

(274) Thang, P. T.; Patrick, S.; Teik, L. S.; Yung, C. S. Anti-Oxidant Effects of the Extracts from the Leaves of Chromolaena Odorata on Human Dermal Fibroblasts and Epidermal Keratinocytes against Hydrogen Peroxide and Hypoxanthine-Xanthine Oxidase Induced Damage. *Burns* **2001**, *27* (4), 319–327. https://doi.org/10.1016/S0305-4179(00)00137-6.

(275) Fu, P. P.; Xia, Q.; Hwang, H.-M.; Ray, P. C.; Yu, H. Mechanisms of Nanotoxicity: Generation of Reactive Oxygen Species. *J. food drug Anal.* **2014**, *22* (1), 64–75.

(276) Abbade, L. P. F.; Lastoria, S. Venous Ulcer: Epidemiology, Physiopathology, Diagnosis and Treatment. *Int. J. Dermatol.* **2005**, *44* (6), 449–456. https://doi.org/10.1111/j.1365-4632.2004.02456.x.

(277) C, F.; D, W.; B, T.; M, C. Limitations of Daily Living Activities in Patients With Venous Stasis Ulcers Undergoing Compression Bandaging: Problems With the Concept of Self-Bandaging. *Wounds a Compend. Clin. Res. Pract.* **2007**, *19* (10), 255–257.

(278) FISHMAN; T. How to Manage Venous Stasis Ulcers. *Pod. Today* **2007**, *20*, 66–72.

(279) Nelzen, O.; Bergqvist, D.; Lindhagen, A. Long-Term Prognosis for Patients with Chronic Leg Ulcers: A Prospective Cohort Study. *Eur. J. Vasc. Endovasc. Surg.* **1997**, *13* (5), 500–508. https://doi.org/10.1016/S1078-5884(97)80179-7.

(280) Bjellerup, M. Determining Venous Incompetence: A Report from a Specialised Leg Ulcer Clinic. *J. Wound Care* **2006**, *15* (10). https://doi.org/10.12968/jowc.2006.15.10.26978.

(281) Phillips, T. J.; Machado, F.; Trout, R.; Porter, J.; Olin, J.; Falanga, V. Prognostic Indicators in Venous Ulcers. *J. Am. Acad. Dermatol.* **2000**, *43* (4), 627–630. https://doi.org/10.1067/mjd.2000.107496.

(282) Persoon, A.; Heinen, M. M.; Van Der Vleuten, C. J. M.; De Rooij, M. J.; Van De Kerkhof, P. C. M.; Van Achterberg, T. Leg Ulcers: A Review of Their Impact on Daily Life. *Journal of Clinical Nursing*. Blackwell Publishing Ltd 2004, pp 341–354. https://doi.org/10.1046/j.1365-2702.2003.00859.x.

(283) Thomson, B.; Hooper, P.; Powell, R.; Warin, A. P. Four-Layer Bandaging and Healing Rates of Venous Leg Ulcers. *J. Wound Care* **1996**, *5* (5), 213–216. https://doi.org/10.12968/jowc.1996.5.5.213.

(284) Grabs, A. J.; Wakely, M. C.; Nyamekye, I.; Ghauri, A. S. K.; Poskitt, K. R. Colour Duplex Ultrasonography in the Rational Management of Chronic Venous Leg Ulcers. *Br. J. Surg.* **1996**, *83* (10), 1380–1382. https://doi.org/10.1002/bjs.1800831016.

(285) Jayachandran, M.; Rodriguez, S.; Solis, E.; Lei, J.; Godavarty, A. Critical Review of Noninvasive Optical Technologies for Wound Imaging. *Adv. Wound Care* **2016**, *5* (8), 349–359. https://doi.org/10.1089/wound.2015.0678.

(286) Hurst, D. T.; Griffiths, E.; Vayianos, C. Inhibition of Uricase by Pyrimidine and Purine Drugs. *Clin. Biochem.* **1985**, *18* (4), 247–251. https://doi.org/10.1016/S0009-9120(85)80050-3.

(287) Fridovich, I. The Competitive Inhibition of Uricase by Oxonate and by Related Derivatives of S-Triazines. *J. Biol. Chem.* **1965**, *240* (6), 2491–2494. https://doi.org/10.1016/s0021-9258(18)97351-5.

(288) Attinger, C.; Wolcott, R. Clinically Addressing Biofilm in Chronic Wounds. *Adv. Wound Care* **2012**, *1* (3), 127–132. https://doi.org/10.1089/wound.2011.0333.

(289) Omar, A.; Wright, J.; Schultz, G.; Burrell, R.; Nadworny, P. Microbial Biofilms and Chronic Wounds. *Microorganisms* **2017**, *5* (1), 9. https://doi.org/10.3390/microorganisms5010009.

(290) James, G. A.; Swogger, E.; Wolcott, R.; Pulcini, E. deLancey; Secor, P.; Sestrich, J.; Costerton, J. W.; Stewart, P. S. Biofilms in Chronic Wounds. *Wound Repair Regen.* **2008**, *16* (1), 37–44. https://doi.org/10.1111/j.1524-475X.2007.00321.x.

(291) Serra, R.; Grande, R.; Butrico, L.; Rossi, A.; Settimio, U. F.; Caroleo, B.; Amato, B.; Gallelli, L.; De Franciscis, S. Chronic Wound Infections: The Role of Pseudomonas Aeruginosa and Staphylococcus Aureus. *Expert Review of Anti-Infective Therapy*. Taylor and Francis Ltd May 1, 2015, pp 605–613. https://doi.org/10.1586/14787210.2015.1023291.

(292) Löffler, M.; Zieker, D.; Weinreich, J.; Löb, S.; Königsrainer, I.; Symons, S.; Bühler, S.; Königsrainer, A.; Northoff, H.; Beckert, S. Wound Fluid Lactate Concentration: A Helpful Marker for Diagnosing Soft-Tissue Infection in Diabetic Foot Ulcers? Preliminary Findings. *Diabet. Med.* **2011**, *28* (2), 175–178. https://doi.org/10.1111/j.1464-5491.2010.03123.x.

APPENDIX 1

Sensor Toxicity Assessment using Image Analysis

Chapter 6 detailed the toxicity assessment of a wound monitoring sensor and its constituent active materials through *in vitro* assays carried out on human keratinocytes (HaCaT) and fibroblasts (HDFa). To assess the toxicity profile, all the treatment groups were investigated at different concentrations and time points using the gold standard MTT assay. The toxicity profile of the treatment groups was further assessed by performing fluorescence staining using the Live/Dead Cell assay (Thermo Fisher). This appendix provides the cell viability values calculated using analysis of the captured images.

The Live/Dead cell assay works on a simple method of differential staining where fluorescent dyes, ethidium homodimer and calcein AM, are used to stain the dead and live cells respectively. Ethidium homodimer intercalates in the DNA of dead cells due to loss of plasma membrane integrity, while calcein AM is an amine-reactive cell membrane permeant dye that binds to a live cell. Differential staining was performed using these dyes and images were captured using a fluorescence microscope (objective: 20x) at different concentrations and time points. Each experiment was carried out in triplicate (three independent wells) and five images were captured per well to account for the spatial cell distribution. In summary, a total of 15 images were captured for a treatment group at a given concentration and time point. This assay was carried out as a supporting study to the quantitative MTT assay. The captured images were analyzed using a manual cell counting method, based on which the percent cell viability was determined using the below formula (ref),

$$\%\ Cell\ viability = \frac{Total\ number\ of\ live\ cells}{Total\ number\ of\ cells} x\ 100 \qquad \text{Equation 1}$$

For a treatment group at a given concentration and time point, the cell viability for each of the 15 images was calculated first, following which the cell viability obtained from the five images captured per well was averaged. For the final cell viability, we computed the mean and standard deviation by averaging the cell viabilities obtained from each independent well. These calculated cell viability values for the dermal and epidermal cell lines are provided in Table 1 and 2 respectively.

Table 1. Cell viability of dermal cells (HDFa) on exposure to the different treatment groups at 12 and 24 h time points. The cell viability values as calculated from image analysis. Five images were captured for each well (n = 3) to account for the spatial cell distribution. All the data is presented as mean ± SD obtained from the images.

Treatment Group	**Concentration (µg/ml)**	**Cell viability (%) (Mean ± SD)**	
		12 h	**24 h**
AuNPs	0.5	80.32 ± 3.52	95.29 ± 1.38
	5	77.13 ± 2.49	92.13 ± 3.43
	50	81.36 ± 4.79	84.32 ± 1.29
MWCNTs	0.001	82.40 ± 0.50	92.97 ± 3.42
	0.01	75.79 ± 1.26	89.37 ± 3.94
	0.1	81.61 ± 5.31	80.63 ± 6.95
UOx	0.2	80.49 ± 5.19	83.87 ± 1.97
	2	83.22 ± 6.41	87.37 ± 1.96
	20	80.44 ± 0.82	84.02 ± 3.51
HRP	0.02	83.94 ± 3.38	92.78 ± 4.95

	0.2	77.36 ± 7.44	82.24 ± 5.17
	2	84.73 ± 2.99	85.53 ± 0.92
Sensor	Unfunctionalized	84.06 ± 2.40	83.69 ± 1.56
	Functionalized	82.76 ± 2.42	76.35 ± 3.91

Table 2. Cell viability of epidermal cells (HaCaT) on exposure to the different treatment groups at 12 and 24 h time points. The cell viability values as calculated from image analysis. Five images were captured for each well (n = 3) to account for the spatial cell distribution. All the data is presented as mean ± SD obtained from the images.

Treatment Group	**Concentration (µg/ml)**	**Cell viability (%) (Mean ± SD)**	
		12 h	**24 h**
AuNPs	0.5	87.73 ± 7.21	89.48 ± 2.49
	5	84.59 ± 8.06	89.42 ± 7.87
	50	84.86 ± 2.15	89.68 ± 1.90
MWCNTs	0.001	88.38 ± 5.74	90.34 ± 0.38
	0.01	83.99 ± 1.93	92.25 ± 2.38
	0.1	88.07 ± 0.30	92.65 ± 2.73
UOx	0.2	88.64 ± 6.58	92.75 ± 5.84
	2	88.19 ± 0.89	91.11 ± 6.70
	20	85.50 ± 1.34	93.83 ± 0.84
HRP	0.02	87.01 ± 4.76	89.32 ± 3.30
	0.2	86.97 ± 5.77	81.51 ± 0.32
	2	79.75 ± 0.87	84.58 ± 7.65
Sensor	Unfunctionalized	90.99 ± 2.41	92.48 ± 2.66
	Functionalized	90.79 ± 4.58	86.25 ± 1.67

The cell viability values calculated from the manual cell counting method followed a similar trend to that of the values obtained from the MTT assay. For both the cell lines, a time and dose-dependent decrease in cell viability was seen when treated with the different treatment groups. The cell viability for each treatment group was observed to be >70%, confirming no cytotoxic effect (IC70). The toxicity assessment carried out using the cell counting method was in agreement with the results obtained with the MTT assay for both the cell lines.

The raw images and the cell viability calculations for each image is available at the following link,

https://fiudit-my.sharepoint.com/:f:/g/personal/pbhushan_fiu_edu/Eqm_AmXZzKpAuiPJ6vdp7tcB0N8ZmgREabclmMCx7L000w?e=QF2i0q

APPENDIX 2

Informed Consent Form

Title of Study: **Continuous monitoring of Uric Acid levels in wound exudate and its correlation with wound healing**

<u>Key Information</u>: The following is a short summary of this study to help you decide whether or not to be a part of this study. More detailed information is listed later on in this form.

Why am I being invited to take part in a research study?

We ask you to take part in a research study because you have a wound in one of your extremities for more than 4 weeks and we would like to place a biosensor embedded in a gauze to monitor the characteristics of the secretions of your wound. A person who takes part in a research study is called a research or study subject. In this consent form "you" always refers to the research subject.

What should I know about this research study?

- Someone will explain this research study to you.
- Whether or not you take part is up to you.
- You can choose not to take part.
- You can agree to take part and later change your mind.
- Your decision will not be held against you.
- You can ask all the questions you want before you decide.

PURPOSE

The purpose of this research study is to place a sensor in your wound to have a continuous measurement of chemical parameters of the secretion of your wound,

through an enzymatic biosensor designed by the Department of Electrical and Computer Engineering at Florida International University, Miami.

Why is this research being done?

We would like to test a wearable sensor of wound secretion parameters. Wearable sensors have the capacity for real-time health and environmental monitoring. Continuous wound monitoring techniques can track healing visually or through individual measurements and allow remote patient-physician engagements to enhance quality of care and time and validate treatment based on data acquired at a personal scale.

How long will the research last and what will I need to do?

We expect that you will be in this research study for 1 month. You will need to come to your regular weekly clinic appointments for wound care and dressing changes. During the dressing changes we will replace the monitor for a new one and your wound will be treated with Standard of Care (e.g. in case of venous leg ulcers debridement and compression therapy will be administrated). We will collect personal information such as past medical and surgical history, medication history, wound specific information such as ulcer size, ulcer duration, current and prior treatment of ulcer. Photographs of the ulcer and healthy skin nearby to the wound will be taken. A sensor will be placed over the wound and over nearby non-wounded area on the same limb. You will be asked to return to the clinic in approximately one week to ensure proper healing, get dressing changes and change the sensor to a new one. More detailed information about the study procedures can be found later in this document under

"What happens if I say yes, I want to be in this research?"

Is there any way being in this study could be bad for me?

There is little if no risk to have allergic reactions to dressings.

Will being in this study help me in any way?

There are no benefits to you from taking part in this research. However, since you are going to receive a standard of care, we expect some improvement in wound healing.

What happens if I do not want to be in this research?

Participation in research is completely voluntary. You can decide to participate or not to participate. You can say no now or leave the study at any time later. This will not affect your care or benefits at UM/Jackson Memorial Hospital. The researcher may remove you from the study if he/she believes that staying in the study is no longer in your best interest. If you stop being in the study, the study staff will stop collecting new information about you but they may need to use the information they have already collected.

Detailed Information:

The following is more detailed information about this study, in addition to the information listed above.

Who can I talk to?

If you have questions, concerns, or complaints, or think the research has hurt you, talk to the research team at Dermatology and Cutaneous Surgery Research Office at (305)689-3376.

This research has been reviewed and approved by an Institutional Review Board ("IRB"). The Human Subject Research Office (HSRO) provides administrative support to the University of Miami's IRBs.

Please call the HSRO at 305-243-3195 if:

- Your questions, concerns, or complaints are not being answered by the research team.
- You cannot reach the research team.

- You want to talk to someone besides the research team.
- You have questions about your rights as a research subject.
- You want to get information or provide input about this research.

How many people will be studied?

We expect about 20 people will be in this research study.

What happens if I say yes, I want to be in this research?

After signing Informed Consent your ulcer will be treated with Standard of Care, for example, in case of venous leg ulcers debridement and compression therapy will be administrated). Debridement (if necessary) will be performed after anesthetizing the wound. Data collection will include personal information such as age, gender, race, ethnicity, Body Mass Index, past medical and surgical history including medication history. Wound specific information such as ulcer size, ulcer duration, current and prior treatment of ulcer. Photographs of the ulcer and healthy skin nearby to the wound will be taken. A small sensor will be placed over the wound and a nearby non-wounded area on the same limb, and then appropriate dressings and compression therapy will be provided. You will be asked to return to the clinic in approximately one week to ensure proper healing, get dressing changes, and change the sensor to a new one.

What happens if I say yes, but I change my mind later?

You can leave the research at any time, it will not be held against you.

What if I get hurt as a result of my participation in this study?

Although risks are unlikely, if injury should occur, treatment will in most cases be available. If you have insurance, your insurance company may or may not pay for these costs. If you do not have insurance, or if your insurance company refuses to pay, you will be expected to pay. Funds to compensate for pain, expenses, lost wages, and other damages caused by injury are not available.

What happens to the information collected for the research?

Efforts will be made to limit the use and disclosure of your personal information, including research study and medical records, to people who need to review this information. We cannot promise complete confidentiality.

We are asking you to let us collect some information from your medical records for this study. We will not need to look at all your records. Instead, we will use a computer to find information about your use of health care services, including:

- clinic visits;
- lab test results;
- trips to the hospital;
- medicines;
- wound measurements;
- pictures of your wounds.

If you are or have been, a patient at a University of Miami facility, you will have a University of Miami medical record. We use an electronic medical record system known as UChart, which improves access to information important to your medical care. UChart will show that you are in a research study and a copy of this signed consent form will be included. To provide as complete a record as possible, some or all of your study-related research information may also be placed in UChart. This specifically includes investigational drugs, devices, biologics, or anything else that may, separately or together with other substances or activities, interfere with your clinical treatment or place you at greater risk of harm. Other information from the research study may be included as well.

This information will be available to University of Miami doctors, nurses, and other authorized staff who may not be part of the research team but who are involved in providing you medical care, or who are otherwise allowed to access your information. The confidentiality of the results and other documents in UChart will be governed by

laws, such as HIPAA, that concern medical records. We suggest that you tell any non-University of Miami doctors that you are in a research study and that more information may be made available to them at your request. The research team may use your information to notify you of appointments, send you appointment reminders, or schedule additional appointments.

Federal law provides additional protection of your medical records and related health information. These are described in the University of Miami HIPAA authorization for research known as Form B.

Will the information collected be used in future research?

Records will be in a locked cabinet in the Dermatology research office, 1321 NW 14 St, Room 504. Dressings will be sent to Dr. Shekhar Bhansali's laboratory, Alcatel Lucent Professor and Chair located at Florida International University, Department of Electrical and Computer Engineering. The samples will be coded with a number but with no patient identifying information. Once analyses of the samples are completed, the samples will be destroyed.

Your information or samples that are collected as part of this research will not be used or distributed for future research studies, even if all of your identifiers are removed.

What else do I need to know?

Your information and samples (both identifiable and de-identified) may be used to create products or to deliver services, including some that may be sold and/or make money for others. If this happens, there are no plans to tell you, or to pay you, or to give any compensation to you or your family.

PARTICIPANT'S STATEMENT/SIGNATURE

- *I have read this form and the research study has been explained to me.*

- *I have been given the chance to ask questions, and my questions have been answered. If I have more questions, I have been told who to call.*
- *I agree to be in the research study described above.*

I will receive a copy of this consent form after I sign it.

_____ _____

Signature of Participant Date

_____ _____

Printed Name of Participant

_____

Printed Name of Person Explaining Consent Date

(Investigator/Delegate)

_____

Signature of Person Explaining Consent

(Investigator/Delegate)

VITA

PULAK BHUSHAN

2009-2013	BSE in Electronics Asian Institute of Technology, Thailand
2013-2015	ME in Microelectronics and Embedded Systems Asian Institute of Technology, Thailand
2017-2021	Doctor of Philosophy in Electrical Engineering Florida International University, USA

PUBLICATIONS

1. Bhushan, P., Umasankar, Y., RoyChoudhury, S., Hirt, P.A., MacQuhaec, F.E., Borda, L.J., Lev-Tov, H.A., Kirsner, R.S. and Bhansali, S., 2019. Biosensor for Monitoring Uric Acid in Wound and Its Proximity: A Potential Wound Diagnostic Tool. *Journal of The Electrochemical Society*, *166*(10), p.B830.

2. RoyChoudhury, S., Umasankar, Y., Bhushan, P., Hirt, P.A., MacQuhae, F.E., Borda, L.J., Lev-Tov, H.A., Kirsner, R. and Bhansali, S., 2019. Nanocomposite Bienzymatic Sensor for Monitoring Xanthine in Wound Diagnostics. *Journal of The Electrochemical Society*, *166*(9), pp.B3295-B3301.

3. Bhushan, P., Umasankar, Y., Hutcheson, J.D. and Bhansali, S., 2019. Toxicity assessment of wearable wound sensor constituents on keratinocytes. *Toxicology in Vitro*, *58*, pp.170-177.

4. Songkakul, T., Bhushan, P., Umasankar, Y., Yokus, M., Daniele, M.A., Bhansali, S. and Bozkurt, A., 2019, October. Towards a Long-Term Multi-Site Electrochemical Wound Monitoring System. In *2019 IEEE SENSORS* (pp. 1-4). IEEE.

5. Hirt, P., Umasankar, Y., Bhushan, P., Borda, L., McNamara, S., Chen, C., MacQuhae, F., Bhansali, S., Kirsner, R. and Lev-Tov, H., 2019. Uric acid levels in chronic wounds are elevated compared with adjacent normal skin: 10511. *Journal of the American Academy of Dermatology*, *81*(4).

6. RoyChoudhury, S., Bhushan, P., Umasankar, Y., Hirt, P.A., Lev-Tov, H.A., Kirsner, R.S. and Bhansali, S., 2018. Multimodal Enzymatic Sensing for Continuous Wound Monitoring. *ECS Transactions*, *88*(1), p.419.